ILLINOIS CENTER FOR TRANSPORTATION

Report No. FHWA-ICT-25-002

Testing, Analysis, and Load Rating of Precast Prestressed Concrete Deck Beams with Transverse Cracks

Bassem Andrawes
Dachina Gunasekaran

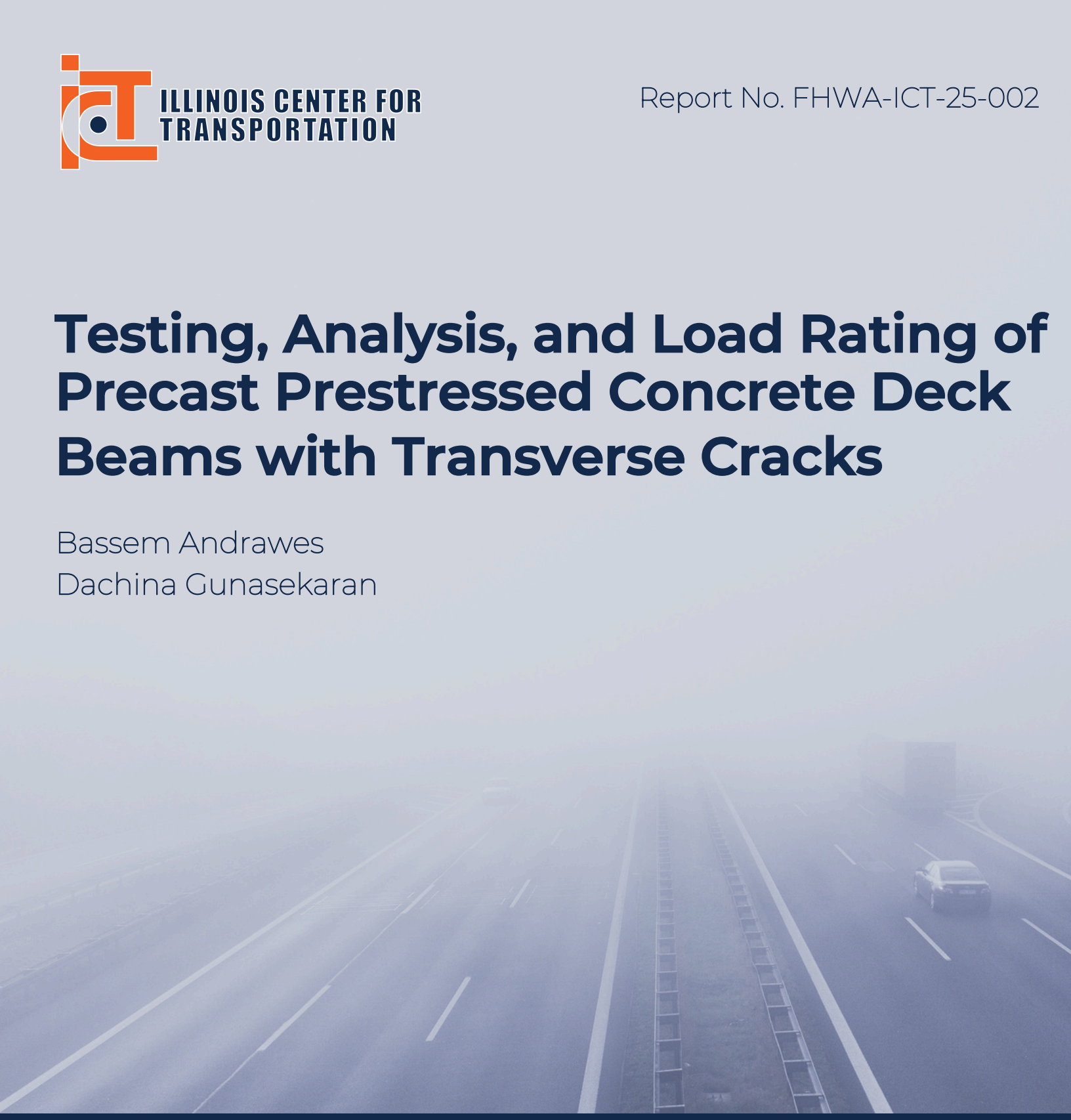

ICT Project R27-226

May 2025

ISSN: 0197-9191
ICT Series Report No. 25-002
https://doi.org/10.36501/0197-9191/25-002

TECHNICAL REPORT DOCUMENTATION PAGE

1. Report No.	2. Government Accession No.	3. Recipient's Catalog No.
FHWA-ICT-25-002	N/A	N/A

4. Title and Subtitle	5. Report Date
Testing, Analysis, and Load Rating of Precast Prestressed Concrete Deck Beams with Transverse Cracks	May 2025
	6. Performing Organization Code N/A

7. Authors	8. Performing Organization Report No.
Bassem Andrawes, https://orcid.org/0000-0002-8954-3751 Dachina Gunasekaran, https://orcid.org/0000-0003-1431-6324	ICT-25-002 UILU-2025-2002

9. Performing Organization Name and Address	10. Work Unit No.
Illinois Center for Transportation Department of Civil and Environmental Engineering University of Illinois Urbana-Champaign 205 North Mathews Avenue, MC-250 Urbana, IL 61801	N/A **11. Contract or Grant No.** R27-226

12. Sponsoring Agency Name and Address	13. Type of Report and Period Covered
Illinois Department of Transportation (SPR) Bureau of Research 126 East Ash Street Springfield, IL 62704	Final Report 8/16/20–5/15/25 **14. Sponsoring Agency Code**

15. Supplementary Notes

Conducted in cooperation with the U.S. Department of Transportation, Federal Highway Administration.
https://doi.org/10.36501/0197-9191/25-002

16. Abstract

This study focused on understanding the impact of transverse cracks on the residual capacity and load rating analysis of in-service precast prestressed concrete (PPC) deck beams. Two decommissioned (33 × 36 and 21 × 36) PPC deck beams were tested under four-point bending loads to assess the impact of transverse cracks on the structural performance of the beams. Finite element and theoretical cracked section analyses were also performed to investigate the capacity of the as-built and cracked PPC deck beam. Transverse cracks reduced the load rating capacity of the 33 × 36 beam by almost 34%, which subsequently reduced the capacity-based load rating factor by 22% under the HS-20 truck load. The experimental investigation of the 21 × 36 PPC deck beam showed that the load required to induce visible cracks in the beam was 95.5% of its AASHTO live load capacity. The load rating of the cracked 21 × 36 beam was 73.6% lower than its as-built capacity, exhibiting a severe reduction in its load-bearing capacity. A parametric study was conducted to understand the effect of the influencing parameters, like the beam geometry and material properties, on the damaged beams' behavior. For PPC deck beams with rectangular voids, the statistically significant parameters were span length, strand diameter, and skew angle. In the parametric study, the inventory load rating factor of the prestressing strands in tension was predicted to decrease linearly for a crack width up to 0.64 mm, while the capacity inventory rating factor was predicted to decrease up to 73.8% for a crack width of 0.64 mm.

17. Key Words	18. Distribution Statement
Box Beams, Transverse Cracks, Residual Capacity, Prestressed Concrete, Load Rating, Parametric Study	No restrictions. This document is available through the National Technical Information Service, Springfield, VA 22161.

19. Security Classif. (of this report)	20. Security Classif. (of this page)	21. No. of Pages	22. Price
Unclassified	Unclassified	69	N/A

Form DOT F 1700.7 (8-72) **Reproduction of completed page authorized**

ACKNOWLEDGMENT, DISCLAIMER, MANUFACTURERS' NAMES

This publication is based on the results of **ICT-R27-226: Residual Capacity of Precast Prestressed Concrete (PPC) Deck Beams with Transverse Cracks**. ICT-R27-226 was conducted in cooperation with the Illinois Center for Transportation; the Illinois Department of Transportation; and the U.S. Department of Transportation, Federal Highway Administration.

Members of the Technical Review Panel (TRP) were the following:

- Robert Perkins, TRP Chair, Illinois Department of Transportation
- Ruben Boehler, Illinois Department of Transportation
- Spencer Koehler, Illinois Department of Transportation
- James Krstulovich, Illinois Department of Transportation
- Nick Lombardi, Federal Highway Administration
- Daniel Tobias, Illinois Department of Transportation

EXECUTIVE SUMMARY

One of the main concerns with adjacent precast prestressed concrete (PPC) deck beams is their durability due to cracking. Although extensive research has focused on the effects and mitigation measures for longitudinal cracks in PPC deck beam bridges, insufficient knowledge remains regarding the impact of transverse cracking on structural integrity. Transverse cracks in PPC beams may adversely affect their safety and performance. Therefore, this research aimed to quantify the effect of transverse cracks by relating crack width to residual capacity, stresses, and load rating of damaged beams.

To achieve this, both experimental and numerical studies were conducted to assess the effects of transverse cracks on residual capacity and state of stress in the beams. Two full-scale PPC deck beams (33 × 36 and 21 × 36) that had previously been in service were experimentally assessed to evaluate the impact of transverse cracks. These beams were subjected to a four-point bending load to isolate the flexural behavior. Experimental test results were used to determine flexural behavior, residual capacity, and concrete and strand stresses in the damaged beams. A finite element model of the 33 × 36 PPC deck beam was developed and analyzed to understand the effect of transverse cracking on load-bearing capacity and strand stresses. The influence of bond-slip behavior between concrete and strands, modeled using nonlinear springs, was compared to that of a perfect bond. Results indicated that strand stresses were sensitive to bond strength and crack width. Incorporating bond-slip behavior ensured that stress predictions from the finite element analysis are more closely aligned with those observed in an in-service beam. Findings revealed that transverse cracks reduced the load rating capacity of the 33 × 36 beam by nearly 34%, leading to a 22% reduction in the capacity-based load rating factor under the HS-20 truck load. Although serviceability-based load rating from theoretical crack width models conservatively provided a negative rating, the flexural testing indicated the beam retained over 50% of its nominal and residual capacities while remaining in the elastic range. A theoretical cracked section analysis was conducted to predict the load capacity and state of stresses in the 21 × 36 PPC deck beam. Experimental and analytical investigations revealed that nearly 95.5% of the 21 × 36 PPC deck beam's AASHTO live load capacity was required to induce visible transverse cracks. The load rating of the cracked 21 × 36 beam was 73.6% lower than its as-built capacity, indicating a severe reduction in load-bearing capacity.

A parametric study was conducted to examine the influence of beam geometry and material properties on the behavior of cracked beams. For PPC deck beams with rectangular voids, the statistically significant parameters were span length, strand diameter, and skew angle. Results showed that the inventory rating factor for prestressing strands in tension decreased linearly for crack widths up to 0.64 mm. In comparison, the capacity inventory rating factor was predicted to decrease up to 73.8% for a crack width of 0.64 mm.

TABLE OF CONTENTS

LIST OF FIGURES

LIST OF TABLES

CHAPTER 1: INTRODUCTION

PROBLEM STATEMENT

Precast prestressed concrete (PPC) adjacent deck beam bridges consist of box beams stacked next to each other and connected using grouted shear keys and transverse tie rods. These bridges are widely used for short-to-medium-span applications and account for nearly 35% of all bridges in Illinois (NBI 2024). According to NBI (2024), 7.5% of Illinois' PPC deck beam bridges are structurally deficient and rated as "poor." By the next decade, an additional 6.0% of PPC deck beam bridges are projected to deteriorate further and receive ratings ranging from "fair" to "poor." Therefore, there is an urgent need to assess the damage in these bridges and evaluate their impact on structural performance.

The primary issues affecting these bridges are structural and durability concerns arising from longitudinal and transverse cracking as well as corrosion. Longitudinal cracks are a common problem encountered in PPC deck beam bridges. Since the late 1980s, numerous researchers have investigated the causes of longitudinal cracks and potential mitigation strategies (Lall et al. 1998; Sharpe 2007; Grace et al. 2012; Attanayake and Aktan 2017). The cracks occur in the shear key, propagate through the depth, and appear as reflective cracks on the riding surface. Such deterioration compromises the ability of beams to act as an integral unit, disrupts load distribution, and increases localized loads on individual beams. The various mitigation measures adopted include the use of improved grouting material (Gulyas et al. 1995), improved shape and depth of the shear key, and the application of transverse post-tensioning (Miller et al. 1999; Lall et al. 1998). While extensive research has been conducted on longitudinal cracks and their mitigation, there remains a knowledge gap regarding the effects of transverse cracks.

This issue of transverse cracking in PPC deck beam bridges has only recently gained attention and has yet to be extensively studied. These cracks, observed near the midspan of the beams in service, occur when the tensile demand on the beam soffit exceeds the tensile strength of concrete, leading to cracking under stress. Transverse cracks may reduce the beam's flexural capacity and stiffness, compromising structural integrity. They may also increase the stresses in the strands and concrete at the crack section, which may lead to localized bond failures. Cracks also allow for water seepage, which could lead to corrosion in the strands. In Xiaohong (2019), transverse cracks were observed in a prestressed box beam bridge, which led to deflections exceeding allowable limits and increased tensile stresses in concrete. Understanding the relationship between transverse crack characteristics—such as location and width—and residual capacity is crucial for accurately determining the load rating of cracked PPC deck beams.

The residual capacity of a damaged bridge section refers to its remaining load-bearing capacity after experiencing deterioration or damage. Many researchers have related the residual capacity of the section to the intensity of corrosion (Kashani et al. 2019; Kioumarsi et al. 2021), impact loads (Nylen 2020; Zhang et al. 2022), and fire (Yu et al. 2021). These studies do not discuss the relationship between the residual capacity and any existing transverse cracks in the beam. Thus, further research is necessary to explore how transverse crack characteristics influence residual capacity and how these cracks affect load rating calculations for PPC deck beams.

Periodic load rating analysis is conducted to determine the maximum truck loads a bridge can safely support, given its current condition. The *Manual for Bridge Evaluation* (*MBE*), published by the American Association of State Highway and Transportation Officials, determines the guidelines and procedures used in the load rating analysis of bridges (AASHTO, 2018). This analysis yields the inventory and operating ratings, which give the maximum allowable and maximum permissible live loads on the bridge, respectively. The residual capacity and the built-up stresses in the damaged beam would be used in the rating equations to ensure the damaged beam is still safe and serviceable. Therefore, for the load rating analysis to be accurate, there is a need to analyze the effects of a transverse crack on the residual capacity and stresses in a damaged bridge beam.

REPORT OUTLINE

This study, initiated and supported by the Illinois Department of Transportation (IDOT), investigates the impact of transverse cracks on the behavior and load rating of PPC deck beams. The details and results of the experimental tests conducted on two PPC deck beams with rectangular and circular voids are described in Chapters 2 and 3 of this report, respectively. Chapter 4 describes the results of the load rating analysis on the cracked PPC deck beams tested as a part of this study. Chapter 5 describes the theoretical evaluations conducted on beams with circular voids, while Chapter 6 presents the parametric study conducted on beams with rectangular voids. Chapters 7 and 8 present the recommendations and the conclusions of the study.

CHAPTER 2: FLEXURAL TEST OF A DAMAGED 33 × 36 PPC DECK BEAM (RECTANGULAR VOID)

The first PPC deck beam specimen tested in this study was a 33 × 36 one, hereby named G1 beam. It was extracted from a bridge (bridge ID: SN 085-4209) in Schuyler County, Illinois, constructed in 1984. The bridge featured three simply supported spans and was skewed at a 10° angle. It had a total length of 50 m (163.94 ft) and a width of 7.3 m (24 ft), accommodating two lanes of traffic. The internal span was 13.9 m (71.3 ft), while the two exterior spans were 21.7 m (46.3 ft) each. The bridge deck had eight 33 × 36 PPC deck beams in its cross-section.

During an inspection, IDOT found an exterior beam and an interior beam in one of the approach spans had transverse cracks at the bottom. Figure 1 presents the location and photos of the transverse cracks in the approach span. The exterior beam with the transverse crack was extracted and tested at the Newmark Structural Engineering Lab at the University of Illinois Urbana-Champaign.

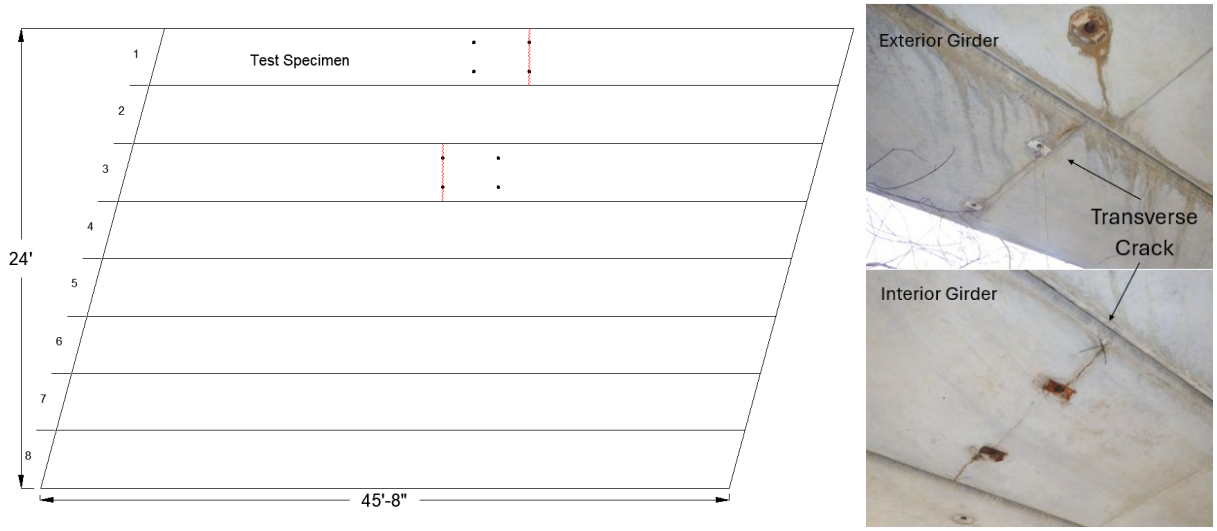

Figure 1. Photos. Transverse cracks in bridge 085-4209.

TEST SPECIMEN

Figures 2-A and 2-B present the cross-sectional and plan views of the G1 beam test specimen. The G1 beam had a 28-day design concrete strength of 34.5 MPa (5 ksi) and contained seven 12.5 mm (0.5 in.) diameter, G270 low-relaxation prestressing strands (ultimate strength = 1862 MPa, 270 ksi), located in the bottom flange with an eccentricity of 331.5 mm (13.1 in.) at the bottom flange of the beam. The beam had an 838 mm (18.4 in.) wide diaphragm at its midspan and a 467 mm (33 in.) wide diaphragm at both ends.

As an initial step, the uncracked beam section's nominal moment capacity was computed per the AASHTO Standard Specifications for Highway Bridges (AASHTO 2002). To reflect design practices from the 1980s, when the bridge was constructed, the *Manual for Bridge Evaluation* (*MBE*) (AASHTO 2018) recommends the use of the load factor design (LFD) method, as outlined in the AASHTO standard

specifications (AASHTO 2002), for analyzing the nominal capacity of the beam section. After calculating the prestressing strand losses (251 MPa, ~20% prestress losses), the nominal moment capacity of the section was 976.9 kN-m (720.5 kip-ft). The dead load moment due to the beam's self-weight at the midspan section was calculated to be 243.6 kN-m (179.7 kip-ft). Therefore, the superimposed nominal moment capacity (after excluding the moment due to self-weight) of the midspan section was 733.3 kN-m (476.9 kip-ft).

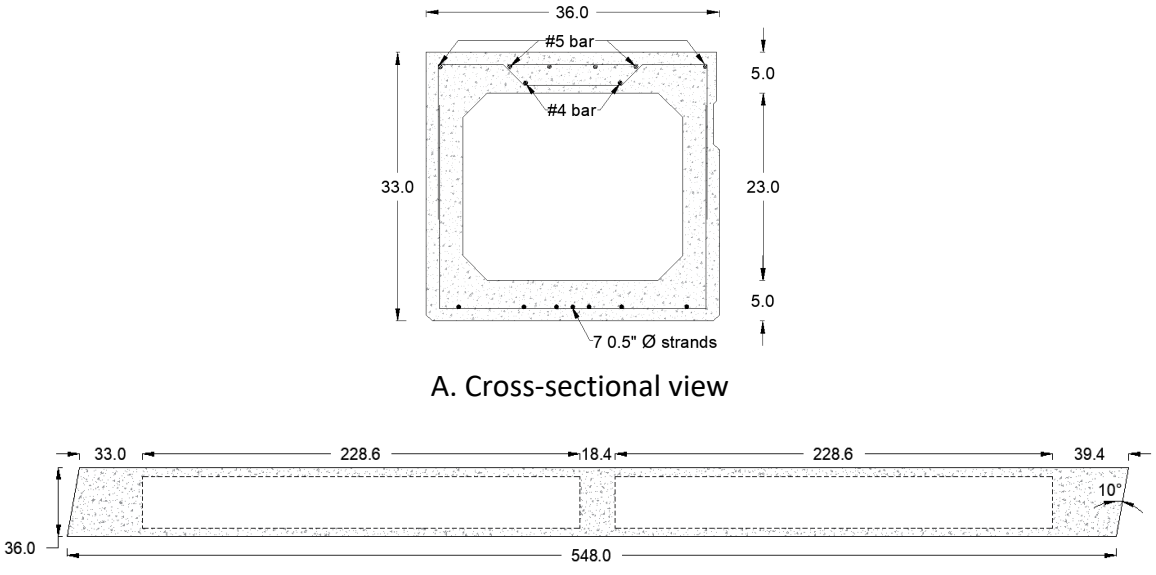

Figure 2. Illustration. 33 × 36 (G1) PPC deck beam.

IDENTIFICATION OF DAMAGE (CRACKS)

The G1 beam was cracked while in service. As a result, the existing cracks on the surface of the beam were identified and marked. Figures 3-A and 3-B present the cracks on the exterior side of the beam; Figure 3-C presents the cracks on the beam's interior side; and Figures 3-D and 3-E present the cracks on the bottom of the beam. Except for cracks C1 to C8, all identified cracks were located on the exterior, top, and interior sides of the beam. As shown in Figures 3-B and 3-D, all cracks except C6 stopped propagating well above the strands and did not extend to the beam's bottom. This indicates that these cracks resulted from the beam's shear-torsional response. Crack C6, measuring 0.25 mm (0.01 in.) at the bottom, was located adjacent to the middle diaphragm and was the sole through-depth crack observed in the beam.

NUMERICAL ANALYSIS OF AS-BUILT BEAM

A numerical analysis of the as-built G1 beam was conducted in ABAQUS to compare the predicted behavior of the undamaged and damaged beam specimens. The finite element model was built using sectional details and material properties available in the bridge plan. The beam's concrete section (Figure 4-A) was modeled using 3D solid elements (C3D8) with eight integration points. Figure 4-B presents the internal reinforcements, including the prestressing strands, longitudinal rebars, and

stirrups, modeled using 3D truss elements (T3D2) with two nodes. The loading and support plates designed as part of the test setup were modeled using 3D solid elements (C3D8) with the exact geometric configuration as the test setup. The first beam, G1, had a skew angle of 10°. It was loaded under four-point bending loads (Figure 4-C) to simulate a tandem load and observe the behavior of the transverse crack under pure flexural behavior. The four-point loading and support plates were modeled with a skew angle of 10° to minimize the influence of torsional behavior and isolate the flexural response.

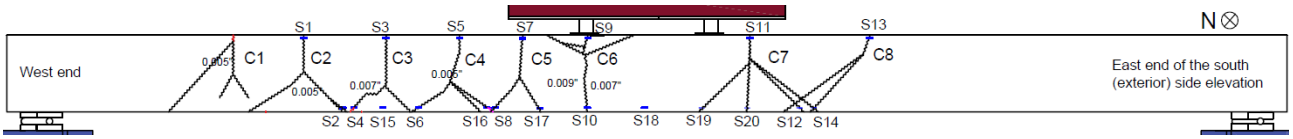

A. Cracks on the exterior (south elevation) side

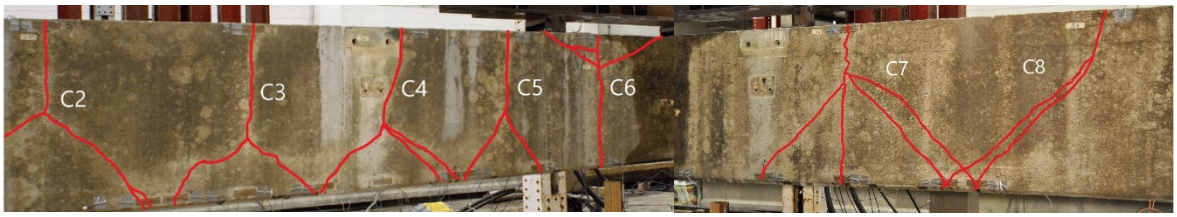

B. Cracks on the exterior (south elevation) side

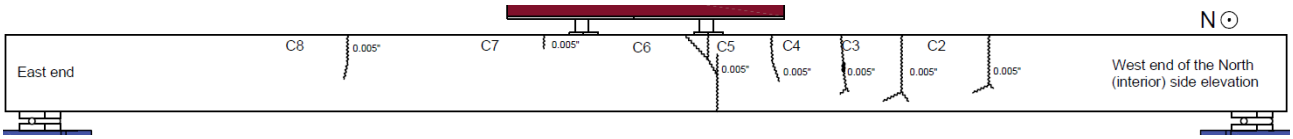

C. Cracks on the interior (north elevation) side

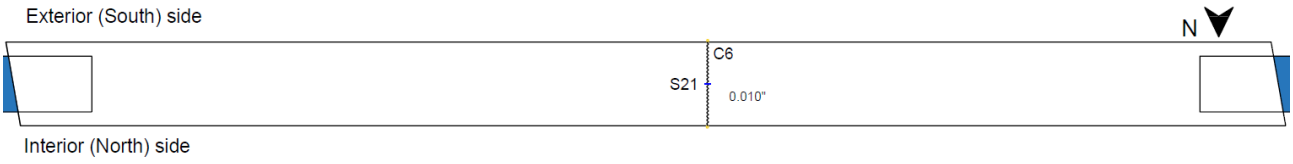

D. Crack on the bottom side

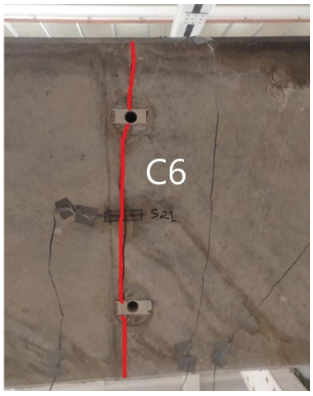

E. Crack on the bottom side

Figure 3. Illustration and photo. Cracks on the 33 × 36 G1 beam.

The concrete material behavior was modeled using the concrete damage plasticity model. The material properties of the concrete were defined using the Hognestad model (Hognestad 1951), with the damage parameters calculated as per the ABAQUS user manual. The nonlinear behavior of the prestressing strands was modeled using the Menegotto-Pinto model (Menegotto and Pinto 1973), while a bilinear model was chosen for Grade 60 rebars. The internal reinforcement was embedded (fully bonded) in the concrete section, and the plates were tied to the beam section. The beam was modeled as a simply supported structure, with a pinned and roller support condition on either end of the beam. To simulate a tandem loading condition, the model was analyzed under a displacement-controlled mode under two concentrated point loads (i.e., four-point bending), 1.37 m (4.5 ft) apart.

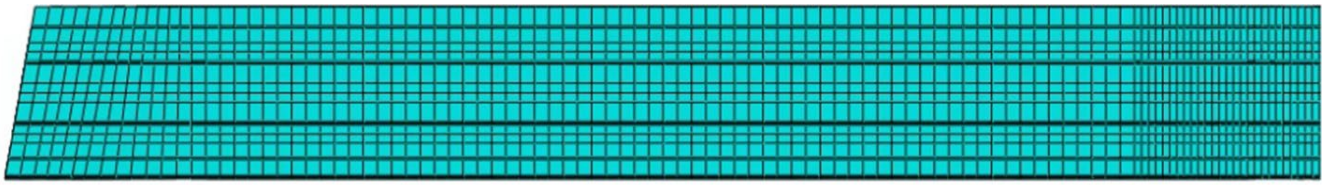

A. Partial plan view of the concrete beam

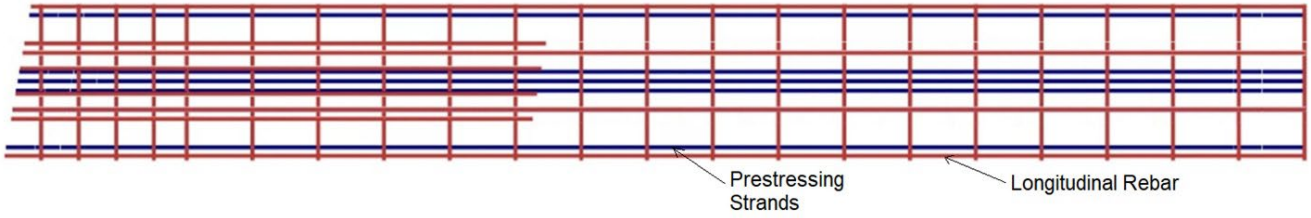

B. Partial plan view of the internal reinforcement

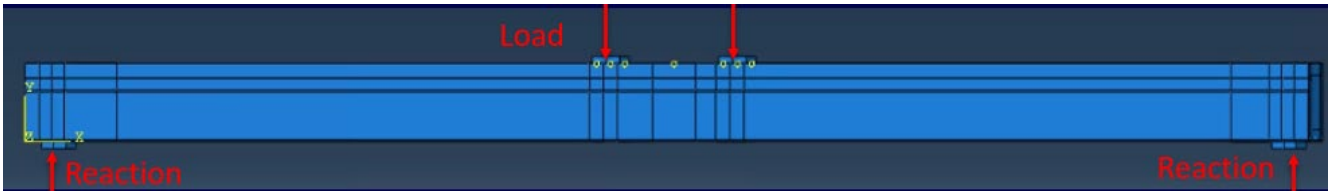

C. Elevation view of the four-point loading setup

Figure 4. Rendered View. 33 × 36 (G1) beam in ABAQUS simulation.

The numerical load-deflection behavior of the G1 specimen under a four-point loading setup is shown in Figure 5. The behavior of the G1 beam was elastic up to the cracking load of 186.5 kN (41.9 kips) at a deflection of 9.1 mm (0.36 in.). As the load increased and the nonlinear behavior of the beam set in, tensile cracks started at the extreme tensile fiber at the bottom of the beam and continued to propagate through the bottom flange until the peak load of 298.7 kN (67.14 kips) was reached at a deflection of 18.2 mm (0.72 in.). A significant drop in the load carried by the beam was observed as the crack propagated through the bottom flange and into webs. This can be attributed to the change in flexural rigidity as the bottom flange was completely cracked. During the post-peak region, the load-bearing capacity of the beam increased gradually until reaching 266.89 kN (60.0 kips) before failure. At failure, the concrete under the loading plates began to crush, and the prestressing strands

reached a stress of 1703 MPa (246.99 ksi, 91.4% of the strand's ultimate strength). The nominal live load capacity (246.5 kN, 55.4 kips) calculated using AASHTO load specifications for a four-point load, excluding the dead load effect of the beam, showed good agreement with the finite element (FE) analysis post-peak behavior.

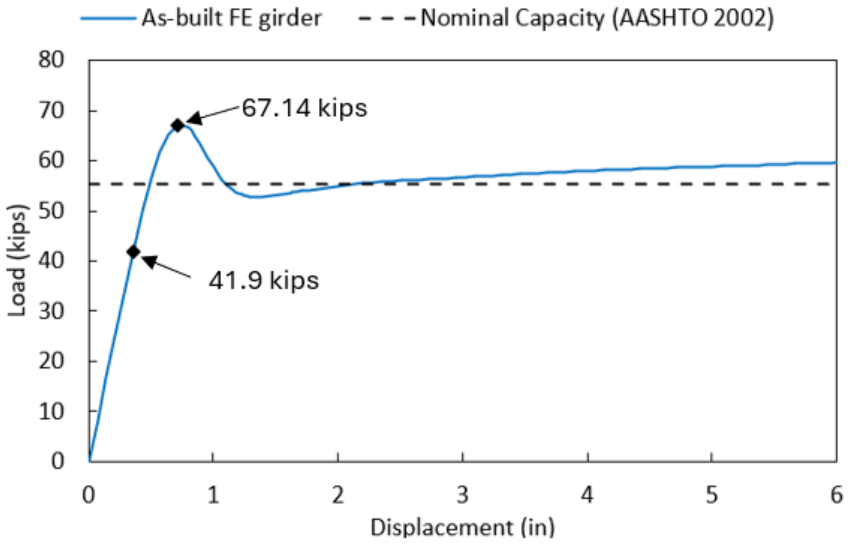

Figure 5. Graph. Load-displacement behavior of the as-built beam.

EXPERIMENTAL FOUR-POINT BENDING TEST

Test Setup

Figures 6-A and 6-B present the schematic plan view and a side elevation photo of the four-point loading setup used to evaluate the damaged PPC beam. Two L-shaped concrete blocks were used on either end to support the beam. The roller and pinned supports were placed at either end of the beam with a clear spacing of 13.4 m (43.78 ft). The four-point load was applied using two plates with a skew angle of 10° and placed 1.37 m (4.5 ft) apart to simulate a tandem load. A spreader beam was used to distribute the load from the actuator to the plates. At midspan, two spring potentiometers and a linear variable differential transformer (LVDT) were placed to measure the deflection of the beam. A displacement-controlled load was applied at a rate of 1 mm/min (0.0394 in./min), and the rate was later doubled once the response of the beam plateaued.

Figure 6-C illustrates the 20 strain gauges attached to the exterior side (denoted by the small dark rectangles) near each crack's top and bottom ends and between a few individual cracks near the bottom. Figure 3-E shows strain gauge S21, the only gauge mounted on the bottom surface across crack C6. The strain gauges mounted across the cracks were used to enable the monitoring of the changes in the crack widths during the test, while the strain gauges placed between the cracks, near the bottom, allowed for monitoring stress redistribution as the cracks propagated.

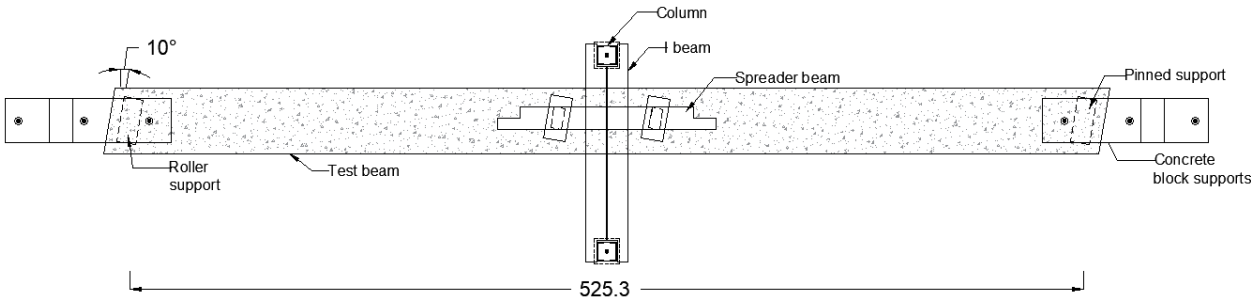

A. Plan view

B. Side elevation view

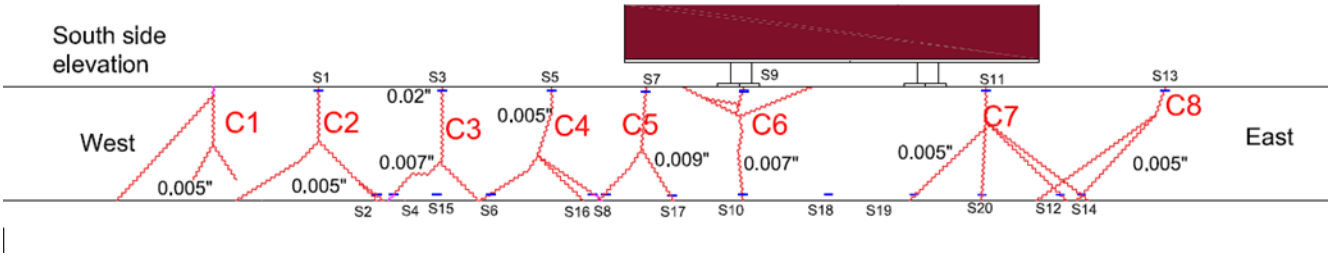

C. Strain gauge locations

Figure 6. Illustration and photo. Four-point bending test setup of G1 beam.

Results and Discussion

Figure 7 shows the load-deflection response of the tested PPC beam under four-point bending. The blue and black curves represent the load-deflection responses from the numerical analysis and the experimental test, respectively. During the experimental test, the damaged PPC beam exhibited linear behavior until reaching a load of 133.3 kN (30 kips) at midspan deflection of 6.25 mm (0.26 in.). At the end of its elastic range, the behavior of the damaged beam differed markedly from the FE analysis predictions for the as-built beam. The damaged beam did not exhibit the analytically predicted peak load and the subsequent drop in capacity. Still, it exhibited the predicted behavior

after the crack had propagated through the bottom flange (soffit slab). This discrepancy can likely be attributed to crack C6 in the damaged beam, which had propagated beyond the bottom flange.

As the beam's behavior became nonlinear, crack C6 opened, and multiple new cracks began to form. Each dip in the experimental load-deflection curve could be attributed to the opening of a new crack, the propagation of an existing crack, and the stress redistribution that might have occurred. The load steadily increased to 263.5 kN (59.2 kips) at a deflection of 93.75 mm (3.67 in.), at which point the beam experienced complete failure.

Along the load-deflection curve, three distinct limit states (capacities) were identified: elastic limit capacity (113.4 kN, 30 kips); theoretical yield capacity (223.3 kN, 50.2 kips); and residual (ultimate) capacity (263.5 kN, 59.2 kips). The elastic limit capacity was identified at the end of the elastic response of the damaged beam. The theoretical yield capacity was located at the intersection of the tangential lines (stiffness) from the elastic and post-yield stages, assuming an idealized bilinear behavior for the damaged specimen. The residual capacity was the capacity of the beam at failure. The elastic limit capacity and the theoretical yield capacity showed 45.9% and 9.4% reduction, respectively, while the residual capacity showed a 6.9% increase compared to the AASHTO nominal load capacity of 246.5 kN (55.4 kips). Furthermore, the damaged beam's residual capacity (263.5kN, 59.2 kips) was 13.4% lower than the capacity predicted from the FE analysis of the as-built beam (298.7kN, 67.14 kips).

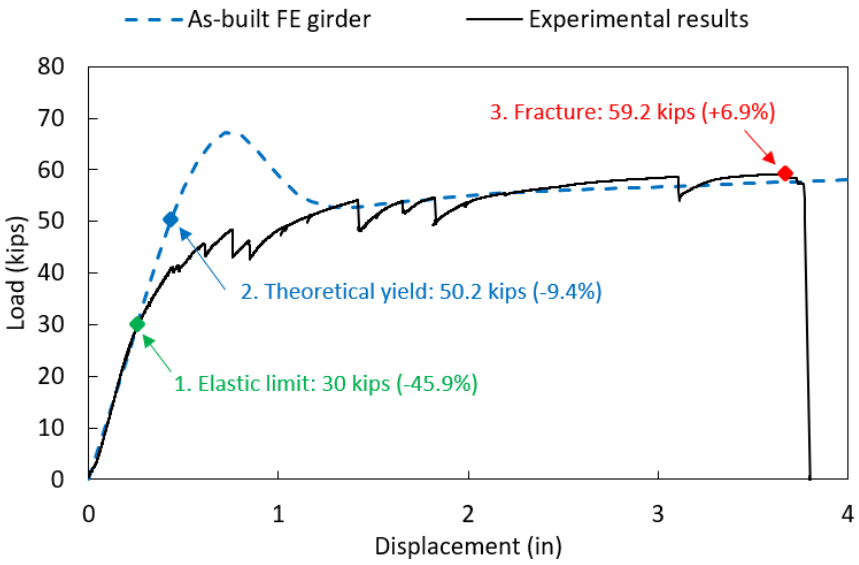

Figure 7. Graph. Load-displacement behavior of the damaged G1 beam.

The close-up photos of the tested PPC beam in Figure 8 indicate that its behavior was predominantly flexural. This resulted in a failure due to the crushing of the midspan top concrete fibers and the simultaneous fracture of the prestressing strands at crack C6. At the failure point, the concrete at the top was crushed, and the compression steel exhibited signs of yielding. Notably, the beam did not fail at the midspan location because of the presence of the middle diaphragm.

Comparing the numerical (undamaged) behavior with the experimental (damaged) behavior reveals that the cracked beam exhibited less peak strength and earlier signs of nonlinear response than the as-built beam. This reduction in performance can be attributed to the loss of the beam's section due to in-service cracking. Although the prestressing strands were still intact before testing, and the prestressing force was not fully compromised, the cracked beam showed a considerably softer (more flexible) response compared to the uncracked beams, especially during the pre-yielding stage. The built-up stress in the strands due to cracking resulted in the early yielding of the prestressing strands and reinforcing bars, causing the cracked beam to exhibit early signs of nonlinear response at a lower load than the uncracked beam. Considering the AASHTO nominal load capacity (Figure 5) of 246.5 kN (55.4 kips), an uncracked beam would sustain almost no damage, remaining elastic under this load. A cracked beam, however, would experience considerable deflection of 55.6 mm (2.19 in.) and inelastic deformation (damage). This finding was essential for evaluating the damaged beam's live load capacity and load rating analysis presented in Chapter 4.

Figure 8. Photo. Failed G1 beam specimen.

ANALYSIS OF DAMAGED PPC DECK BEAM

One of the major challenges in analyzing a damaged beam is determining the built-up stresses caused by the presence of a crack. Cracking can significantly increase the stress in the prestressing strands, leading to additional stress accumulation in the compression zone at the top of the beam. In this study, finite element analysis was conducted to predict the elastic capacity of damaged beams and evaluate the built-up strand stress in the prestressing strands.

Numerical Analysis of Damaged Beam

A numerical model simulating the behavior of the damaged beam specimen was built in ABAQUS to predict the behavior of the damaged beam specimen. This model was used to understand the behavior of the damaged beam and to determine the built-up stresses in the stands and the beam section due to a transverse crack. The beam was initially loaded in the model to introduce a transverse crack near the middle diaphragm, like in the tested specimen. The cracked beam was then loaded using four-point loading to simulate the experimental test conditions. The behavior of the cracked beam under the four-point bending test was used to validate the finite element model.

Model Description

The FE model for the G1 beam was developed using the existing bridge plans. The beam was modeled as a simply supported beam with a pinned and roller support condition on either end of the beam. The beam cross-section, loading, and support plates were modeled using the 3D solid elements (C3D8) with eight integration points, and the internal reinforcements (strands and rebars) were modeled using 3D truss elements (T3D2) with two nodes. The concrete damaged plasticity model was used in ABAQUS to model the concrete material behavior. The stress-strain behavior of concrete and prestressing strands was modeled using the Hognestad (1951) and Menegotto-Pinto models (1973), respectively, while a bilinear model was adopted for the rebars. The internal reinforcement was embedded (fully bonded) in the concrete section, and the support and loading plates were tied to the beam section.

Concrete-Strand Bond Model

To capture the interaction between the prestressing strands and the surrounding concrete, two bond conditions were considered at the beam concrete-strand interface: a perfect bond condition and a bond-slip model. In the perfect bond condition, the embedded constraint in ABAQUS (2022) was used to enforce full bonding between the prestressing strand and the surrounding concrete nodes. This constraint ensured a perfect bond between the concrete beam and strand elements. This method would result in upper bound limits for the built-up strand stresses as it neglects the bond-slip in the strands at the cracks. The nonlinear spring ("SPRING2" in ABAQUS) was used to model the bond-slip condition in the second case. SPRING2 allows the user to define the force-displacement behavior between two nodes in the model (ABAQUS 2022).

The bond strength between strands and concrete depends on mechanical interlock, adhesion, and friction (Janney 1954; Hanson and Kaar 1959). Mechanical interlock between the concrete and the strand wires, adhesion (chemical bond) between the strands and the concrete, and the frictional resistance to the interfacial movement between the strands and concrete contribute to the bond strength of the strands. Adhesion in the concrete-strand interface is negligible. Hence, friction and mechanical interlock are the predominant contributors to the strength of the concrete-strand bond. The friction and the mechanical interlock create radial compressive stresses that allow force transfer between the prestressing strand and the concrete. Thus, the bond stress between the seven-wire prestressing strand and concrete increases linearly up to the debonding limit, beyond which it remains constant or increases marginally with slip. This differs from a plain wire's bond-slip behavior, which decreases drastically beyond the debonding limit. The additional bond strength of the seven-wire strands is attributed to the mechanical interlock between the strand and the surrounding concrete (Uijl 1998; Steensels et al. 2017).

The bond-slip model was used to evaluate the influence of prestressing strand bond strength on beam behavior and state of stresses at the crack. Historically, pull-out tests have been used to quantify the bond characteristics of prestressing strands embedded in concrete. Since Dinsmore et al. (1958) conducted a pull-out test on an 11.1 mm (7/16 in.) diameter strand, pull-out tests have been widely used to identify the bond strength between the strands and concrete. Later, Moustafa (1974) performed pull-out tests on specimens with an embedded strand length of 305 mm (12 in.) to 762 mm (30 in.) for different strand diameters. The pull-out test method established in Moustafa (1974)

was adopted with a modified embedded strand length of 457.2 mm (18 in.) and used by many researchers, including Rose and Russell (1996) and Logan (1997), to identify the bond strength of prestressing strands.

Several studies, including those by Stocker and Sozen (1969), Cousins et al. (1992), Logan (1997), Peterman (2009), and Loflin (2008), have demonstrated that the bond strength of prestressing strands depends on the concrete strength, strand diameter (surface area), and the strand surface condition. Variables like epoxy coating, grease, and corrosion significantly influence bond behavior. These researchers have recorded pull-out bond strengths for various strand diameters and grades. As presented in Table 1, the modified bond strengths for the various diameters of 1723.7 MPa (G250) and 1861.6 MPa (G270) grade strands were obtained using the results of the pull-out test from Stocker and Sozen (1969), Logan (1997), Peterman (2009), Loflin (2008), and Andrawes et al. (2009) for 34.5 MPa (5ksi) strength concrete.

In the pull-out test, force is averaged over the embedded length of the strand to calculate the average bond strength of the strand. Using data from Anderson et al. (1964), Andrawes et al. (2009) found that the maximum-to-average bond strength ratio was 2.1. Cousins et al. (1992) conducted a tensioned pull-out test to find the average bond strength while considering the effects of friction, the Hoyer effect, and the effects of adhesion and mechanical interlock. The ratio of average bond stress for tensioned to untensioned pull-out tests was 1.9 for uncoated 12.7 mm (0.5 in.) diameter strands. Andrawes et al. (2009) suggested a modification factor of 4.0 (~1.9*2.1) to account for the difference between the non-tensioned bond strength from the pull-out tests to the tensioned bond strength in a prestressed beam and the difference between the maximum and average bond strength observed over the embedded length of a pull-out specimen. The bond-slip model produced more realistic bond stresses at the crack.

Table 1. Modified Bond Strengths for Different Diameters

Strand Diameter	**G250**	**G270**
In.	ksi	ksi
7/16	0.78	0.85
0.5	0.79	1.03

Loading Sequence

Figure 9-A presents a schematic of the HS-20 wheel load setup used to introduce a transverse crack in beam G1 similar to the in-service crack C6. HS-20 wheel loads were applied in the initial step to crack. Figure 9-B presents the DamageT contour of the G1 beam, illustrating the formation of a crack similar to C6. The crack in the numerical model passed through the drain holes in the bottom. This showed that drain holes in high-moment regions could act as a nucleus for cracking.

Once cracked, the wheel loads were removed, and a four-point bending load was applied to understand the behavior of the damaged beam. The four-point loading plates were skewed at 10 degrees to match the test specimen's skew and minimize the beam's torsional response. The extent of damage was determined by comparing the numerical and experimental load-deflection behavior under four-point loading conditions.

Results and Discussion

Figure 10 presents the load-deflection behavior of the damaged beam (red curve) from numerical analysis. This response is compared with the blue curve, representing the numerical results for the as-built beam, and the black curve, which represents the experimental results of the four-point loading test on the damaged beam. The initial stiffness, peak, and post-peak behavior of the numerical results of the damaged beam under the four-point bending load resembles the experimental results of the damaged beam. This shows that the general global behavior of the damaged beam from the numerical analysis resembles that of the experimental beam. The response of the damaged beam under four-point loading was consistent with experimental results, confirming the validity of the numerical model. The built-up stresses in the prestressing strands and extreme concrete compression fiber were recorded and incorporated into load rating equations to assess the effect of transverse cracking on beam capacity and load rating. The difference in the elastic limit of the damaged beam in the numerical and experimental results was attributed to the extensive shear-torsional damage in the experimental beam. The numerical analyses only considered the effect of the transverse crack on the performance of the cracked beam.

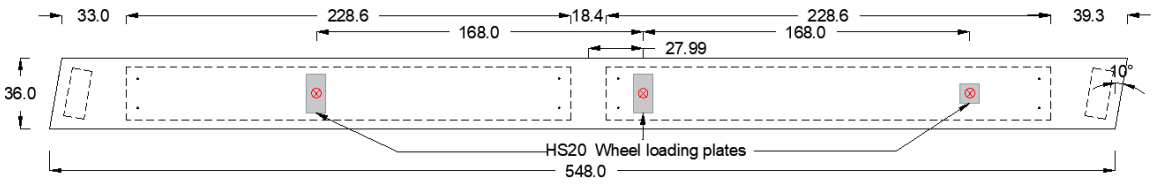

A. Plan view with HS-20 wheel loads

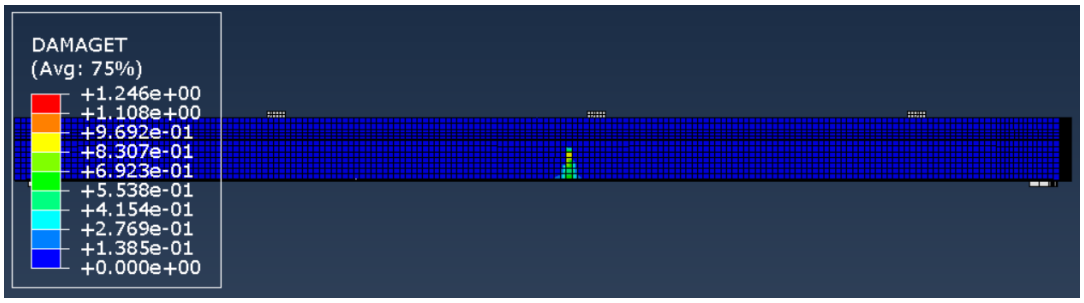

B. DamageT contour with the location of the crack

Figure 9. Illustration. Numerical model of the damaged G1 beam.

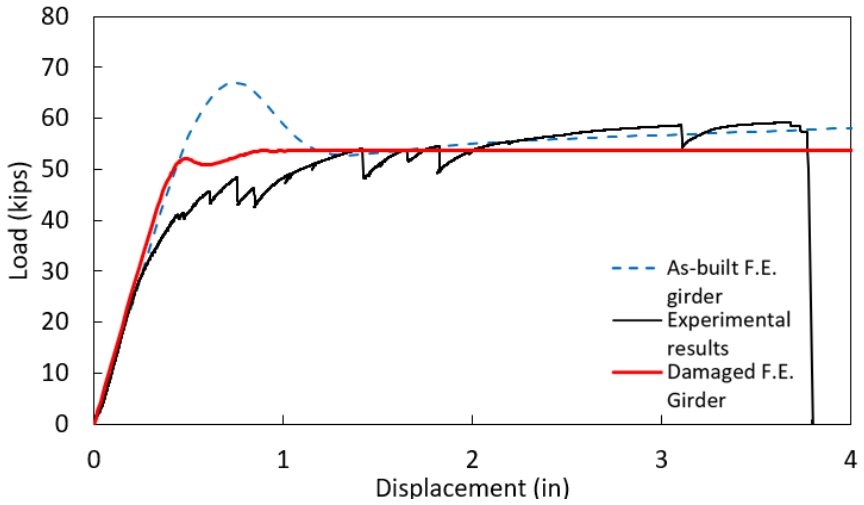

Figure 10. Graph. Load-deflection behavior of damaged and as-built G1 beams.

The difference in the load-deflection behavior and location of the transverse crack for both perfect bond and bond-slip cases was negligible. The notable differences between the two models were the crack width and the built-up stresses in the strands and the concrete beam.

Under gravity, the maximum built-up stress in the strands at the crack for the damaged beam with the perfect bond was 1425 MPa (206.8 ksi) compared to 1081.1 MPa (156.8 ksi) for the as-built beam for a crack width of 0.254 mm (0.01 in.). The strand showed a 31.9% increase in stress (~0.85 times the amount of stress yields) at the crack. The compressive stress in concrete increased from 1.17 MPa (0.17 ksi) in the as-built beam to 3.03 MPa (0.44 ksi) in the damaged beam. For the damaged beam with the bond-slip model, the crack width was slightly larger, measuring 0.305 mm (0.012 in.). In this case, the maximum built-up stress in the strands and concrete was 1258.29 MPa (182.5 ksi) and 2.83 MPa (0.41 ksi), respectively, representing a 16.4% increase in strand stress and a 139.4% increase in concrete compressive stress compared to the as-built beam.

The stresses predicted using the perfect bond case presented the upper limit of the built-up prestressing strand stress at the crack. This model did not account for bond-slip and the resulting reduction in strand stresses due to the bond deterioration between the concrete member and prestressing strands at the crack. Meanwhile, the bond-slip model captured the strand slip due to bond deterioration at the crack. Thus, the strand stress predicted using the bond-slip model was 11.7% lower than the perfect bond model. The capacities and strand stress obtained from the experimental testing, numerical modeling, and analytical equations were used in the load rating analysis of the G1 beam, as presented in Chapter 4.

CHAPTER 3: FLEXURAL TEST OF A 21 × 36 PPC DECK BEAM (CIRCULAR VOIDS)

The second PPC deck beam specimen tested in this study was 21 × 36, hereby named the G2 beam. It was extracted from a single-span bridge (bridge no. 042-3020) in Jersey County, Illinois. Figure 11-A presents a view of the single-span bridge, which was constructed in 1962 and demolished after nearly 60 years of service. The bridge had a total span of 15.24 m (50 ft) and a total width of 6.1 m (20 ft). The bridge cross-section had seven 21 × 36 PPC deck beams (Figure 11-B) connected via a dry-packed shear key and 25.4 mm (1.0 in.) transverse tie rods at one- and two-thirds of the span length. A bituminous material layer was present on the deck surface. As shown in Figure 11-C, the bridge exhibited signs of distress, including corrosion and water leakage caused by longitudinal cracks under the deck. One interior beam (G2) was extracted and tested at the University of Illinois' Newmark Structural Engineering Lab to assess the performance of cracked and repaired PPC deck beams.

A. View of the single-span bridge

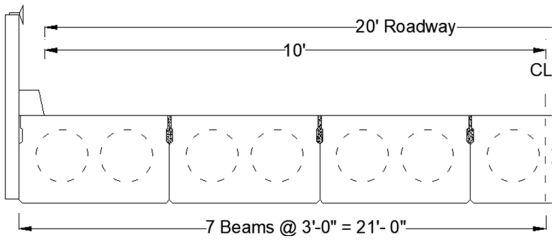

B. Bridge deck cross-section

C. Corrosion and water damage under the deck

Figure 11. Photo. Bridge no. 042-3020 in Jersey County.

As shown in Figure 12-A, the test specimen contained 26 G250 prestressing strands with a diameter of 11.11 mm (7/16 in.) and an eccentricity of 161.54 mm (6.36 in.). It had a design concrete compressive strength of 34.47 MPa (5 ksi). The beam had two circular voids with a diameter of 317.5 mm (12.5 in.) in its cross-section. In the place of stirrups, a #2/5 wire mesh with #2 bars spaced 76.2 mm vertically and 203.2 mm horizontally (3 in. × 8 in.) was provided at the top and sides of the beam, extending along its entire length. Figure 12-B shows the plan view of the G2 beam with two 203.2 mm (8 in.) wide diaphragms at one-third and two-thirds of the span length with 762 mm (30 in.) wide end diaphragms.

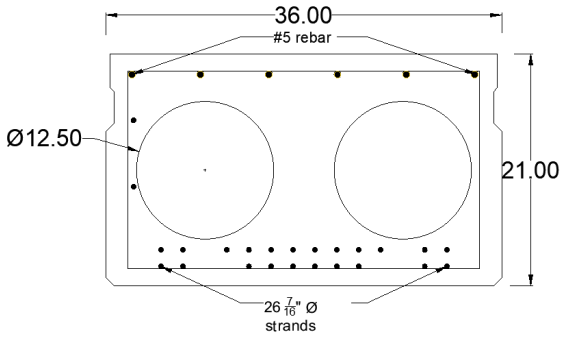

A. Cross-section

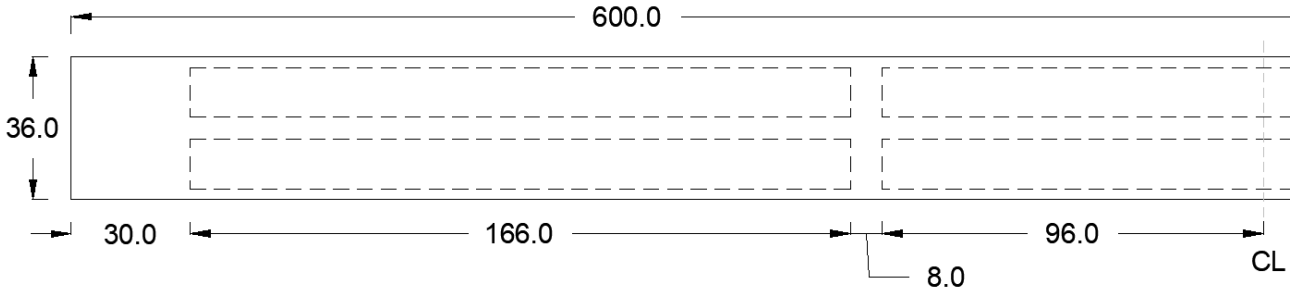

B. Partial plan view

Figure 12. Illustration. 21 × 36 (G2) PPC deck beam.

TEST SETUP

The G2 beam was subjected to a four-point bending load test. The test setup, depicted in Figures 13-A and 13-B, featured roller and pinned supports at either end of the beam, providing a clear span of 14.89 m (48.88 ft). A 489.3 kN (110 kip) capacity servo-controlled hydraulic actuator was used to apply the load, with the force and stroke clearance calculated according to AASHTO (2002) standard specifications. The load was applied using two loading plates with a center-to-center spacing of 1.2 m (4 ft), simulating the effect of a tandem load.

After placing the beam in the test setup, its surfaces were cleaned, and no visible cracks or damages were observed. Figure 13-C shows the layout of strain gauges on the surface of the G2 beam. A total of 18 strain gauges were installed: 5 gauges at the top to measure compressive strains and 13 at the

bottom to measure tensile strains. The gauges were placed within two loading plates to capture strains due to purely flexural cracks. One LVDT and two spring potentiometers were placed at midspan to measure the deflections of the beams under the applied load.

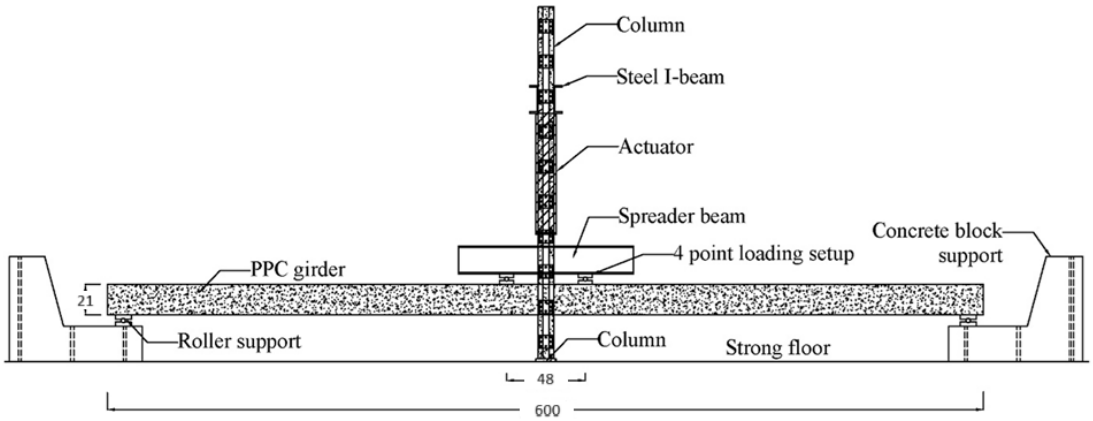

A. Side elevation view

B. Plan view

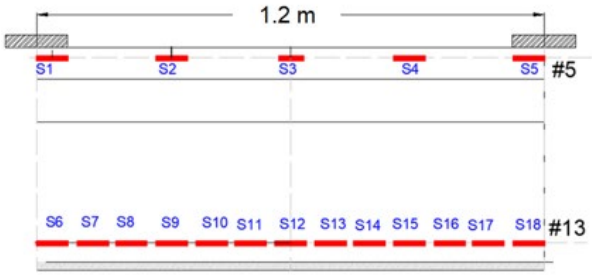

C. Strain gauge locations

Figure 13. Illustration and photo. Test setup and instrumentation of G2 beam.

INITIAL CRACKING LOAD STEPS

The G2 beam was initially loaded under a monotonic four-point bending load to induce transverse cracks. Based on the beam design specifications, the AASHTO nominal capacity of the beams was calculated to be 1040.4 kN-m (767.36 kip-ft), and the dead load moment was estimated to be 2434.7 kN-m (166.83 kip-ft). This results in a live load moment capacity of 814.22 kN-m (600.54 kip-ft), equivalent to a total four-point bending load of 239.23 kN (53.78 kips). The G2 beam was initially loaded at 3 mm/min (0.118 in./min) to 178.91 kN (40.22) to introduce transverse cracks. The initial applied load of 178.91 kN (40.22 kips) was 75% of the live load capacity, and this load step was named Load Step 1 (LS1).

Figure 14-A presents the load-deflection behavior (blue curve) of the G2 beam under LS1. The G2 beam had an initial uncracked stiffness of 37.1 kip/in., and the elastic limit (cracking load) was 88.96 kN (20 kips), after which the behavior became nonlinear due to the propagation of the transverse cracks through the depth of the bottom flange. After the initial change in stiffness at the elastic limit, the behavior of the beam remained elastic as the cracks continued to propagate through the depth. After the beam had reached the target load, the loading was stopped, and the beam was unloaded at a rate of 6 mm/min (0.236 in./min) to observe the residual crack widths and deflection at rest. Remarkably, no visible cracks remained, as all cracks had closed after unloading. This demonstrated the beam's high resilience, as it exhibited no visible signs of damage even despite being loaded to 75% of its live load capacity.

To induce cracks with measurable widths at rest, the specimen was reloaded in Load Step 2 (LS2) to 228.64 kN (51.4 kips), which was 95.5% of its live load capacity and 74.8% of its total nominal capacity. The loading rate for LS2 was 6 mm/min (0.236 in./min), and the unloading rate was 12 mm/min (0.472 in./min). Figure 14-B shows eight cracks between the loading plates at the peak load, and the maximum crack width was 0.381 mm (0.015 in.). When the beam was unloaded and at rest, four visible cracks measuring 0.127 mm (0.005 in.) were observed in the G2 beam. The behavior of the beam was still elastic under unloading, and the residual deflection in the beams was 12.7 mm (0.5 in.) for G2. In each load step, the slope of the unloading curve resembled that of the loading curve. The elastic unloading curve was attributed to the elastic recovery of the prestressing strands after the beam was unloaded.

Figure 14-A presents the compression strains recorded from gauge S3 during LS1 and LS2. In LS1, the maximum compression strain at peak load was 0.00073 in./in., with a residual strain of 0.00023 in./in. after unloading. In LS2, the S3 gauge recorded a peak strain of 0.00093 in./in., with a residual strain of 0.00027 in./in. after unloading. The maximum compressive strains in the concrete remained below 46.4% of the peak strain value (0.002 in./in.). If the estimated compressive dead load strain of 0.000097 in./in. were added to the recorded strains, the peak compressive strain would be 0.00103 in./in., which is 51.2% of the peak strain value. This would ensure that the compressive stress in the concrete remained below 60% of its strength when the beam was loaded to nearly 95% of its AASHTO live load capacity. The load-deflection behavior and recorded strains indicated that the concrete and prestressing strands continued to behave nearly elastically. The G2 beam was highly resilient and performed exceptionally well under the applied loads. Note that even after the G2 beam was loaded to 95.5% of its AASHTO load capacity, the widths of observable cracks in the soffit were only 0.127

mm (0.005 in.). It was remarkable that the materials in the beam behaved elastically even when the beam was loaded to 95.5% of its live load capacity.

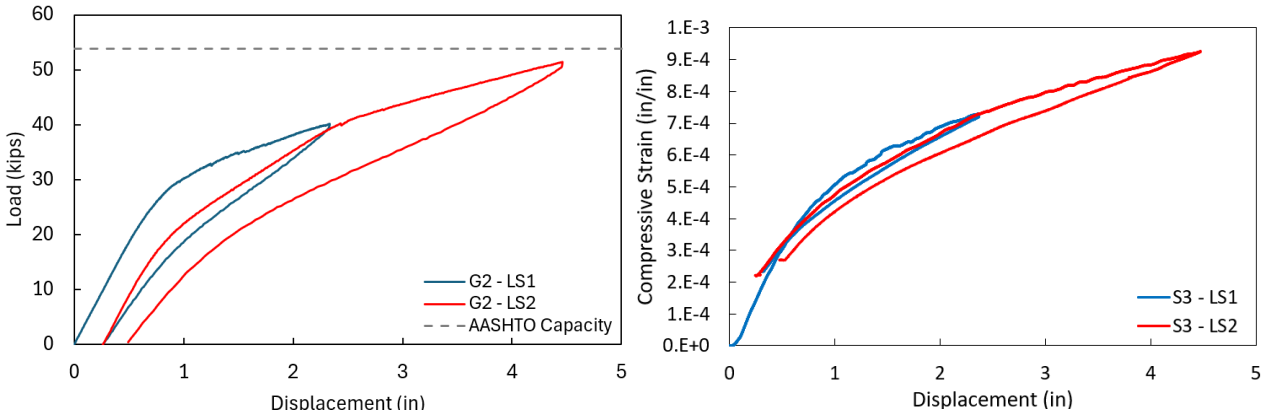

A. Load-displacement curves and compressive strains in gauge S3

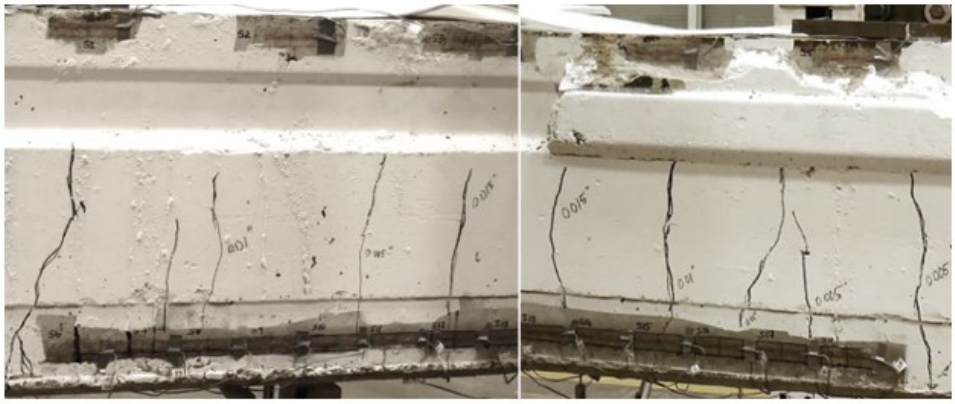

B. Crack propagation at the peak load of LS2

Figure 14. Graph and photo. Cracking load steps of G2 beam.

RESPONSE OF THE CRACKED SECTION: LOAD STEPS 3 AND 4

In the previous cracking load steps (LS1 and LS2), four transverse cracks of width 0.127 mm (0.005 in.) were introduced into the beam. To observe the impact of the transverse cracks on the stiffness, capacity, and behavior of the cracked section, the G2 beam was loaded to 338.06 kN (76 kips) at a rate of 12 mm/min (0.472 in./min) in Load Step 3 (LS3). Figure 15-A presents the load-deflection behavior of the G2 beam in LS3. The response of the G2 beam was linear until 57.83 kN (13 kips) at a deflection of 9.652 mm (0.38 in.). The design truck load (HS-15), including the impact (IM) and distribution factors (DF), was 60.45 kN (13.59 kips), and the observed elastic capacity was 4.3% lower than the HS-15 load requirement. Beyond the elastic limit, the stiffness of the G1 and G2 beam sections began to decrease as the crack opening reached the circular voids. The load-deflection response remained piecewise linear until 231.31 kN (52 kips). Beyond this point, the beam's behavior became nonlinear, and the rate of change in load relative to displacement decreased as the material

(concrete) entered its nonlinear stress-strain range. At 311.37 kN (70 kips), the slope of the load-deflection curve of the G2 specimen changed drastically and began to plateau as the prestressing strands started to yield. The response of the G2 beam plateaued, and LS3 was stopped at 340.51 kN (76.55 kips) at 400.81 mm (15.78 in.) as it reached the end of the actuator stroke length. The specimen was then unloaded at 24 mm/min (0.945 in./min) and had a residual deflection of 134.62 mm (5.30 in.). The maximum crack width (Figure 15-B) at rest was 1.905 mm (0.075 in.), well above any practical crack width limit.

The beam was loaded to failure in Load Step 4 (LS4) at a rate of 24 mm/min (0.945 in./min). The G2 specimen failed at a fracture load of 348.29 kN (78.3 kips) with a final displacement of 481.84 mm (18.97 in.). Figure 16-B presents photos of the failed specimen. The beam failed explosively in compression while the prestressing strands and the longitudinal rebar remained intact. This showed that the beam was over-reinforced, as it failed by compression rather than in tension due to strand fracture. The fracture load was 45.6% higher than the nominal live load capacity for the G2 beam.

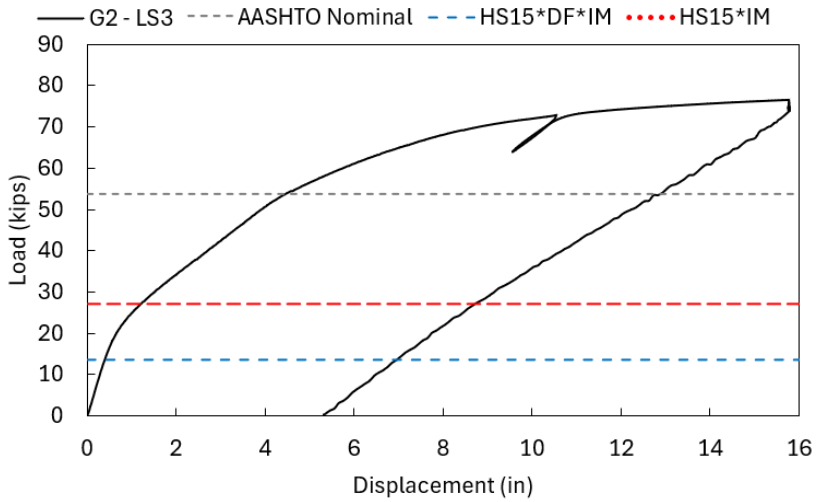

A. Load-displacement behavior of the G2 beam under LS3

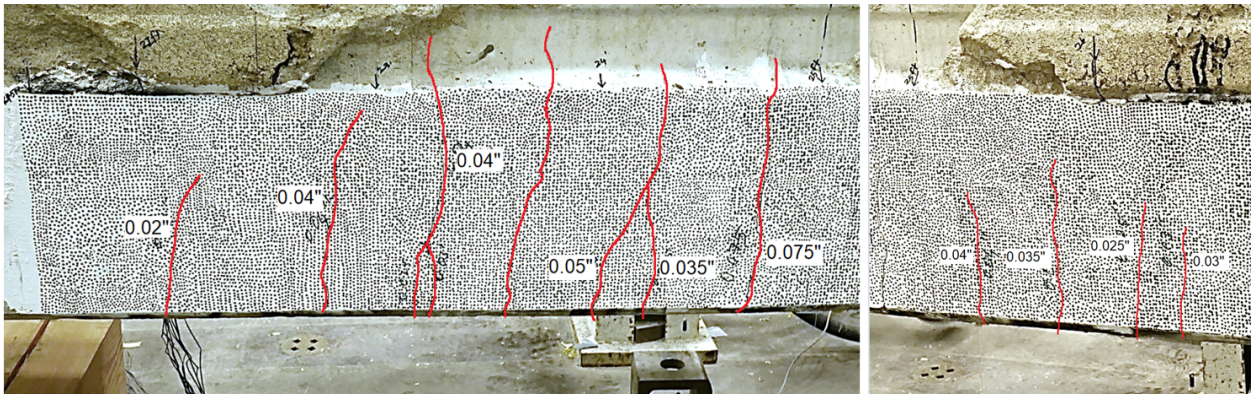

B. Crack propagation at the end of LS3

Figure 15. Graph and photo. Load step 3 of the G2 beam.

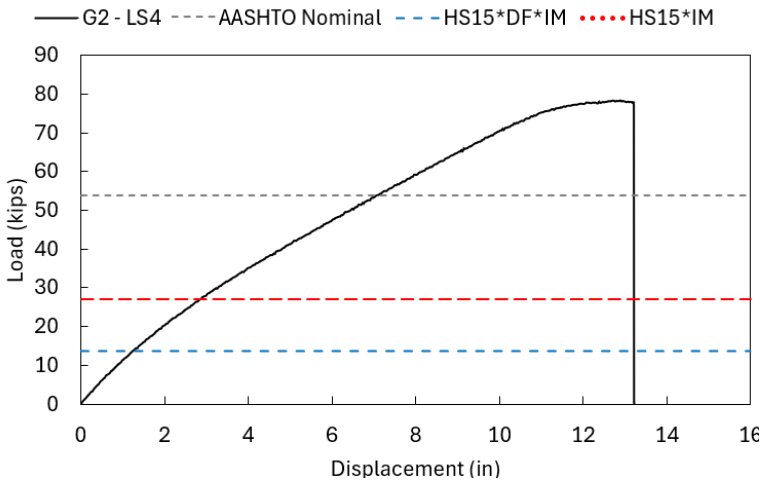

A. Load-deflection response in LS4

B. Failed specimen

Figure 16. Graph and photo. G2 in load step 4.

THEORETICAL CRACKED SECTION ANALYSIS

The theoretical cracked section analysis was conducted to better understand the behavior of the 21 × 36 PPC deck beam under applied loads. The theoretical analysis was based on the fiber section analysis. The analysis considered the effect of the cracked section on the section stresses and deflection. The material behavior of concrete was based on the stress-strain model by Karthik and Mander (2011), and the behavior of the prestressing strands and the longitudinal rebars was assumed to be bilinear. The theoretical calculation of load-deflection behavior was based on the elastic analysis of the cracked section. The residual permanent plastic strain in concrete was accounted for as the beam was unloaded at the end of each load step, and the built-up residual plastic strain was considered in the next step. This resulted in a permanent change in the strains at the end of each load step after cracking.

The cross-section of the G2 beam was divided into 21 fibers, each measuring 25.4 mm (1 in.) in depth. For a given compressive strain at the top, the strain distribution across the cross-section depth was calculated using the assumed neutral axis depth. The average stress in a concrete fiber element and

the corresponding force in the element were calculated by multiplying the average stress by the area of the fiber element. The net compressive and tensile forces in the concrete member were obtained from the sum of the forces in each fiber element. In the G2 beam, the prestressing strands were provided in four layers: 12 strands at 44.45 mm (1.75 in.), 10 strands at 82.55 mm (3.25 in.), 2 strands at 228.6 mm (9 in.) and 304.8 mm (12 in.). The strain, stress, and forces were calculated at the centroid of each prestressing strand layer, and the net tensile force in the prestressing strands was obtained. Similarly, the strain, stress, and force at the centroid of the compression reinforcement were calculated. The neutral axis depth was iterated until the forces in the section were in equilibrium. The net moment in the section was calculated by considering the moments from the concrete beam, the prestressing strands, and the longitudinal rebars about the center of the cross-section. The corresponding four-point bending load was determined based on net moment. The displacement of the beam under the applied loads was computed considering the forces acting on the section (applied prestress, self-weight of the beam, and four-point bending load) and the cracked flexural rigidity. Figure 17 presents the equation for the equivalent flexural rigidity of the section proposed by Branson (1968).

$$I_e = I_{cr} + \left(\frac{M_{cr}}{M_a}\right)^3 \left(I_g - I_{cr}\right) \leq I_g$$

Figure 17. Equation. Equivalent flexural rigidity.

where I_{cr} and I_g are the moments of inertia of the cracked and uncracked sections, and M_{cr} and M_a are the cracking and applied moments in the section. This equation accounted for the change in the second moment of the area due to crack propagation. The results using the equivalent moment of inertia were of sufficient accuracy for the section.

Assumptions

The following assumptions were made in the theoretical analysis of the cracked section:

- Plane sections remain plane after bending (i.e., the strain distribution across the section depth remains linear after cracking).
- A perfect bond was assumed between the concrete and the prestressing strands and between the concrete and the longitudinal rebars.
- The materials' behavior follows the assumed stress-strain models.
- The difference in strength between the core and cover due to the confining effect of the stirrups is ignored in the linear analysis.
- The moment of inertia of the cracked section follows the effective moment of inertia equation by Branson (1974).
- The strains across the width of the section were assumed to be uniform.

Load-Deflection Response of the 21 × 36 (G2) Beam

The load-deflection response of the 21 × 36 PPC deck beam, predicted using the theoretical analysis, is presented in Figure 18-A. The solid line represents the theoretical predictions, while the dashed line represents the experimental results from LS1. The initial cracking point from the experimental curve was used to predict the concrete strength and the stress in the prestressing strands after losses. The concrete strength and the stress in the prestressing strands after losses were modified until the theoretical results for the initial cracking load and deflection in LS1 were coincidental with the experimental results. There was very good agreement between the load-deflection curves from the experimental analysis and theoretical predictions.

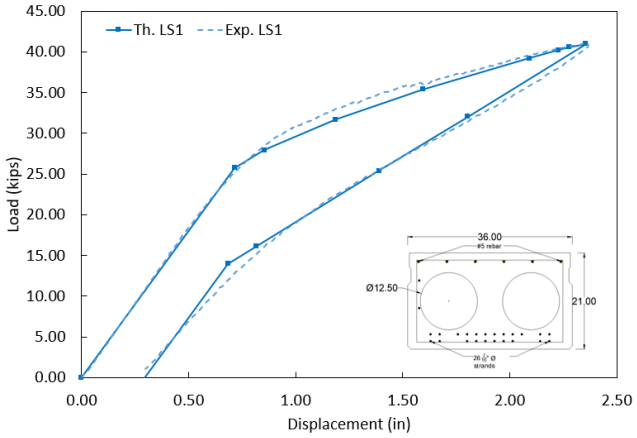

A. Load-deflection response for LS1

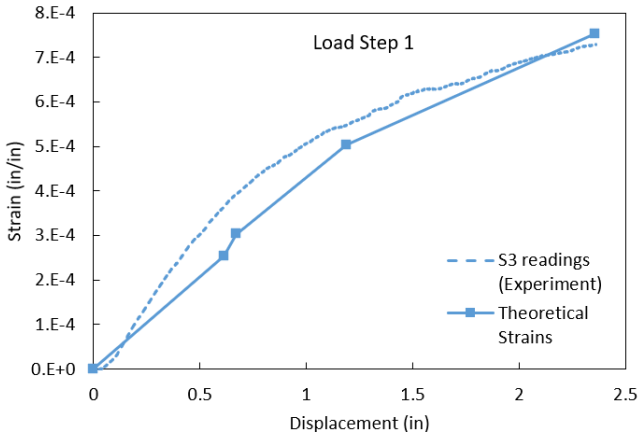

B. Compressive strains at the top of the beam

Figure 18. Graph. 21 × 36 beam: theoretical predictions for G2 beam in load step 1.

Figure 18-B presents the predicted concrete compressive strains at the top of the beam, obtained from the theoretical calculations, and compares them to strain readings from gauge S3 during experimental testing. The results for the loading curve in LS1 demonstrate a very strong correlation between the experimental results and the theoretical predictions of the compressive strain in the

concrete at midspan. Because the analysis assumed a perfect bond between the concrete and prestressing strands, the predicted strains and corresponding stresses in the prestressing strands were expected to be higher than those in the experimental beam.

Figures 19-A and 19-B present the theoretical predictions compared to the experimental results of the 21 × 36 beam under LS2 and LS3, respectively. Again, the theoretical predictions closely matched the experimental data.

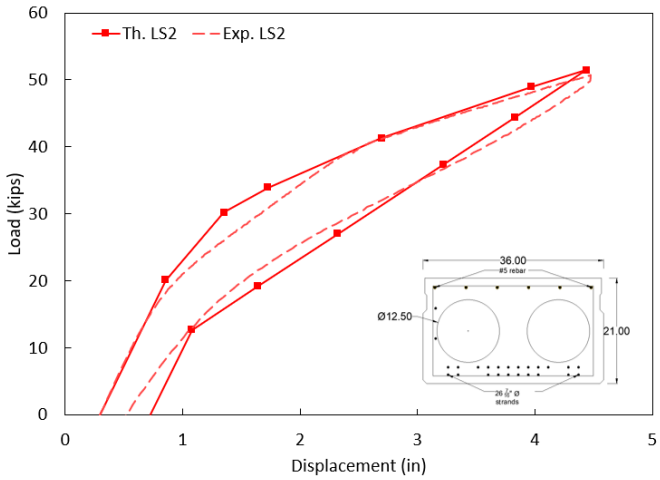

A. Load-deflection response for LS2

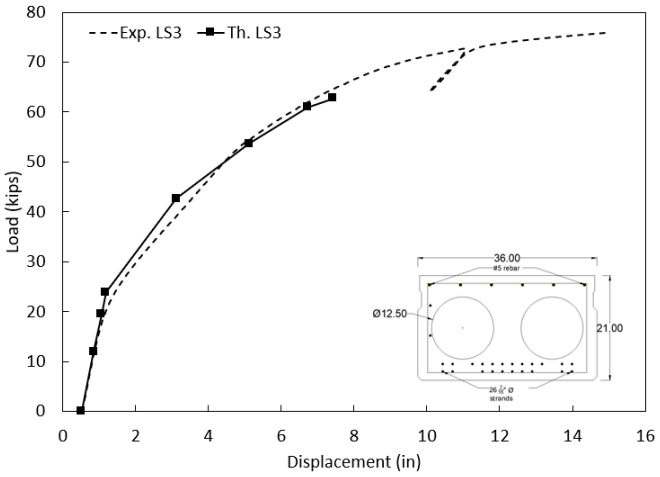

B. Load-deflection response for LS3

Figure 19. Graph. 21 × 36 beam: theoretical predictions for G2 beam in load steps 2 and 3.

For LS3, the elastic capacity predicted by the theoretical analysis was 59.65 kN (13.41 kips). The elastic limit value for the G2 beam was 2.3% higher than the experimental value, which was within the acceptable accuracy limits. At the beginning of LS3, the beam was damaged due to an applied load that was 95.5% of its AASHTO nominal live load capacity. Thus, the elastic capacity observed in LS3 reflected the damaged condition of the beam after this high-load exposure. When the cracked

beam was loaded beyond its elastic limit, it exhibited nonlinear behavior and had excessive deformation, which is undesirable under service loads. When the beam was unloaded beyond its elastic limit, it would accumulate plastic strains in the compressive zone of the concrete member. This is undesirable, as it would imply that the cracked beam accumulates plastic strains, and its performance may deteriorate. Hence, the elastic capacity of the beam was chosen as the limiting capacity, beyond which the beam must not be loaded.

CHAPTER 4: LOAD RATING ANALYSIS OF TEST SPECIMENS

This section discusses the load rating analysis of the tested beams based on the experimental results. The load rating analysis was conducted following the AASHTO *Manual for Bridge Evaluation* (*MBE*) guidelines (AASHTO 2018). The load rating procedures in AASHTO's *MBE* are based on the fundamental principle of determining the maximum vehicular live load that can be safely applied to a bridge without causing structural damage. The AASHTO *MBE* recommends using two rating levels for highway bridges: inventory and operating. The inventory rating level provides a live load allowed on the bridge at the current bridge and material condition indefinitely, while the operating rating results in the maximum allowable live load.

According to AASHTO's *MBE* (2018), the capacity-based load rating factor using the Load Factor Rating (LFR) method at the inventory and operating levels is determined using the following equations in Figure 20:

$$RF_{inventory\_Strength} = \frac{C - 1.3D}{2.17L(1+I)}$$

$$RF_{operating\_Strength} = \frac{C - 1.3D}{1.3L(1+I)}$$

Figure 20. Equation. Capacity-based rating equations.

where, for the tested beam, *C* is the nominal (flexural) strength of the section, *D* is the unfactored dead load moment considering the self-weight of the beam, *L* is the unfactored live load moment considering the design truck loading (HS-20 and HS-15 for G1 and G2, respectively), and *I* is the impact factor. Since the bridges from which the G1 and G2 beams were extracted were designed according to the AASHTO *Standard Specifications for Highway Bridges*, the live load distribution factor and the impact factor used in the load rating analysis in this section were computed as per the AASHTO standard specifications (AASHTO 2002).

Furthermore, to satisfy serviceability limit states, the AASHTO *MBE* specifies that the load rating factors for concrete tension, concrete compression, and prestressing steel tension at the inventory and operating levels can be calculated based on the following equations in Figure 21:

$$RF_{inventory\_Concrete\ Tension} = \frac{6\sqrt{f'_c} - (F_d + F_p + F_s)}{F_l}$$

$$RF_{inventory\_Concrete\ Compression} = \frac{0.6f'_c - (F_d + F_p + F_s)}{F_l}$$

$$RF_{inventory\_Concrete\ Compression} = \frac{0.4f'_c - 0.5(F_d + F_p + F_s)}{F_l}$$

$$RF_{inventory\_Prestress\ Steel\ Tension} = \frac{0.8f_y^* - (F_d + F_p + F_s)}{F_l}$$

$$RF_{operating\_Prestress\ Steel\ Tension} = \frac{0.9f_y^* - (F_d + F_p + F_s)}{F_l}$$

Figure 21. Equation. Serviceability-based rating equations.

where f'_c is the concrete compressive strength, f^*_y is the prestressing steel yield stress, F_d is the unfactored dead load stress considering the self-weight of the beam, F_l is the unfactored live load stress including impact by considering the design truck loading, F_p is the unfactored stress due to prestress force after all losses, and F_s is the unfactored stress due to secondary prestress force, which was taken as zero in this case.

LOAD RATING ANALYSIS OF THE AS-BUILT 33 × 36 BEAMS

In this study, the load rating of the as-built beam was used as a baseline measure to understand the influence of damage on the bridge load rating. In the as-built beam, the stress contributions from the dead, live, and effective prestressing forces were calculated based on the general stress relations for prestressed members (Nawy 2009). To establish a reference point for the load rating analysis of the beams tested experimentally, the first step was to compute the load rating factors of the as-built (undamaged) beam using the conventional analytical approach. The nominal sectional moment capacity of the as-built PPC deck beam was calculated following the LFD method from the AASHTO *Standard Specifications for Highway Bridges*. This nominal capacity was computed considering prestress losses due to shrinkage and creep of concrete and stress relaxation of prestressing strands (AASHTO 2002). The non-prestressing steel in tension and compression at the top flange were also considered in the calculation.

For the 33 × 36 (G1) PPC deck beam, the nominal capacity of the beam was calculated to be 976.9 kN-m (720.5 kip-ft), the unfactored dead load moment was 243.6 kN-m (179.7 kip-ft), and the unfactored live load moment due to HS-20 truck load considering the distribution factor (0.508) and the impact factor (1.29) was 245.43 kN-m (181.02 kip-ft). Using the calculated moments and the calculated stresses in concrete and prestressing strands for the as-built beam, the inventory and operating rating factors were 1.23 and 2.05, respectively. Table 2 summarizes the load rating factors for both the as-built and damaged 33 × 36 PPC deck beam.

LOAD RATING OF THE CRACKED 33 × 36 (G1) BEAM

The load rating analysis of the cracked 33 × 36 PPC deck beam was conducted using the experimental and numerical analysis results, and the resultant load ratings are presented in the following section. Using the experimental results, the capacity-based load rating factors were derived for the tested specimen, and the corresponding serviceability ratings for the test specimen were derived using the analytical crack width models. The finite element analyses results for component stresses and overall capacity were used to calculate both the capacity-based and serviceability-based load rating factors for the cracked 33 × 36 beam.

Capacity-Based Load Factors from Experimental Results

The experimental-based rating factors (RFs) were computed using the load-deflection relationship presented in Figure 7. Figure 22 presents the moment-displacement relationship derived from the experimental and as-built finite element load-deflection curves (Figure 7). Note that the moments shown in Figure 22 exclude the moment due to the self-weight of the beam. The elastic limit capacity (398.3 kN-m, 293.8 kip-ft) ensured the bridge remained in the elastic range under the design live load. To maintain an operating/inventory level ratio of 1.67, as specified in the AASHTO *MBE*, the operating level moment (409.86 kN-m, 302.3 kip-ft) was computed by multiplying the moment corresponding to the HS-20 truck by 1.67. This calculation resulted in an inventory and operating rating factor of 1.0 and 1.67, respectively. Although the inventory level moment corresponding to the HS-20 rating truck fell below the elastic limit capacity, the operating level moment exceeded the elastic limit of 398.3 kN-m (293.8 kip-ft). This indicated that the beam, in the cracked condition, could not withstand the operating level moment without experiencing permanent damage. Thus, the maximum unfactored operating moment was limited to 398.3 kN-m (293.8 kip-ft) to ensure elastic behavior.

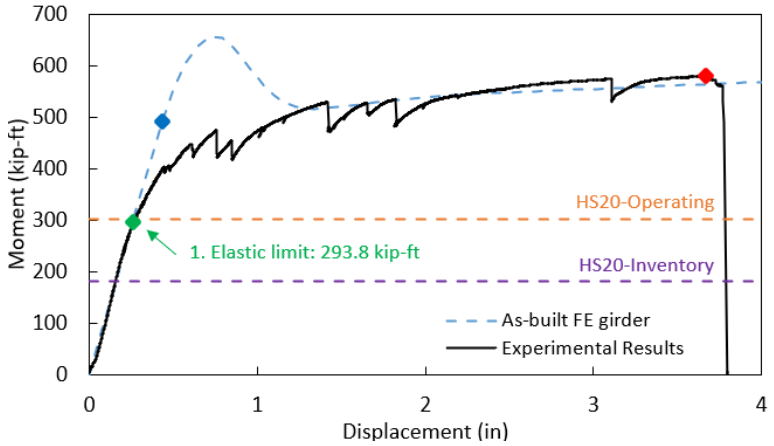

Figure 22. Graph. Moment-displacement behavior of the 33 × 36 beam.

For an operating level moment of 398.3 kN-m (293.8 kip-ft), using the capacity-based operating equation in Figure 20, the ultimate load rating capacity was found to be 517.8 kN-m (381.9 kip-ft), which was 34.2% lower than the experimental residual capacity of the cracked section. Accounting for this reduction in capacity in the load rating analysis was essential, as it reflected the additional flexibility of the beam due to cracking. Using the new reduced load rating capacity (517.8 kN-m, 381.9 kip-ft) in the capacity-based rating equations in Figure 20, along with the HS-20 live load moment, the capacity-based inventory and operating rating factors (Table 2) were computed as 0.96 and 1.60, respectively. For the experimental capacity-based rating, the coefficient for the unfactored dead load moment was taken as 1.0 instead of 1.3, as it was possible to predict dead load moment with sufficient accuracy. Thus, based on the reduced capacity, the cracked beam's inventory and operating rating factors were reduced by 22% compared to the as-built beam. This significant reduction in capacity led to a corresponding reduction in the capacity-based load ratings, which, in turn, imposed restrictions on the allowable vehicular loads on the bridge. As a result, it may be necessary to close or restrict the lane containing the cracked beam to heavy axle loads while still permitting lighter traffic.

Routine monitoring is required to ensure existing cracks do not widen or propagate and that no new cracks develop.

Table 2. Rating Factors Based on AASHTO *MBE* for the 33 × 36 (G1) Beam in the As-Built and Cracked Conditions

Load Rating Category	As Built	Damaged Beam: Experimental Results	Damaged Beam: FEM Perfect Bond	Damaged Beam: FEM—(Bond-Slip)
Inventory Rating—Capacity	1.23	0.96	0.96 < 1	0.96 < 1
Inventory Rating—Concrete Tension	1.72	–	–	–
Inventory Rating—Concrete Compression	6.32	5.73	2.05	5.62
Inventory Rating—Concrete Compression	4.29	3.70	1.4	3.90
Inventory Rating—Prestressing Steel Tension	12.59	–	< 0 (−3.64)	3.50
Operating Rating—Capacity	2.05	1.60	1.6	1.6
Operating Rating—Prestressing Steel Tension	20.48	–	3.5	10.65

Capacity and Serviceability Load Factors from Finite Element Analysis

The strand stresses predicted using the analytical crack width models were highly sensitive to the variations in crack width. Therefore, finite element models of the cracked 33 × 36 beams were developed and analyzed to predict the strand stress at the crack width using two methods: (1) perfect bond case (using embedded conditions), and (2) bond-slip methods (using nonlinear springs).

In the finite element analysis, under self-weight, the maximum built-up stress in the strands at the crack for the damaged beam with the perfect bond was 1425.8 MPa (206.8 ksi), compared to 1081.1 MPa (156.8 ksi) for the as-built beam at a crack width of 0.25 mm (0.01 in.). This represents a 31.9% increase in strand stress (~0.85 times the amount of stress yield) at the crack. The compressive stress in concrete increased from 1.2 MPa (0.17 ksi) in the as-built beam to 3.0 MPa (0.44 ksi) in the damaged beam. For the damaged beam with the bond-slip model, at a crack width of 0.3 mm (0.012 in.), the maximum built-up stress in the strands was 1258.3 MPa (182.5 ksi), while the concrete compressive stress was 2.8 MPa (0.41 ksi). These values represented increases of 16.4% and 139.4%, respectively, compared to the as-built beam. The observed stress values were used to calculate the load rating of the numerical model of the damaged beam section.

In the serviceability-based equations for the tensile stresses in the prestressing strands in Figure 21, the increased strand stresses at the cracks under gravity were used as the sum of prestress and dead load stress ($F_p + F_d$). Similarly, the corresponding increased compressive stresses in concrete under gravity were used as the sum of prestress and dead load stress ($F_p + F_d$) in the serviceability-based equations for the compressive stresses in concrete in Figure 21. The equivalent live load stress from the four-point bending results corresponding to the moment induced by the HS-20 truck (load rating vehicle) on the beam was used as the live load stress (F_l). The numerical analysis shows that the inventory and operating ratings for the tension in the prestressing strands are −3.64 (<0) and 3.5 for the first method with perfect bond. Because the inventory rating is less than zero, it is taken as zero. This shows that the serviceability rating may govern the rating of a damaged beam. For the second method with a bond-slip model, the inventory and operating ratings for the tension in the prestressing strands are 3.5 and 10.65, respectively. Thus, the inventory and capacity rating of the beam are governed by the residual capacity of the cracked beam. This shows that it is essential to consider a bond-slip model for the concrete-strand interface to obtain accurate strand stresses at the crack.

LOAD RATING ANALYSIS OF THE CRACKED 21 × 36 (G2) BEAM

As explained previously, the capacity, prestressing strand, and concrete stress contributions from the dead, live, and effective prestressing forces were used to load rate the as-built 21 × 36 (G2) PPC deck beam. The nominal capacity of the beam was calculated to be 1040.4 kN-m (767.36 kip-ft), the unfactored dead load moment was 226.19 kN-m (166.83 kip-ft), and the unfactored live load moment due to HS-15 truck load considering the distribution factor (0.501) and the impact factor (1.29) was 208.8 kN-m (151.79 kip-ft). Using the computed moments and the calculated stresses in concrete and prestressing strands in the as-built beam, the inventory and operating rating of the beam were found to be 1.67 and 2.79, respectively. Table 3 summarizes the load rating factors of the as-built and damaged 21 × 36 PPC deck beam.

The load rating analysis of the cracked G2 beam was conducted using experimental results and theoretical predictions of the damaged 21 × 36 PPC deck beam. Based on the experimental results and the theoretical analysis of the cracked section, when the cracked beam was loaded beyond its elastic limit, it exhibited nonlinear behavior and had excessive displacement under service loads. Also, when the cracked beam was loaded beyond its elastic limit, its continued performance was adversely affected due to the accumulation of plastic strains in the concrete member. Hence, to avoid any deterioration in performance, the capacity of the cracked beam was limited to its elastic limit.

From the experimental results and theoretical predictions of LS3, the elastic limit of the G2 beam was found to be 13 kips and 13.41 kips, respectively. The load rating of the cracked G2 beam was computed using the results of LS3, and the capacity-based load factors were found to govern the concrete and strand stresses as they were elastic at the elastic limit. The inventory and operating rating factors of the G2 beam were 0.44 and 0.74 for the experimental results and 0.30 and 0.51 for the theoretical predictions.

Table 3. Rating Factors Based on AASHTO MBE for the 21 × 36 (G2) Beam in the As-Built and Cracked Conditions

Load Rating Category	As Built	Damaged Beam: Experimental Results (LS3)	Damaged Beam: Theoretical Predictions (LS3)
Inventory Rating—Capacity	1.67	0.44	0.30
Operating Rating—Capacity	2.79	0.74	0.51

The G2 beam had to be loaded to 95.5% of its live load capacity before visible transverse cracks formed at the end of LS2. The cracked G2 beam had four visible cracks measuring 0.13 mm (0.005 in.), resulting from damage induced by a load equal to 95.5% of its live load capacity. Therefore, at the end of LS2, the load-carrying capacity of the beam had dropped significantly, leading to an 73.6% reduction in load rating factors. This illustrated that beams like the 21 × 36 (G2) beam must be subjected to very high loads before visible cracks form on their soffit. Furthermore, the presence of visible transverse cracks in the soffit in these beams would indicate a significant reduction in load rating, necessitating careful monitoring and potential load restrictions.

CHAPTER 5: THEORETICAL LOAD-DEFLECTION BEHAVIOR OF PPC DECK BEAMS WITH CIRCULAR VOIDS

The experimental tests of the 21 × 36 and 33 × 36 PPC deck beams revealed significant differences in their behavior. The 21 × 36 PPC deck beam was over-reinforced, exhibiting robust nonlinear elastic behavior after sustaining four transverse cracks (0.005 in.) under a four-point bending load that was 95.5% of its live load capacity. It ultimately failed in compression due to concrete crushing at the top, while the prestressing strands remained intact. Despite this, its elastic limit was only 24.2% of its live load capacity, meaning it would experience nonlinear behavior and excessive displacement if loaded beyond that point. In contrast, the 33 × 36 PPC deck beam, with a single transverse crack measuring 0.01 in., exhibited early nonlinear plastic behavior due to the propagation of transverse cracks and yielding of the prestressing strands. Its linear elastic limit was 54.1% of its live load capacity, and it failed due to simultaneous fracture of strands and crushing of concrete. The two beams differ significantly in response to transverse cracks and were treated separately to observe their behavior.

This chapter presents theoretical cracked section analyses for beams with circular voids, similar to the 21 × 36 (G2) beam. The analyzed sections include 21 × 36, 21 × 48, 17 × 36, and 17 × 48 PPC deck beams. Figure 23 presents the cross-sectional details of these four beams. Bridge plans for 28 structures built between 1958 to 1995 were obtained from IDOT, with 15 of these bridges incorporating PPC deck beams with circular voids. The beams from the 15 bridges were analyzed using theoretical cracked section analyses, and the results are presented in this chapter.

OBSERVATIONS FROM IDOT BRIDGE PLANS

The following observations were made from IDOT bridge plans:

- The design concrete strength for the superstructures was 34.5 MPa (5 ksi) at 28 days.
- The span length of PPC deck beams with circular voids ranged from 7.62 m (25 ft) to 15.24 m (50 ft).
- For 914.4 mm (36 in.) wide beams, the minimum number of strands was 6, while the 1219.2 mm (48 in.) wide beams had a minimum of 9 strands for all span lengths.
- The compression zone reinforcement consisted of four #5 G60 rebars in all beams with circular voids.
- Wire meshes were used as stirrups throughout the length of the beams, similar to the wire mesh used in the G2 test specimen.
- These bridges were designed for HS-20 or HS-15 trucks using the LFD methods in AASHTO design specifications.

The details listed above were consistent across all 15 IDOT bridge plans. Therefore, for the theoretical analysis, all beams were assumed to have a concrete design strength of 34.5 MPa (5 ksi), span lengths ranging from 7.62 m (25 ft) to 15.24 m (50 ft), at least 6 strands for the 914.4 mm (36 in.) wide beams and 9 strands for the 1219.2 mm (48 in.) wide beams, and wire mesh reinforcement, consistent with the G2 (21 × 36) beam.

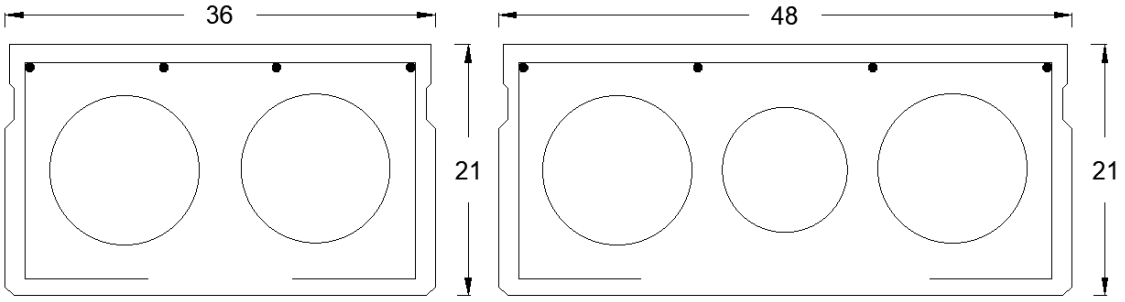

A. 21 × 36 and 21 × 48 PPC deck beams

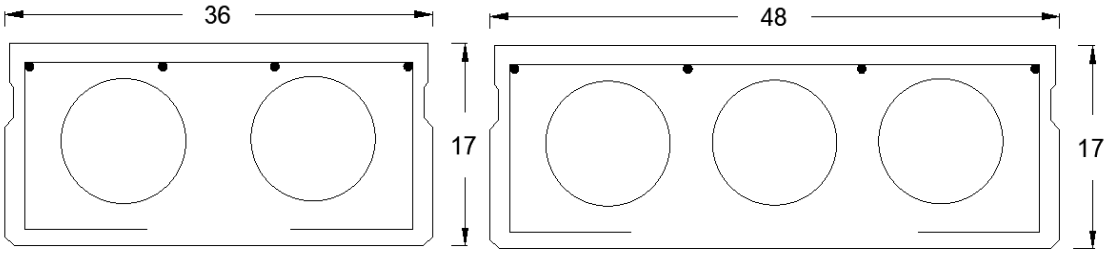

B. 17 × 36 and 17 × 48 PPC deck beams

Figure 23. Illustration. Cross-sectional details of PPC deck beams with circular voids.

LIMITATIONS OF THE ANALYSIS

The assumptions made in the theoretical cracked section analysis were outlined in Chapter 3. The limitations of this analysis are as follows:

- The analysis ignores the effect of skew on the behavior of these beams. The strains across the width of the section were assumed to be uniform.
- The analysis assumed that the applied load would act on the longitudinal axis of the beam with zero eccentricity. It ignores the effect of any torsional and eccentric loading on the performance of the beam.
- It assumed that the beam was in perfect condition, with no damage.
- It assumed that the beam's prestressing strands and other reinforcement were intact with no corrosion. Hence, the entire nominal area of the reinforcement was available.

- The analysis assumed a perfect bond between the prestressing strands and the concrete beam, so the effect of the bond-slip is ignored.

- For the sections analyzed in this chapter, the target load was 80% of its AASHTO live load capacity or a full design truck load (HS-20 / HS-15), whichever was lower. For the sections considered in this study, the prestressing strands and longitudinal rebars were still linear, and the concrete stress was between 0.35f'c and 0.45f'c. Hence, the beams would be expected to unload elastically.

ULTIMATE LIMIT STATE ANALYSIS

The 15 bridge plans with 21 × 36, 21 × 48, 17 × 36 and 17 × 48 PPC deck beams were analyzed, and the results of the ultimate section analysis are presented in Tables 4, 5, 6, and 7. These beams were usually designed such that the stress in the prestressing strands was close to the yield stress (±3%) of the strands. In 10 out of 15 beams, the prestressing strands did not yield stress at the ultimate limit state. These beams were over-reinforced even though their inventory rating factors were close to 1.0. This over-reinforcement was attributed to the limited height of the PPC deck beams with circular voids, which limited the eccentricity of the prestressing strands. As a result, more strands were required to generate the same nominal capacity compared to the deeper sections available with PPC deck beams with rectangular voids. This effect was more pronounced in the shallower (17 × 36 and 17 × 48) sections.

Table 4. Summary of the Ultimate Section Analysis of the 21 × 36 Beam Bridges

Bridge Number	Span Length (ft)	Number of Strands	Strand Diameter (in.)	Strand-to-Concrete Area (%)	Strand Stress at Ultimate to Yield Stress	Vehicle Type	Inv. RF
065-3041	40.6	9	0.5 (G270)	0.27%	1.033	HS-20	1.14
008-3504	41.1	10	0.5 (G270)	0.30%	1.024	HS-20	1.21
079-4252	45.17	12	0.5 (G270)	0.37%	1.007	HS-20	1.18
087-3458	50.0	16	0.5 (G270)	0.49%	0.972	HS-20	1.17
037-3154	50.0	18	7/16 (G250)	0.41%	1.002	HS-15	1.25
G2 beam	50.0	26	7/16 (G250)	0.549%	0.990	HS-15	1.67

Table 5. Summary of the Ultimate Section Analysis of the 21 × 48 Beam Bridges

Bridge Number	Span Length (ft)	Number of Strands	Strand Diameter (in.)	Strand-to-Concrete Area (%)	Strand Stress at Ultimate to Yield Stress	Vehicle Type	Inv. RF
079-3034	40	12	0.5 (G270)	0.27%	1.03	HS-20	1.15
038-3929	45.7	28	7/16 (G250)	0.48%	0.97	HS-20	1.42
079-3034	50	19	0.5 (G270)	0.44%	0.99	HS-20	1.06
098-5403	52	28	7/16 (G250)	0.48%	0.98	HS-15	1.33

Table 6. Summary of the Ultimate Section Analysis of the 17 × 36 Beam Bridges

Bridge Number	Span Length (ft)	Number of Strands	Strand Diameter (in.)	Strand-to-Concrete Area (%)	Strand Stress at Ultimate to Yield Stress	Vehicle Type	Inv. RF
037-3040	38.0	18	7/16 (G250)	0.48%	0.98	HS-15	1.09
042-3006	39.9	14	0.5 (G270)	0.5%	0.97	HS-20	1.22
100-3160	39.9	15	0.5 (G270)	0.53%	0.96	HS-20	1.30

Table 7. Summary of the Ultimate Section Analysis of the 17 × 48 Beam Bridges

Bridge Number	Span Length (ft)	Number of Strands	Strand Diameter (in.)	Strand-to-Concrete Area (%)	Strand Stress at Ultimate to Yield Stress	Vehicle Type	Inv. RF
037-3010	50	31	7/16 (G250)	0.65	0.93	HS-15	1.26
046-3016	33	21	7/16 (G250)	0.38	1.01	HS-15	1.70
037-3093	36	26	3/8 (G250)	0.44	0.99	HS-15	1.48
087-3458	38.6	13	0.5 (G270)	0.363	1.01	HS-20	1.03

THEORETICAL CRACKED SECTION ANALYSIS: RESULTS

Figures 24, 25, 26, and 27 present the results of the cracked section analysis of the 21 × 36, 21 × 48, 17 × 36 and 17 × 48 beams obtained from IDOT bridge plans. The target (peak) load was set at 80% of the AASHTO live load capacity or a full design truck load (HS-20/ HS-15), whichever was lower. The prestressing strands and longitudinal rebars remained elastic, and the concrete stress was between 0.35f'c and 0.45f'c. The materials in the beams were still linear under 80% of their live load capacities, and the beams unloaded elastically, with only minor residual displacements. Similar to the G2 beam, these beams are expected to have no visible cracks after the unloading step (LS1). These beams behaved elastically up to the target peak load. Therefore, they can be loaded safely to the target loads without major adverse impacts on the structural performance.

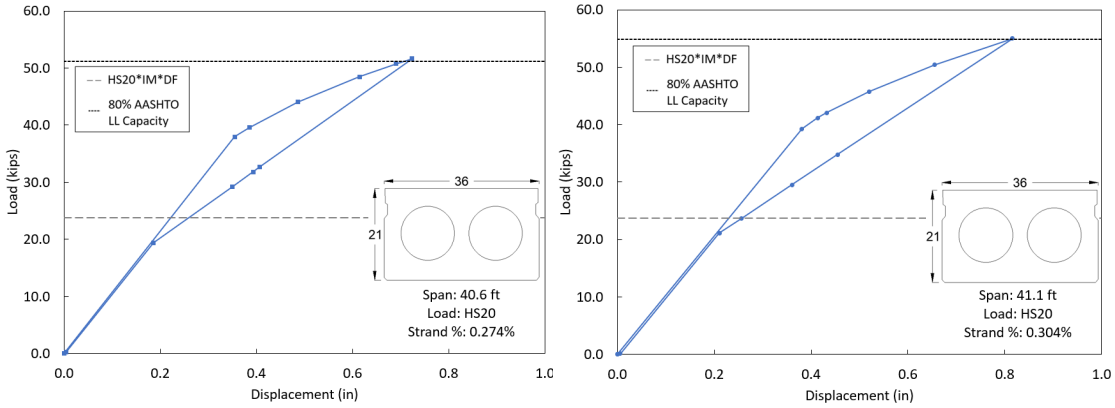

A. Beams with 40.6 ft and 41.1 ft span from bridge 065-3041 and 008-3504

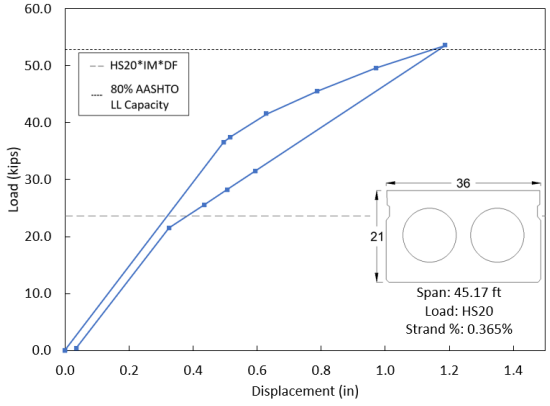

B. Beam with 45.2 ft span from bridge 079-4252

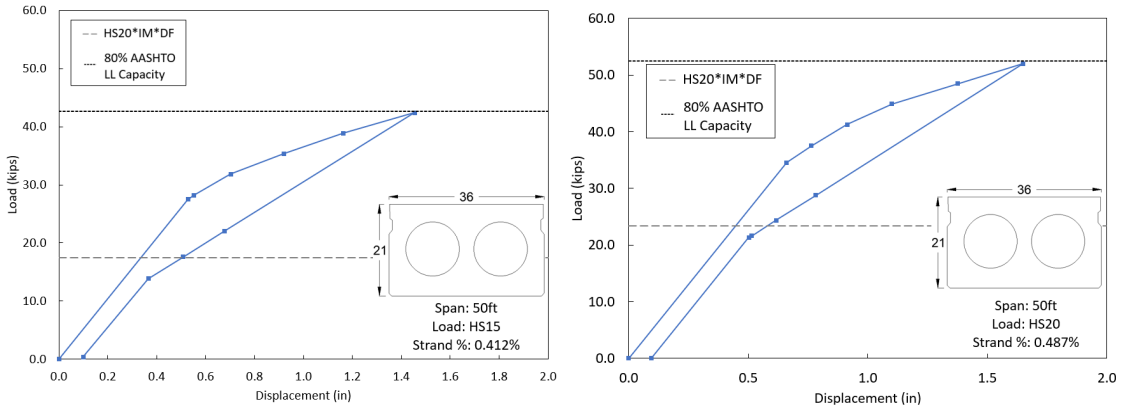

C. Beams with 50 ft span from bridge 037-3154 and 087-3458

Figure 24. Graph. Theoretical load-deflection curves of G21 × 36.

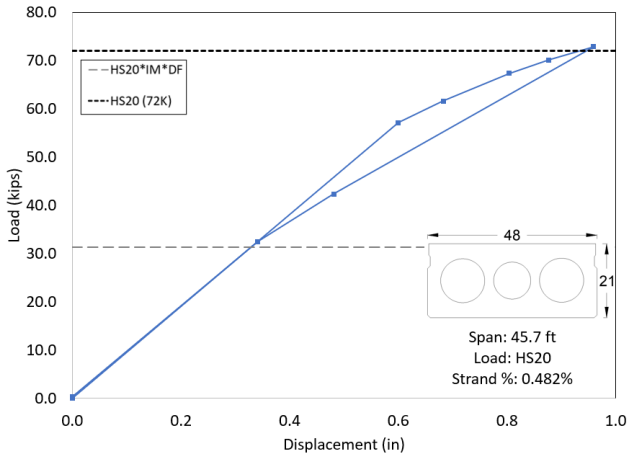

A. Beam with 45.7 ft span from bridge 038-3929

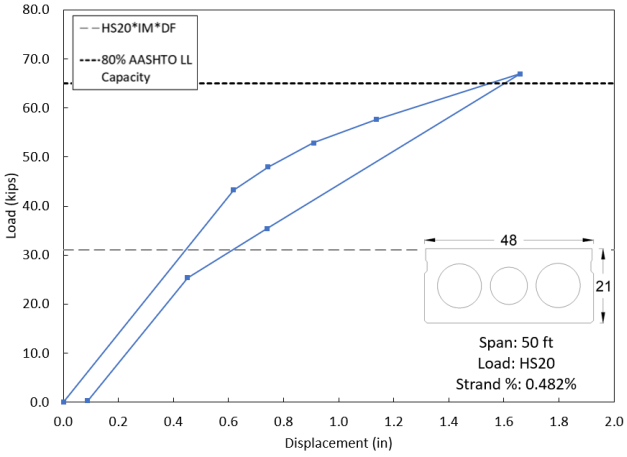

B. Beam with 50 ft span from bridge 079-3034

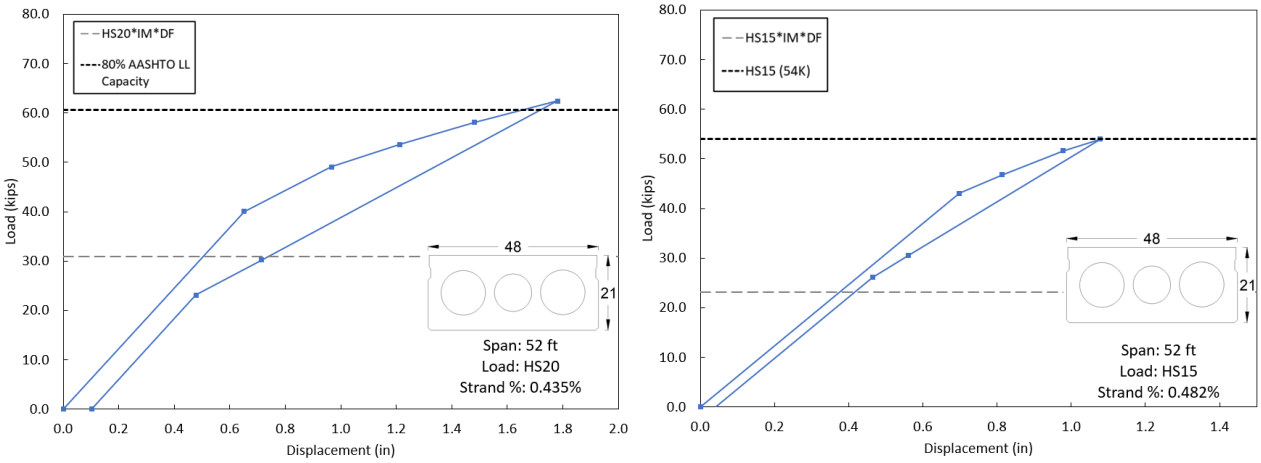

C. Beams with 52 ft span from bridge 100-3136 and 079-3034

Figure 25. Graph. Theoretical load-deflection curves of G21 × 48.

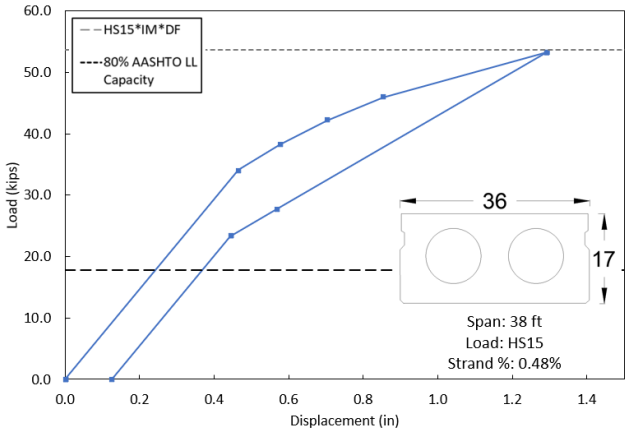

A. Beam with 38 ft span from bridge 037-3040

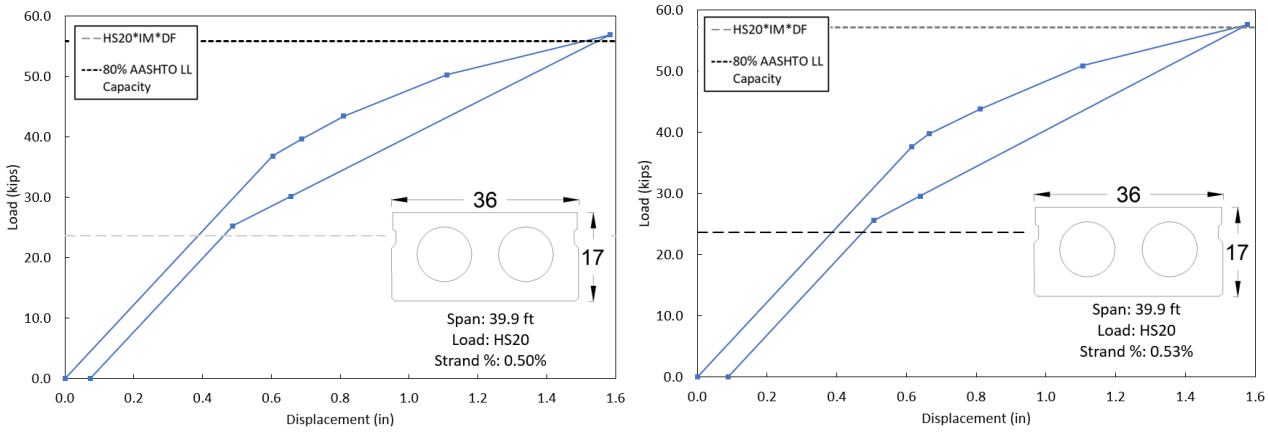

B. Beams with 39.9 ft span from bridge 042-3006 and 100-3160

Figure 26. Graph. Theoretical load-deflection curves of G17 × 36.

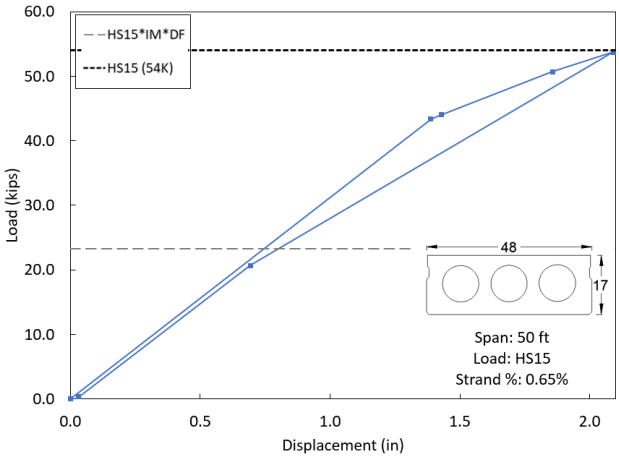

A. Beam with 50 ft span from bridge 037-3010

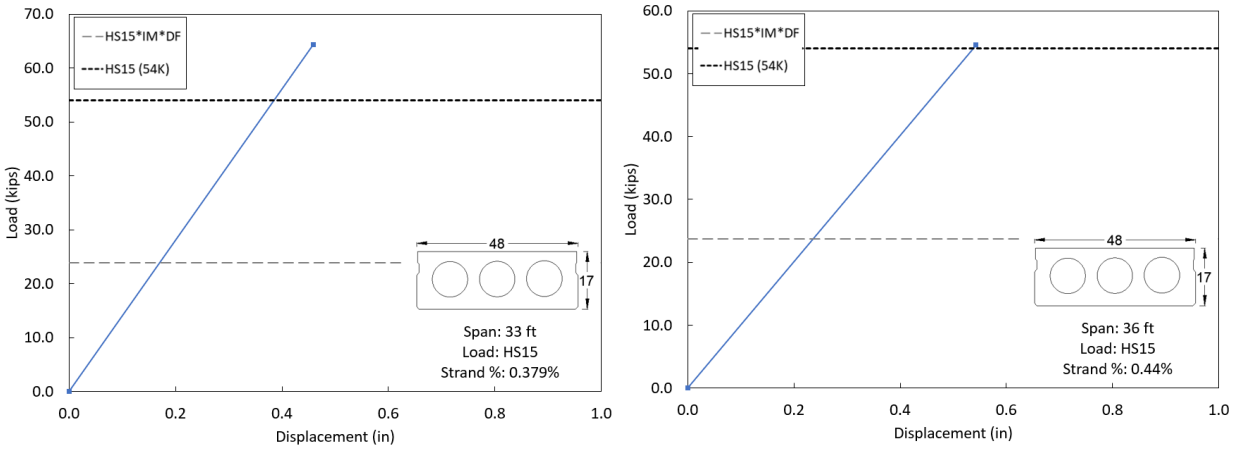

B. Beams with 33 ft and 36 ft spans from bridge 046-3016 and 037-3093

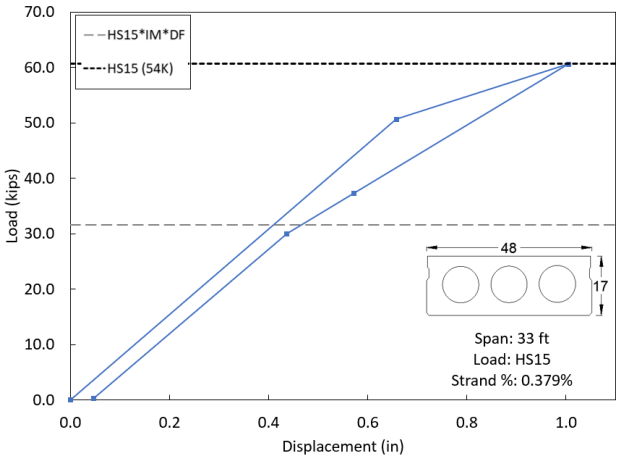

C. Beam with 38.6 ft span from bridge 102-3117

Figure 27. Graph. Theoretical load-deflection curves of G17 × 48.

Figures 28, 29, 30, and 31 present the minimum area of strands required for 21 × 36, 21 × 48, 17 × 36 and 17 × 48 PPC deck beams, respectively. These beams were designed for HS-20 and HS-15 design truck loads, using G270 and G250 grade prestressing strands. The PPC deck beams, with spans ranging from 7.62 m (25 ft) to 15.24 m (50 ft), were analyzed under 80% of their live load capacity, and the minimum strand area required to ensure elastic material behavior in the prestressing strands and concrete was reported. If a beam has a prestressing strand area ratio equal to or greater than the specified minimum value and is loaded to 80% of its live load under flexure, the materials would behave elastically. Note that if these beams have visible transverse cracks, it may imply that they were subjected to very high loads and may significantly reduce their rating factor.

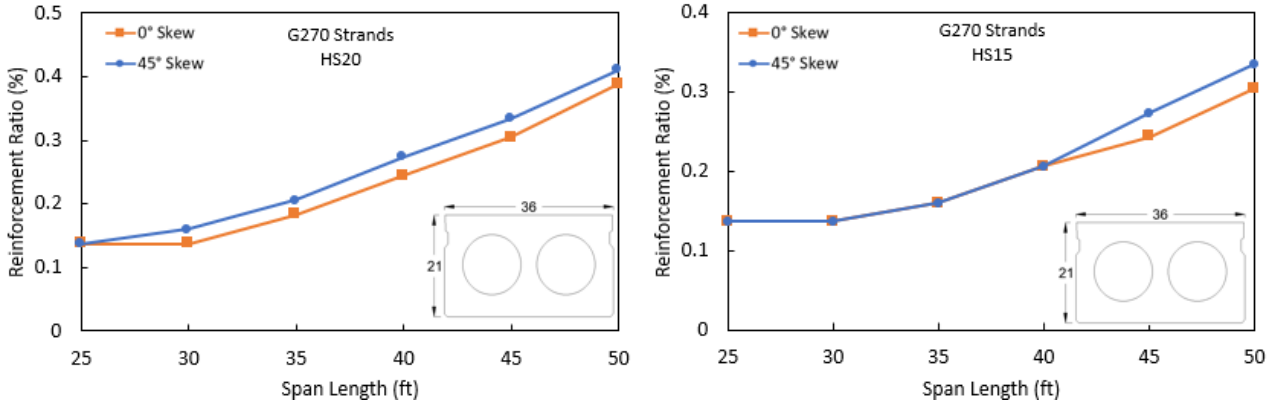

A. Beams with G270 strands

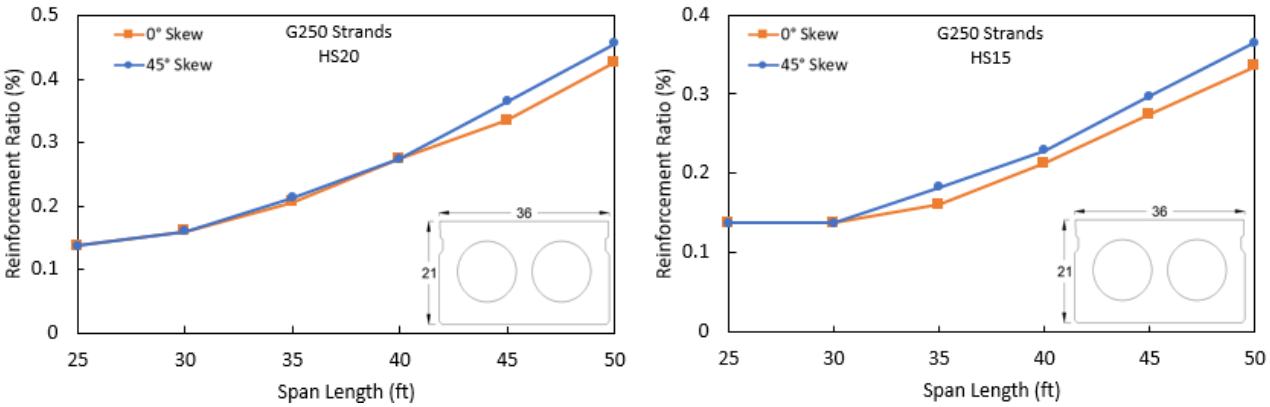

B. Beams with G250 strands

Figure 28. Graph. Minimum strands required for G21 × 36 beams.

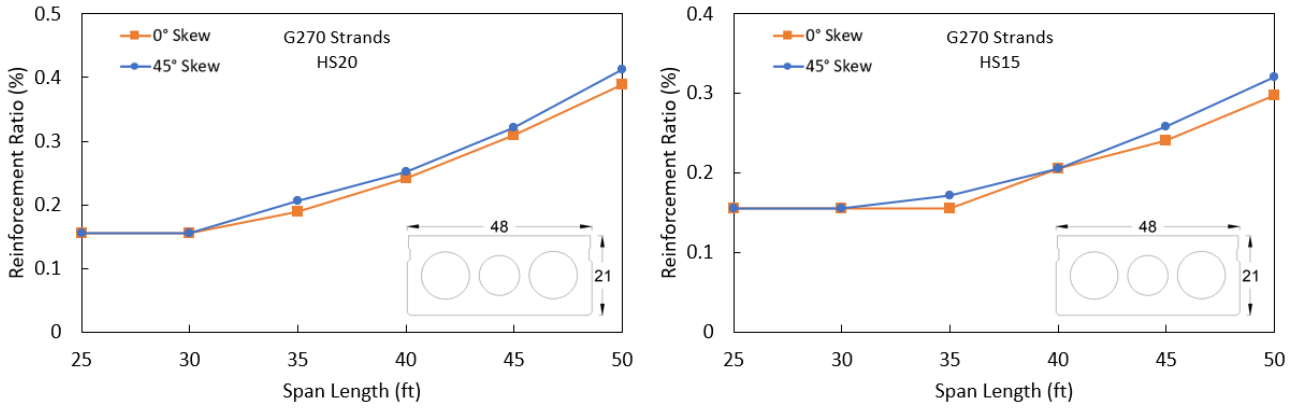

A. Beams with G270 strands

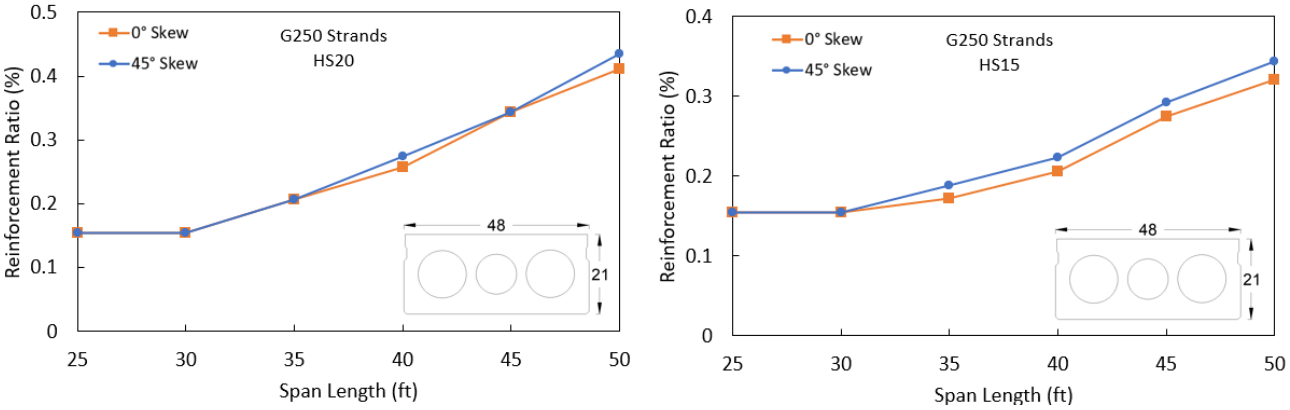

B. Beams with G250 strands

Figure 29. Graph. Minimum strands required for G21 × 48 beams.

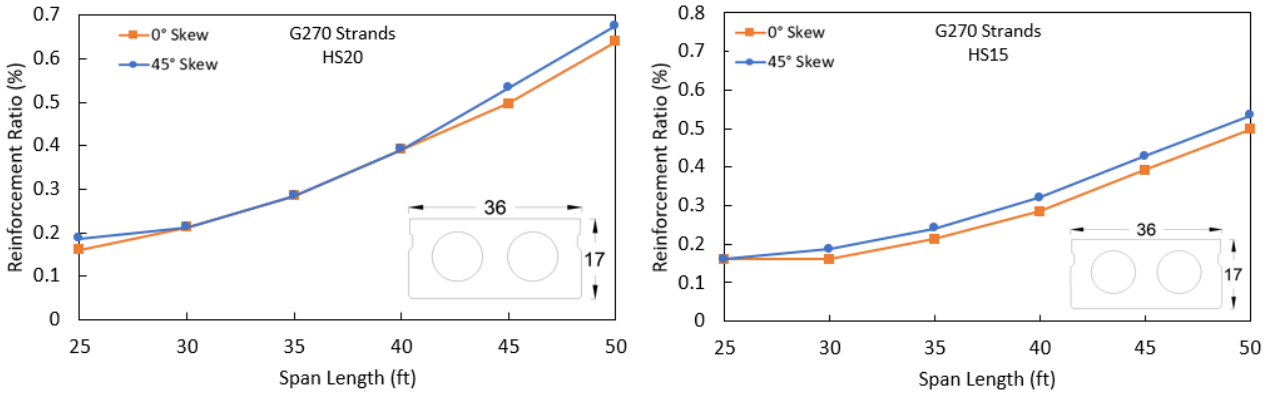

A. Beams with G270 strands

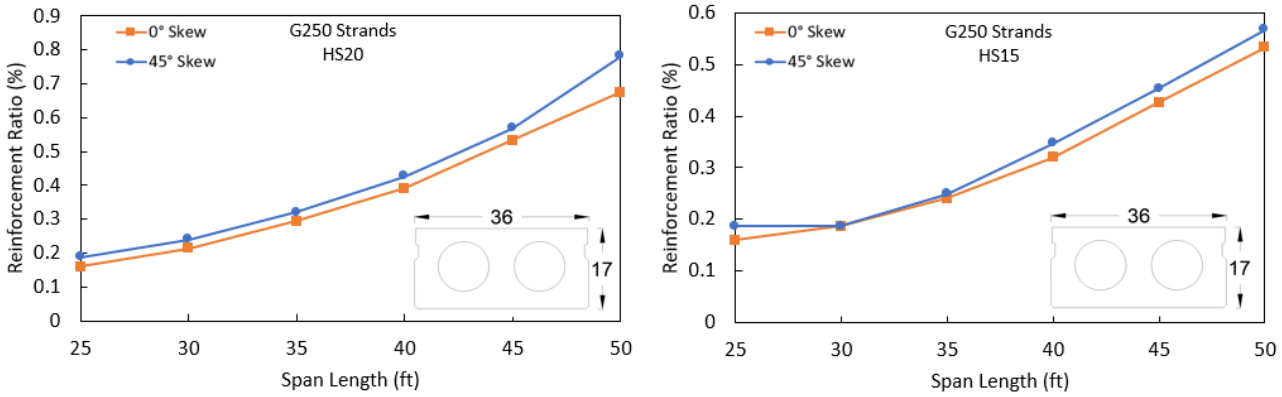

B. Beams with G250 strands

Figure 30. Graph. Minimum strands required for 17 × 36 beams.

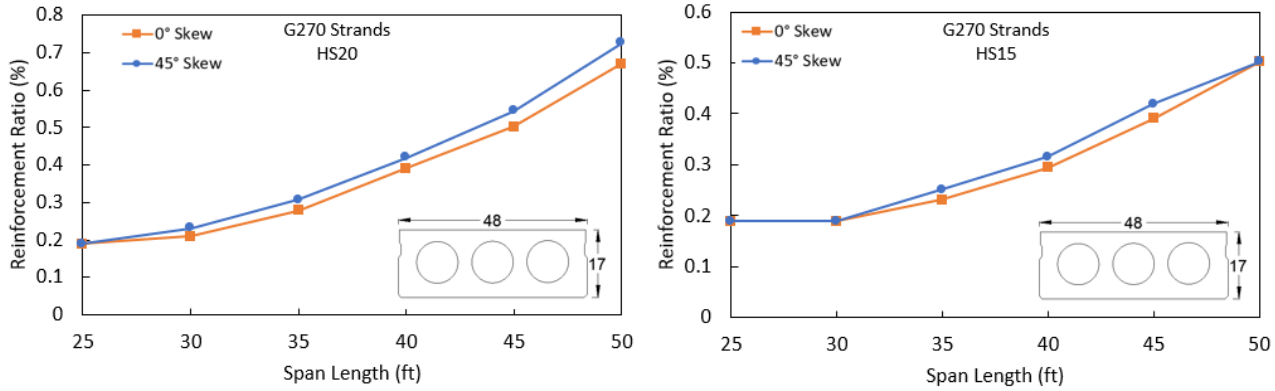

A. Beams with G270 strands

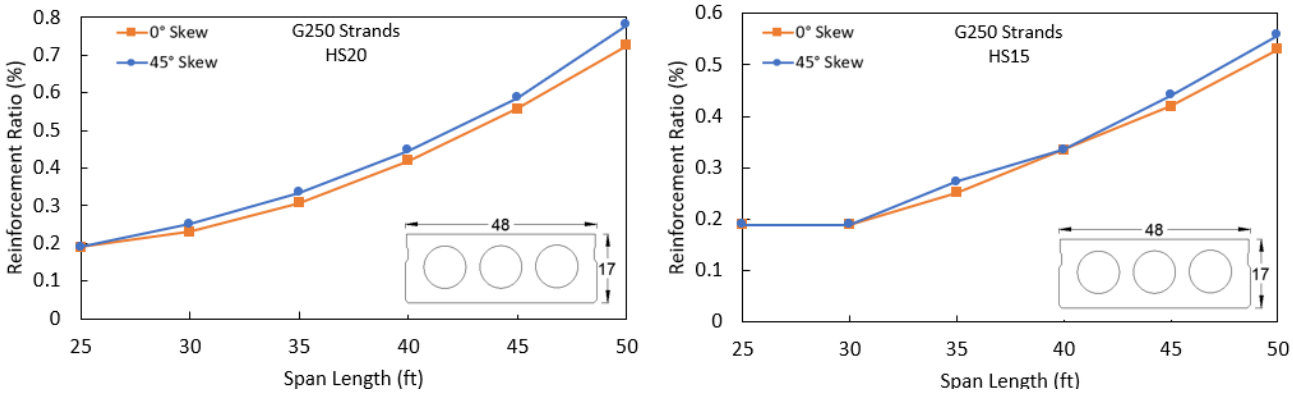

B. Beams with G250 strands

Figure 31. Graph. Minimum strands required for 17 × 48 beams.

CHAPTER 6: PARAMETRIC STUDY ON PPC DECK BEAMS WITH RECTANGULAR VOIDS

A parametric study was conducted on PPC deck beams with rectangular voids to understand the influence of beam material properties and geometric section characteristics on the behavior, residual strength, built-up stresses, and load rating of damaged beams. Routine IDOT inspections revealed that transverse cracks commonly occur in older bridges. To assess their impact, 28 bridge plans for structures built in the latter half of the 20th century were obtained and analyzed. Among these, 13 bridge plans contained PPC deck beams with rectangular voids. The beams used in the bridge plans were 27 × 36, 27 × 48 and 33 × 36 PPC deck beams. Figure 32 presents the cross-sectional details of the 27 × 36, 27 × 48, and 33 × 36 PPC deck beams.

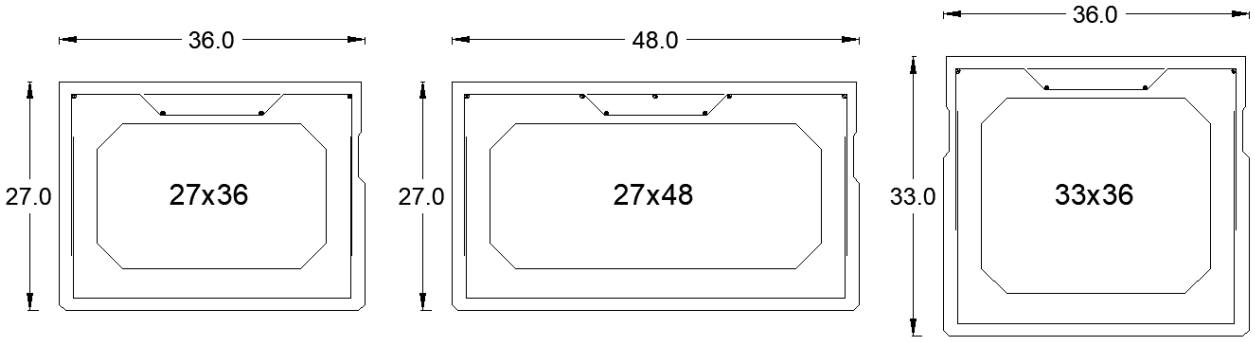

Figure 32. Illustration. Cross-sectional details of PPC deck beams with rectangular voids.

OBSERVATIONS ON IDOT BRIDGE PLANS

The following are the observations made from the IDOT bridge plans:

- The design concrete strength used in the superstructures was 34.5 MPa (5 ksi) at 28 days.
- The span length of the 27 × 36 and 27 × 48 PPC deck beams with the rectangular voids ranged from 10.97 m (36 ft) to 18.29 m (60 ft), and the span length of the 33 × 36 PPC deck beam with the rectangular voids ranged from 10.97 m (36 ft) to 24.38 m (80 ft).
- For the 914.4 mm (36 in.) wide beams, the minimum number of strands used was 6, and the 1219.2 mm (48 in.) wide beams had a minimum of 9 strands for all span lengths.
- For the 914.4 mm (36 in.) wide beams, the longitudinal rebars used in the compression zone of the beams were always two #5 G60 rebars located at a clear distance of 38.1 mm (1.5 in.) from the top of the beam and two #4 rebars located 25.4 mm (1 in.) from the bottom of the top flange.
- For the 1219.2 mm (48 in.) wide beams, the longitudinal rebars used in the compression zone of the beams were always five #5 G60 rebars located at a clear distance of 38.1 mm

(1.5 in.) from the top of the beam and two #4 rebars located 25.4 mm (1 in.) from the bottom of the top flange.

- Transverse ("U" shaped) rebars (Figure 32) were used as stirrups throughout the length of the beams, similar to the stirrups used in the G1 test specimen.

- These bridges were designed for HS-20 or HS-15 trucks using the LFD method in AASHTO design specifications.

The details listed above were consistent across the 13 bridge plans from IDOT, and it was assumed that these details apply to other similar bridges, serving as the standard for analysis. Therefore, all the beams presented in this chapter had a concrete design strength of 34.5 MPa (5 ksi), with spans ranging from 10.97 m (36 ft) to 18.29 m (60 ft) for the 27 × 36 and 27 × 48 PPC deck beams and from 10.97 m (36 ft) to 24.38 m (80 ft) for the 33 × 36 PPC deck beams. The beams had a minimum of 6 strands for the 914.4 mm (36 in.) wide beams and 9 strands for the 1219.2 mm (48 in.) wide beams. The beams had stirrups as the transverse reinforcement, similar to the G1 (33 × 36) beam.

LIMITATIONS OF THE STUDY

The parametric study on PPC deck beams with rectangular voids was subject to the following limitations:

- The analysis assumed that the applied load would act on the longitudinal axis of the beam with zero eccentricity. The effects of any torsional and eccentric loading were not considered.

- It assumed that the beam sustains no damage other than transverse cracks. The analysis focused solely on the impact of transverse cracks on load rating reduction.

- It assumed that the beam's prestressing strands and other reinforcement were intact with no corrosion. Hence, the entire nominal area of the reinforcement was available.

- When available, the original bridge plan designs were used. For other cases, the beams were designed as per the AASHTO standard specifications (2002).

- The bond-slip model used in the analysis was based on the average bond strength obtained from the literature review. Based on the bond condition of a beam, which is dependent on the strand and beam condition during casting and service, concrete strength, etc., the strand stresses at a crack in a beam may differ from the ones predicted by the finite element analysis.

2^N FACTORIAL ANALYSIS

The bridge plans analyzed in this study showed variation in beam section properties (i.e., width and depth), skew angle (θ), span length (L), and the diameter (d_b) and grade (G) of the prestressing strands. Whereas the characteristic concrete strength of the superstructure in all the bridge plans was 34.5 MPa (5 ksi), the longitudinal and transverse rebar layout was identical across all the bridge plans for a given beam width and depth.

Figure 33 presents the schematic cross-section and plan view of a 33 × 36 IDOT PPC deck beam, illustrating the variables considered in the parametric study. There are two steps in a parametric study. In the first step, a 2^n factorial analysis (Johnson 2018) was used to design an analysis in which two (usually, the maximum and minimum) values would be considered for each parameter. Finite element (FE) models were built using the identified combinations of parametric values from the factorial analysis case, and the outcome of all the FE analyses was used to identify the statistically significant parameters. In the second step, the intermediate values for the statistically significant parameters were identified, and FE models were built and analyzed to identify trends over the intermediate values.

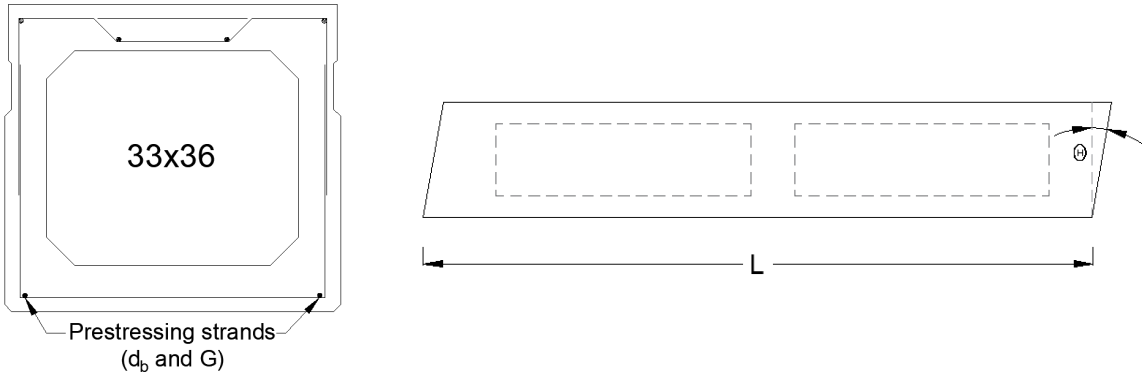

Figure 33. Illustration. Independent variables in the parametric study.

A 2^n factorial analysis was performed for each beam section type to obtain the statistically significant parameters and interactions. For each of the "n" parameters, two levels (i.e., the maximum and minimum values) were considered, as shown in Table 8. Thus, for each of the 2^n parametric variations, a 3D FE model was built using the bond-slip model described in the previous section. The beams were subject to four-point loading to induce a target crack width between two ranges, [0.32 mm, 0.44 mm] (i.e., [0.0125 in., 0.0175 in.]) and 0.44 mm to 0.57 mm (i.e., [0.0175 in., 0.0225 in.]), and the built-up stresses were obtained. The cracked beam was later loaded under an HS-20 wheel load to obtain the live load stresses. It was also subjected to a second four-point load to obtain the residual capacity of the beam.

The expected outcomes of the 2^n finite element analyses were the ratio of capacity (and prestressing strand) inventory rating of the damaged beam to the as-built beam. Once the outcomes of the 2^n factorial analysis were obtained, two-way analysis of variance (ANOVA) was used to assess the

statistical significance of the parameters statistically. ANOVA can assess the effect of varied factors and their interactions on the outcome of the analysis (Johnson 2018).

For the 33 × 36 PPC deck beam, the statistically significant parameters were the length (L), skew (θ), strand diameter (d_b) and the interaction between length and skew angle ($L{:}\theta$). And for the 27 × 36 and 27 × 48 PPC deck beams, the significant parameters were identified to be length (L), skew (θ), and the interaction between length and skew angle (L:θ).

Table 8. Variations in the Variables Considered for the Parametric Study

Independent Parameters	Range
Span (L)	10.97 m (36 ft) to 18.29 m (60 ft) for the 685.8 mm (27 in.) deep beams. 10.97 m (36 ft) to 24.38 m (80 ft) for the 838.2 mm (33 in.) deep beams.
Diameter of the strand (d_b)	11.1 mm and 12.7 mm (7/16 in. and 0.5 in.)
Grade of strand (G)	1723.7 MPa and 1861.6 MPa (250 ksi and 270 ksi)
Skew angle ($\boldsymbol{\theta}$)	0°–45°

A parametric study was conducted on the 33 × 36 and 27 × 48 PPC deck beams to understand the effect of the significant parameters on the load rating of the cracked beams. Finite element models were developed of the 33 × 36 and 27 × 48 PPC deck beams with span lengths ranging from 10.97 m (36 ft) to 24.38 m (80 ft) for the 838.2 mm (33 in.) deep beams and from 10.97 m (36 ft) to 18.29 m (60 ft) for the 685.8 mm (27 in.) deep beams. The skew angles were varied between 0° and 45° with 15° increments. The finite element models were analyzed to assess the influence of the statistically significant parameters, length (L) and skew (θ) and their interaction. A total of 64 FE models were built, and each beam was cracked to different crack widths, and the residual capacity and built-up stresses in the strands were obtained. The analysis was stopped once the crack width exceeded 0.64 mm (0.025 in.). The behavior of the 27 × 36 PPC deck beams was assumed to be similar to the 33 × 36 PPC deck beam.

33 × 36 PPC DECK BEAM: ANALYSIS RESULTS

Variation in Span Length and Skew Angle

Figure 34 shows the relation between the crack width and the inventory rating for the prestressing strands in tension for the 33 × 36 PPC deck beams with spans varying from 13.7 m (45 ft) to 18.3 m (60 ft). The inventory rating of the prestressing strands started to drop drastically with increasing crack width. There was a linear relation between the increase in crack width and the drop in inventory rating of the prestressing strands. The linear relationship between the increasing crack width and the decreasing inventory rating of prestressing strands held true for all span lengths and skew angles of the beam.

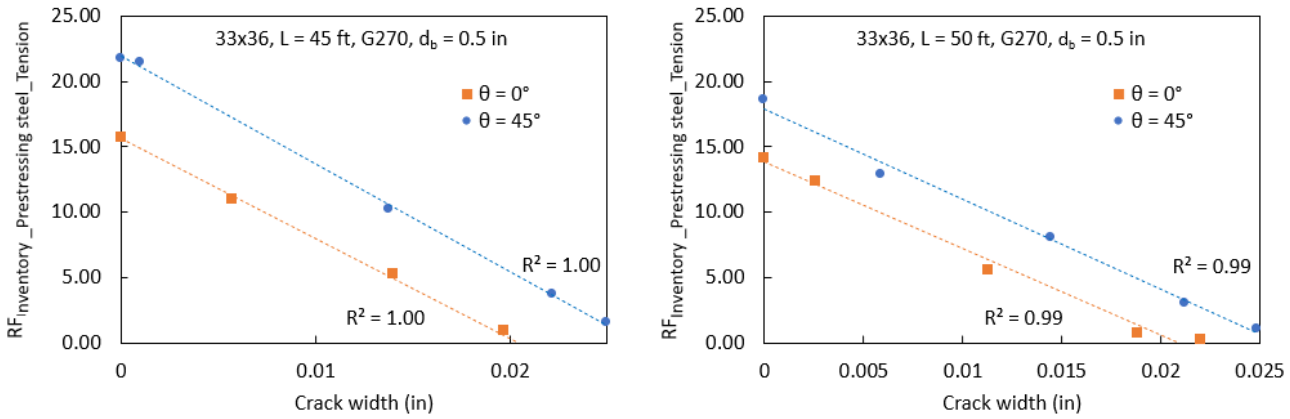

A. Results for span lengths of 45 ft and 50 ft

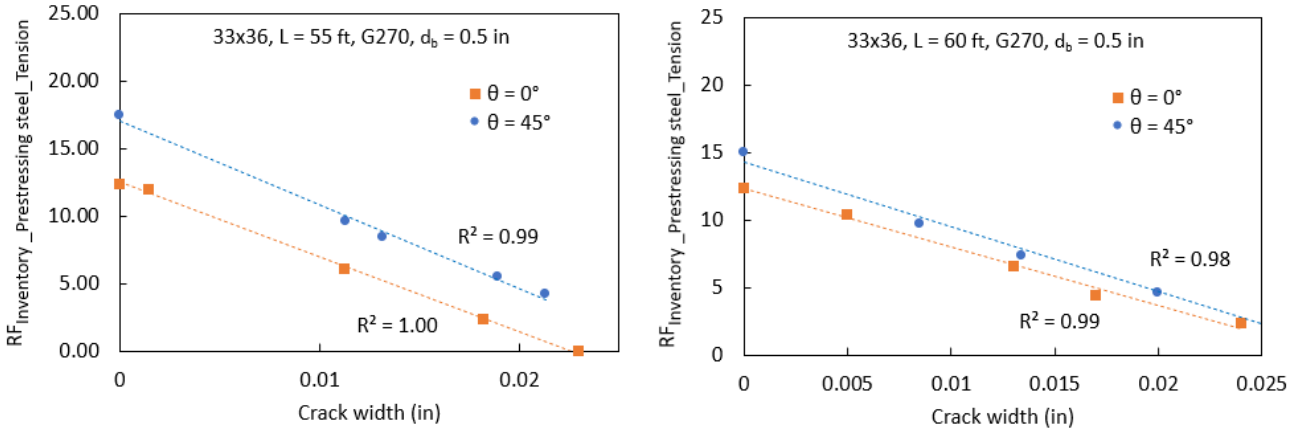

B. Results for span lengths of 55 ft and 60 ft

Figure 34. Graph. Crack width vs. inventory rating for prestressing strand in tension for 33 × 36 PPC deck beams.

Figure 35 shows the relation between the crack width and the capacity inventory rating for the 16.76 m (55 ft) long 33 × 36 PPC deck beams with 0° and 45° skew angles. The capacity inventory rating had a significant drop initially. This was attributed to taking the elastic capacity as the residual capacity of the cracked beam. The capacity-based inventory rating slowly starts to reduce with increasing crack width for both skewed and non-skewed beams. The inventory rating of the cracked beams was taken as the minimum of the capacity and serviceability-based inventory ratings.

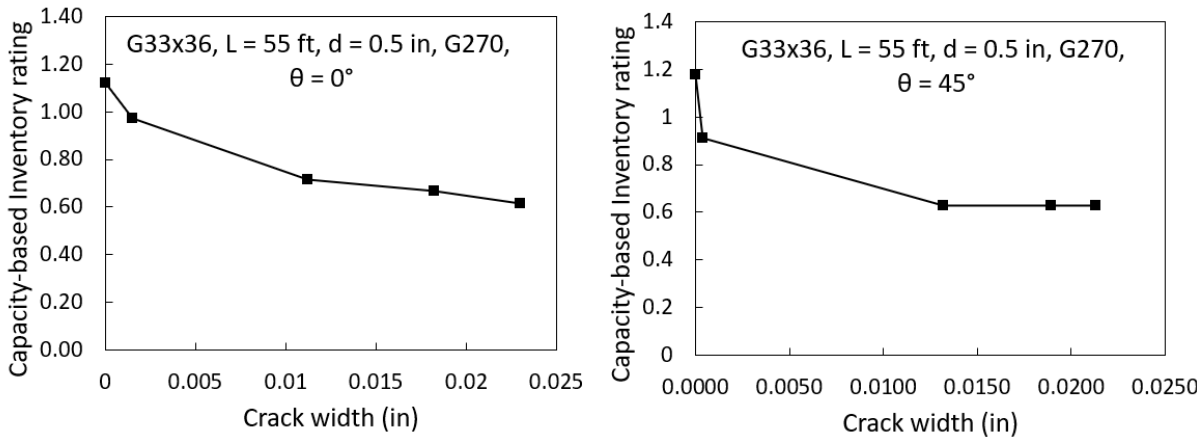

Figure 35. Crack width vs. capacity-based inventory rating for 55 ft long 33 × 36 PPC deck beams.

The reduced inventory ratings and the reduction factors (R_{RF}) for the cracked 33 × 36 PPC deck beams with span lengths between 10.97 m (36 ft) to 24.38 m (80 ft) and skew angles of 0°, 15°, 30°, and 45° are presented in the subsequent figures. Figure 36 presents the results for the 33 × 36 PPC deck beams with spans ranging from 10.97 m (36 ft) to 24.38 m (80 ft) for the four skew angles. The capacity-based inventory rating governed until the beam had a crack width of 0.51 mm (0.02 in.) for 10.97 m (36 ft) for all skew angles. A similar trend was observed at the 12.19 m (40 ft) and 13.72 m (45 ft) long for beams with skew angles of 0° to 30°, for 15.24 m (50 ft) for beams with skew angles of 0° to 15°, and for the 16.76 m (55 ft) long beams with zero skew. The inventory rating of the other beams was governed by capacity. This showed that the influence of the prestressing strand on the inventory rating of the cracked beam reduced with increasing span length and skew angle.

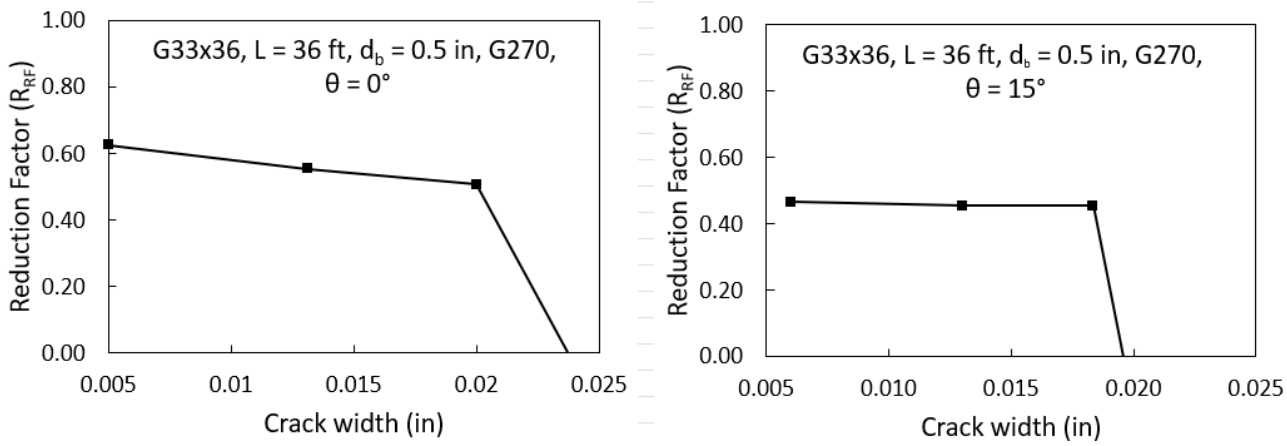

A. Results for 36 ft long beam with θ = 0° and 15°

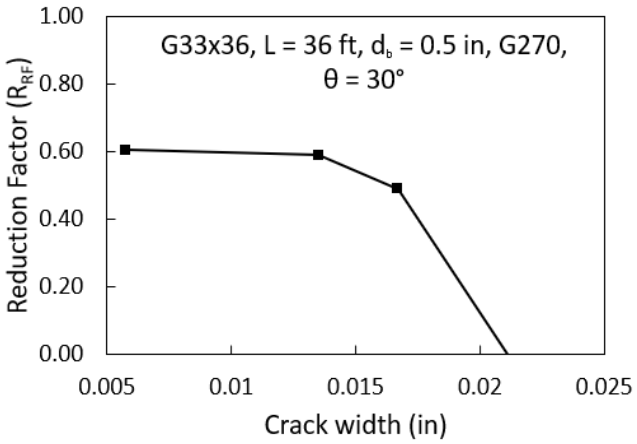

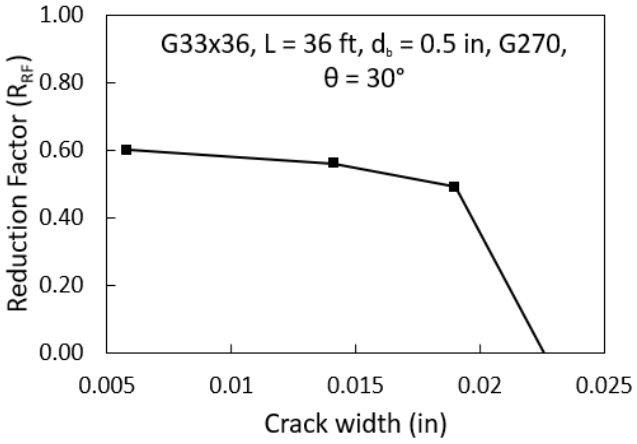

B. Results for 36 ft long beam with θ = 30° and 45°

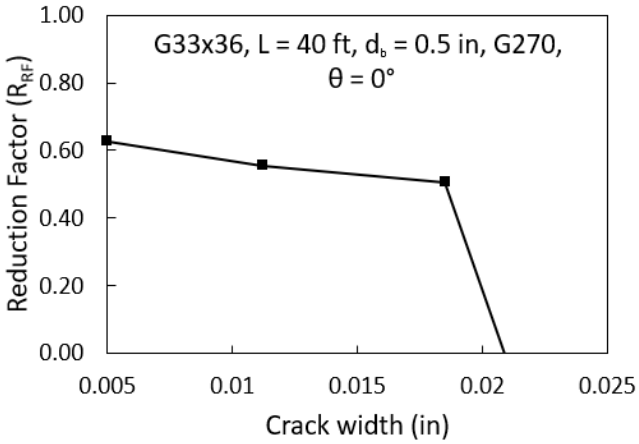

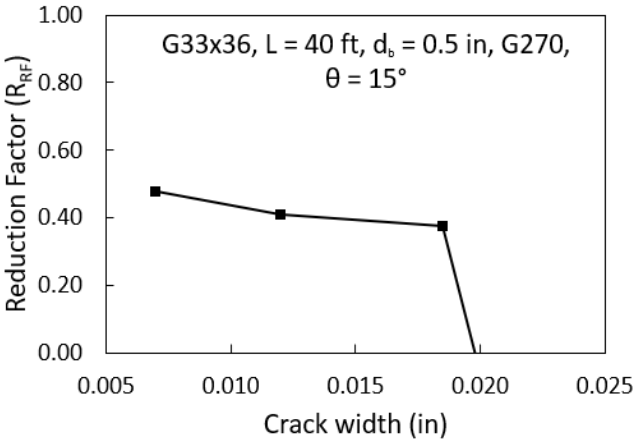

C. Results for 40 ft long beam with θ = 0° and 15°

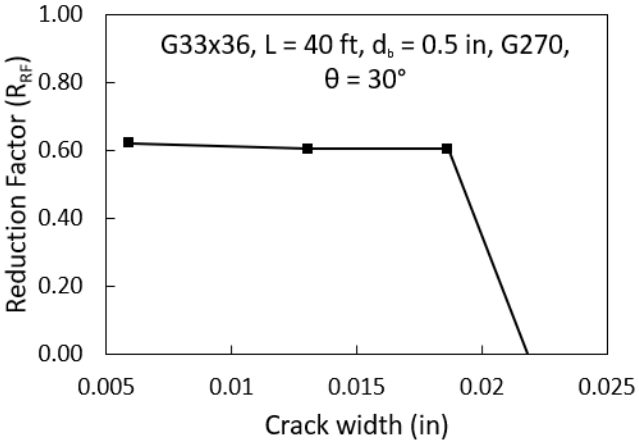

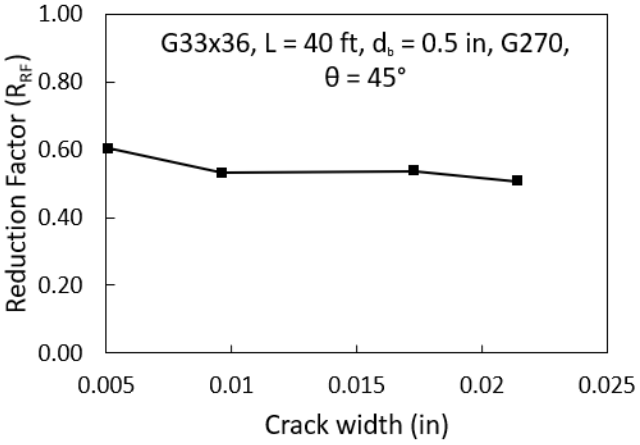

D. Results for 40 ft long beam with θ = 30° and 45°

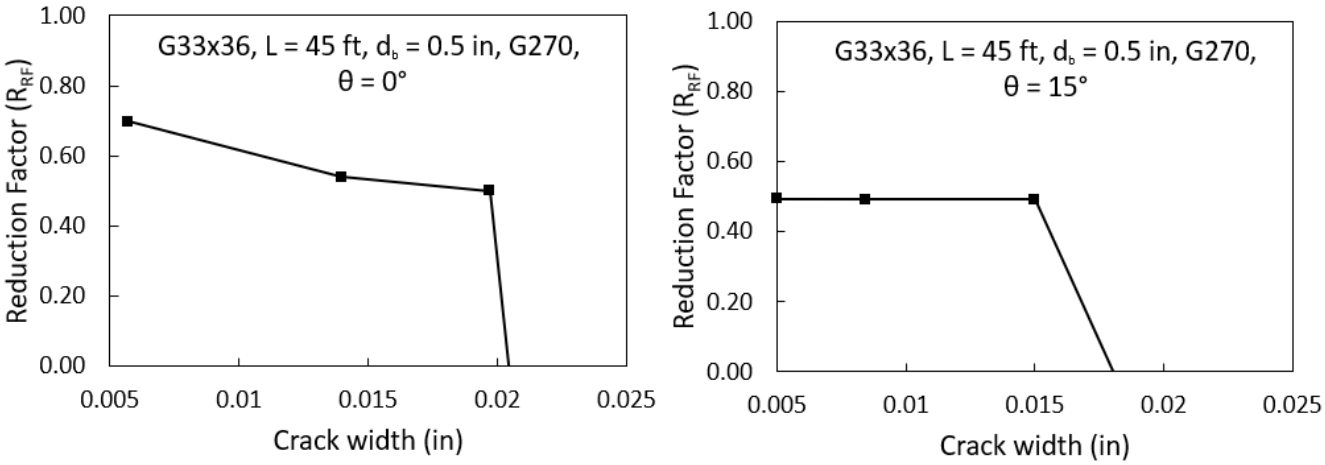

E. Results for 45 ft long beam with θ = 0° and 15°

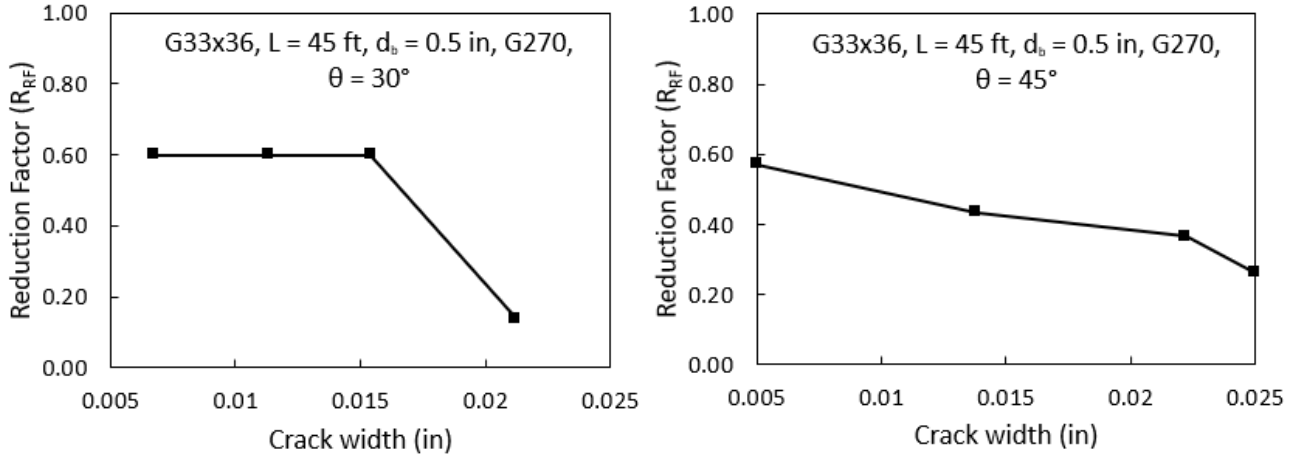

F. Results for 45 ft long beam with θ = 30° and 45°

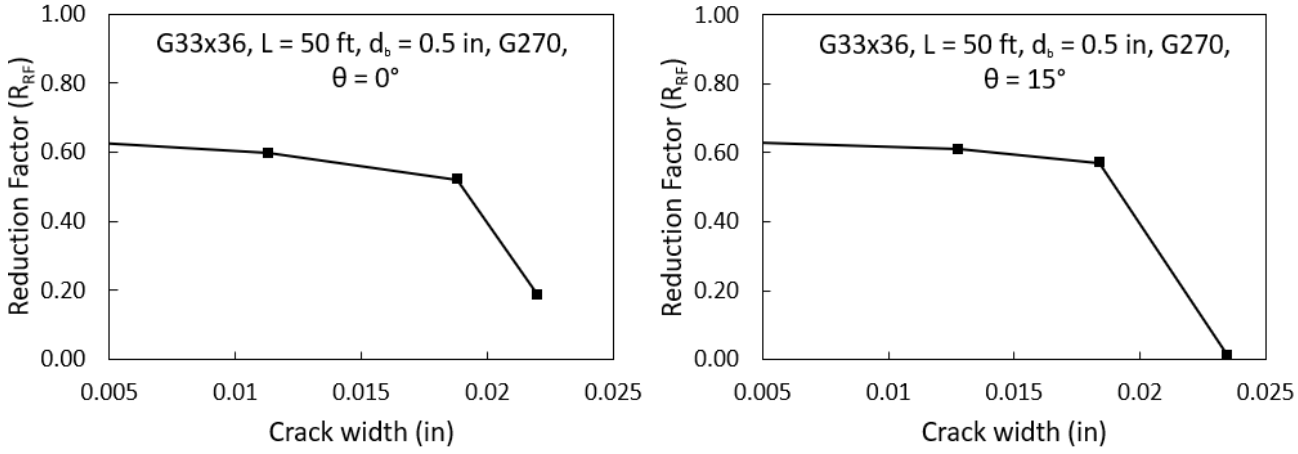

G. Results for 50 ft long beam with θ = 0° and 15°

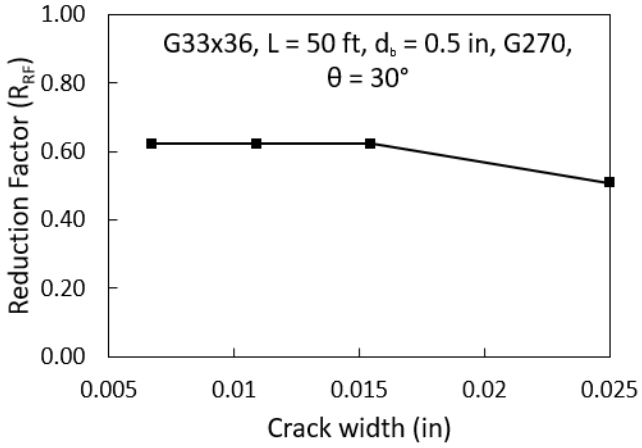

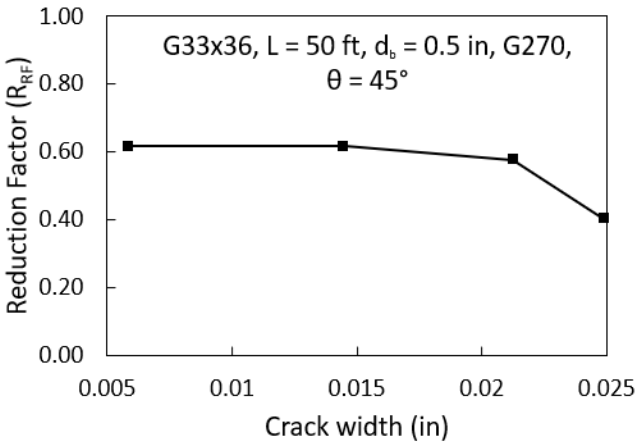

H. Results for 50 ft long beam with θ = 30° and 45°

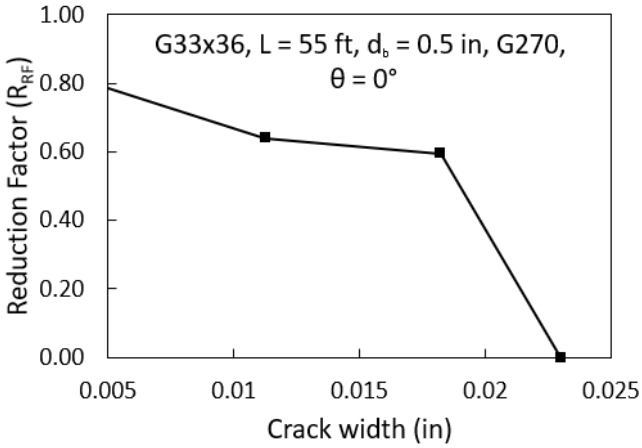

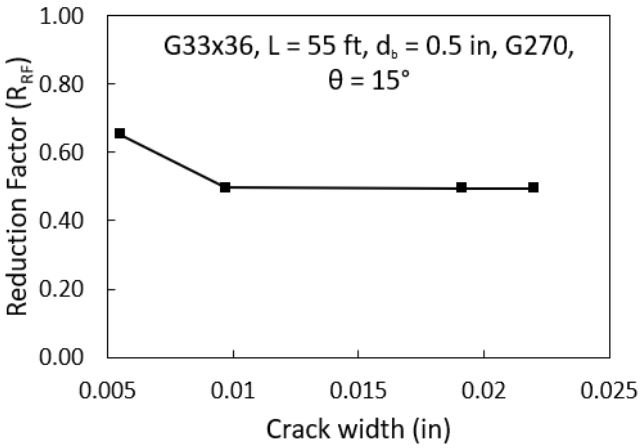

I. Results for 55 ft long beam with θ = 0° and 15°

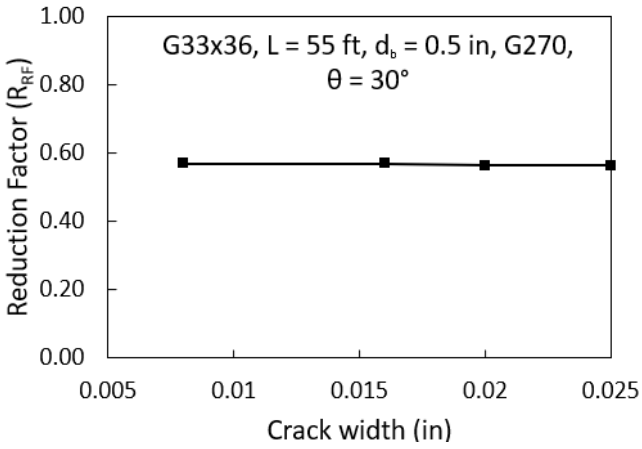

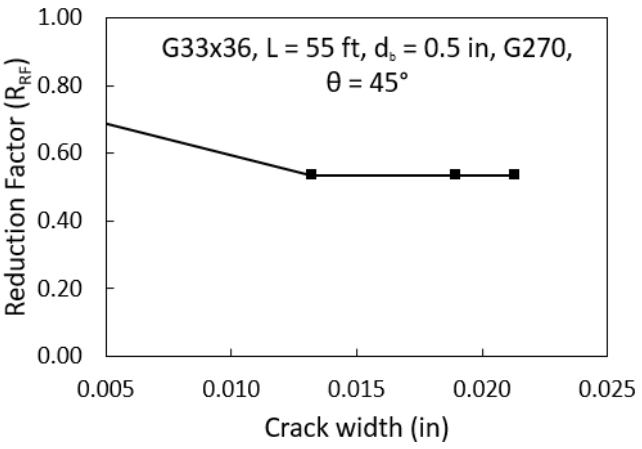

J. Results for 55 ft long beam with θ = 30° and 45°

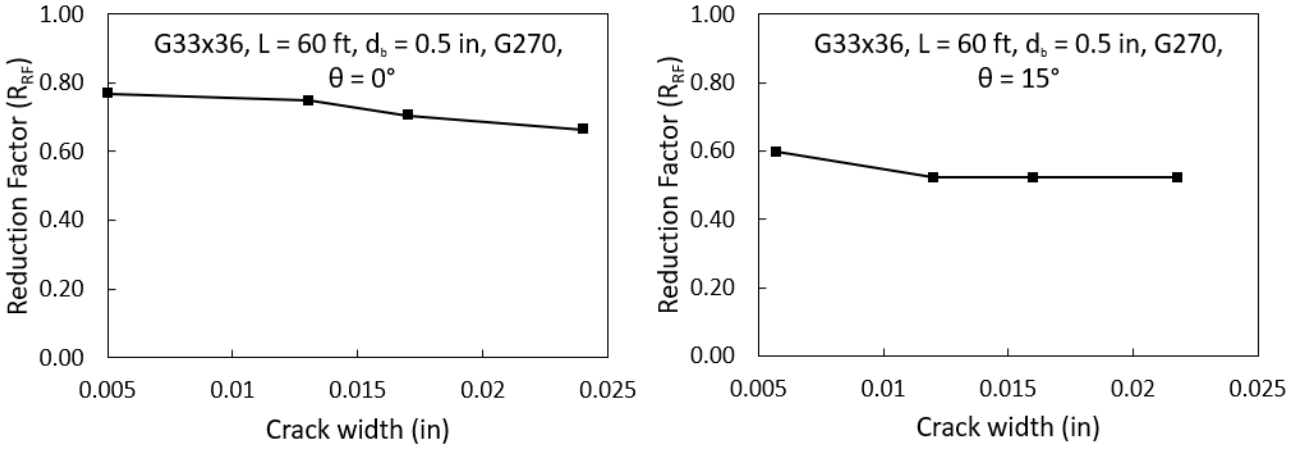

K. Results for 60 ft long beam with θ = 0° and 15°

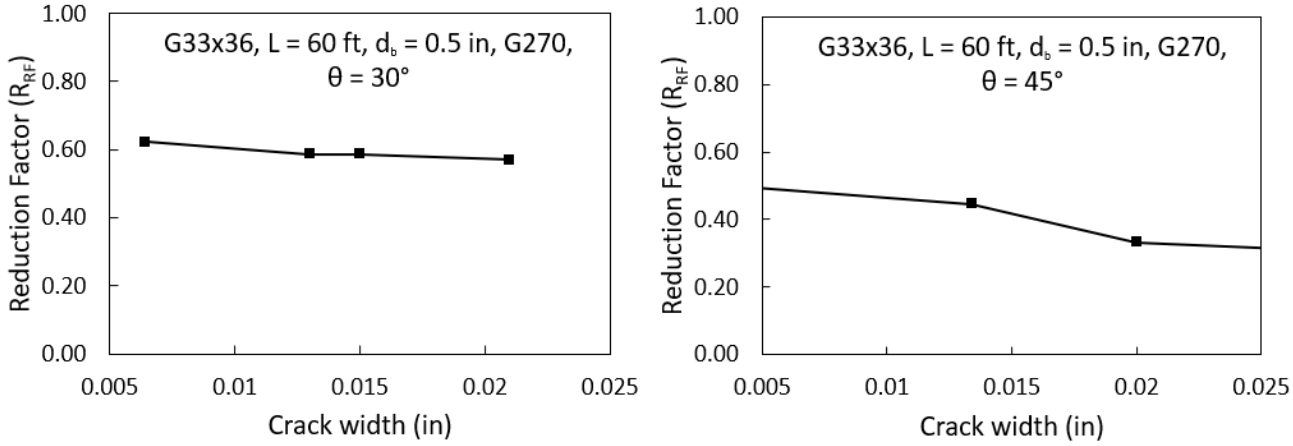

L. Results for 60 ft long beam with θ = 30° and 45°

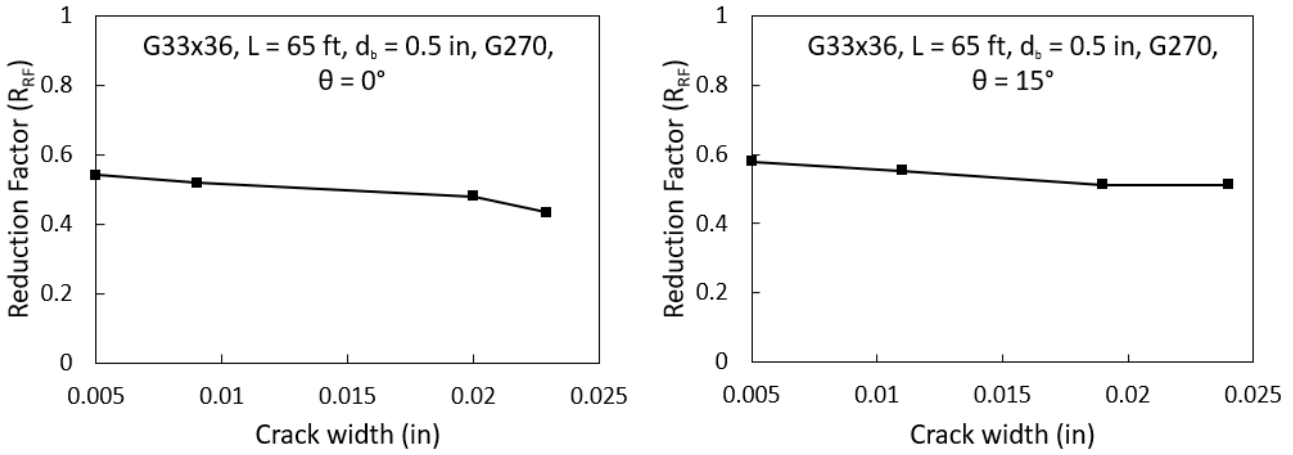

M. Results for 65 ft long beam with θ = 0° and 15°

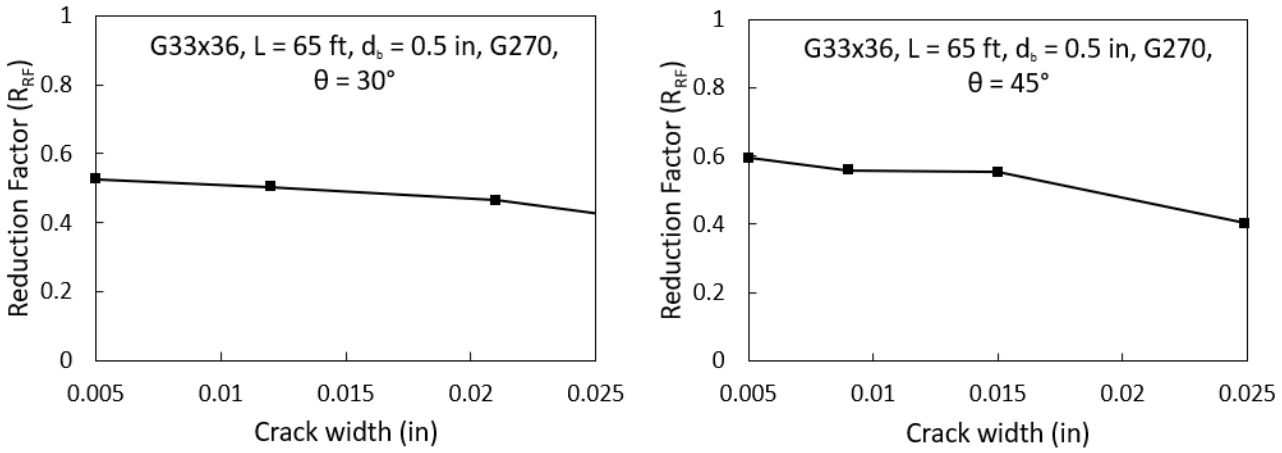

N. Results for 65 ft long beam with θ = 30° and 45°

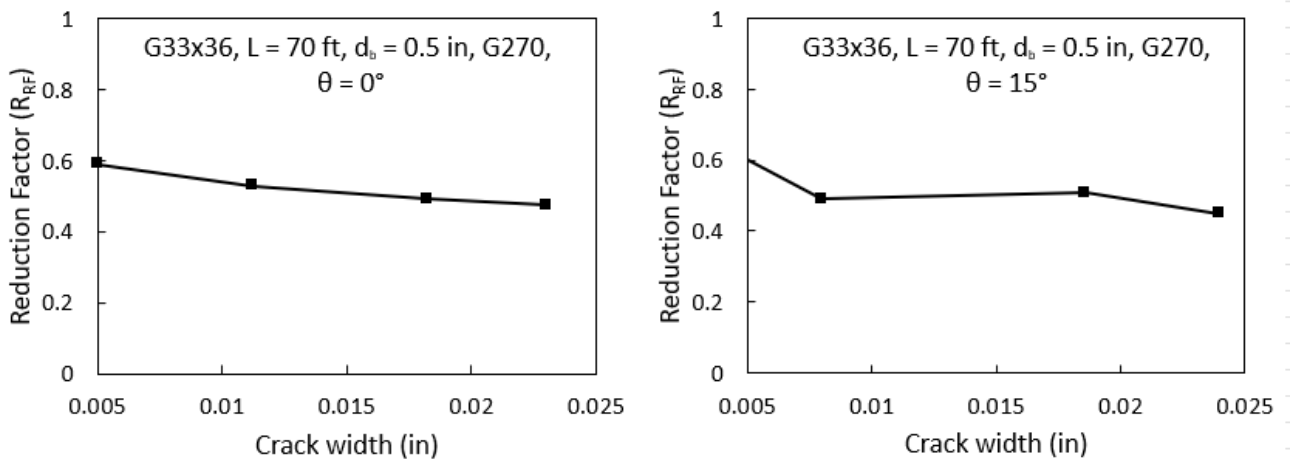

O. Results for 70 ft long beam with θ = 0° and 15°

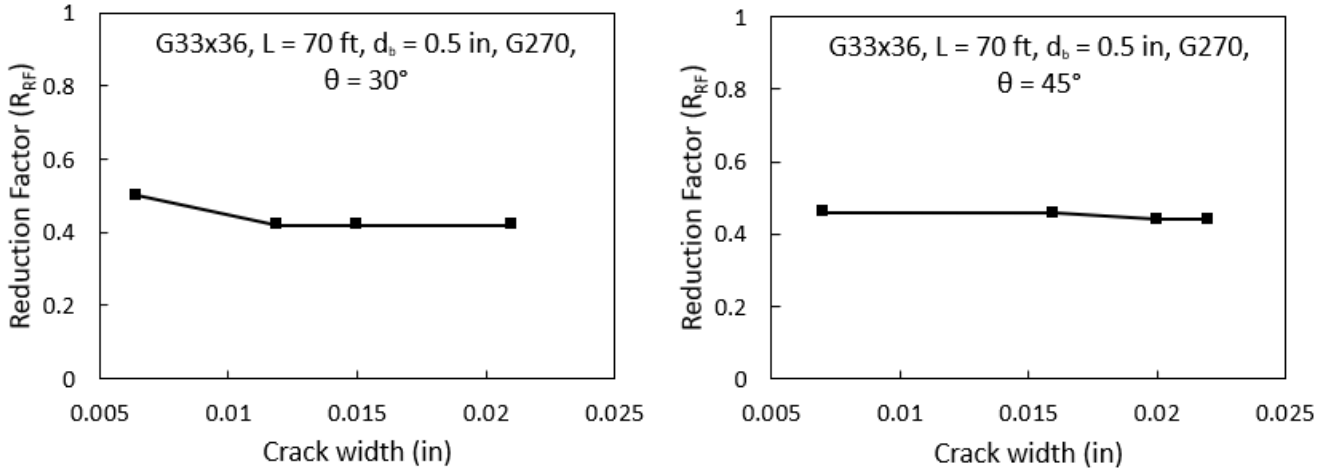

P. Results for 70 ft long beam with θ = 30° and 45°

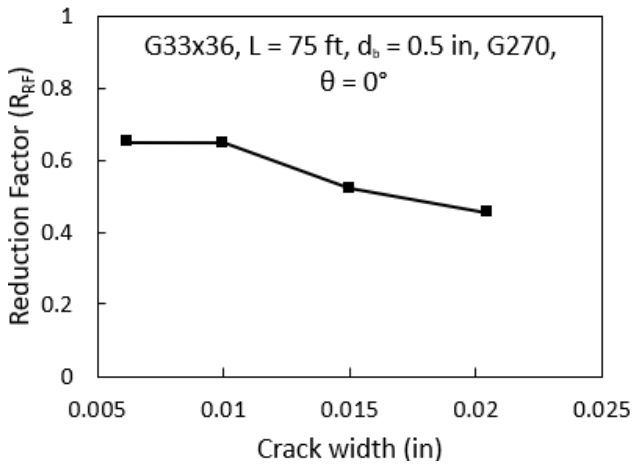

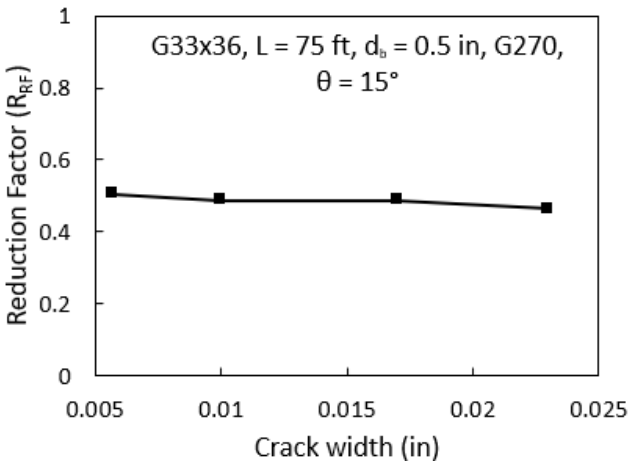

Q. Results for 75 ft long beam with θ = 0° and 15°

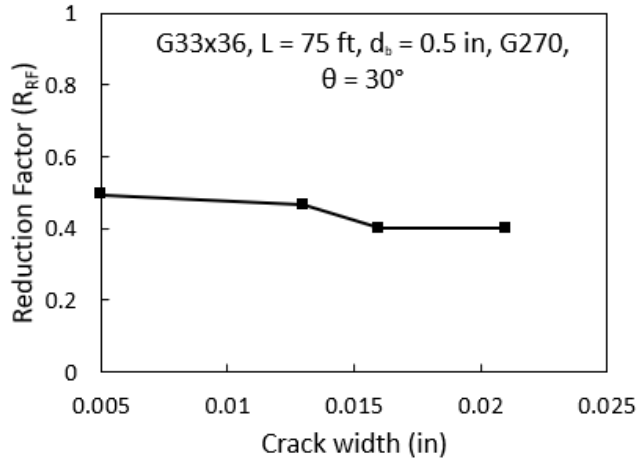

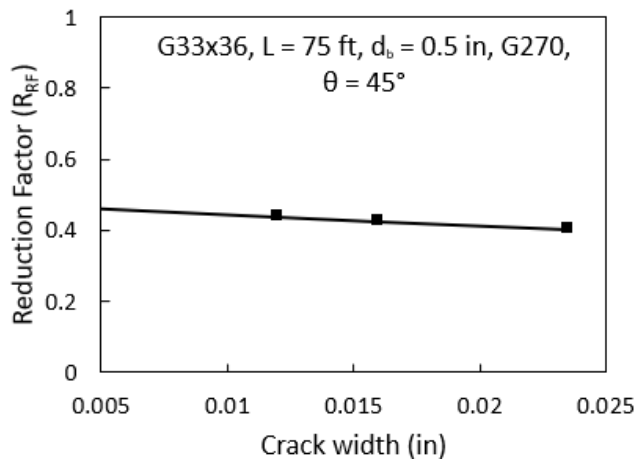

R. Results for 75 ft long beam with θ = 30° and 45°

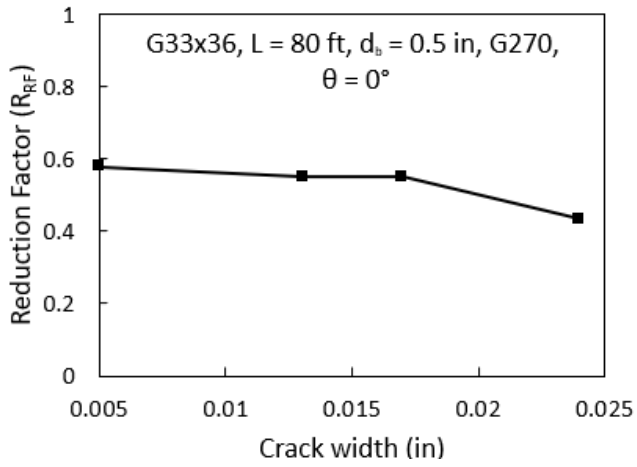

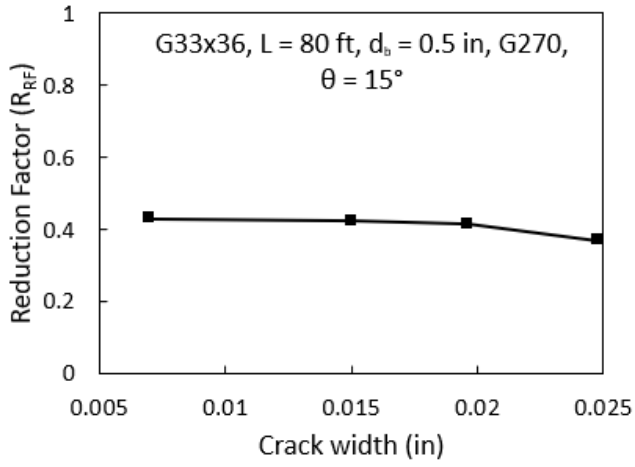

S. Results for 80 ft long beam with θ = 0° and 15°

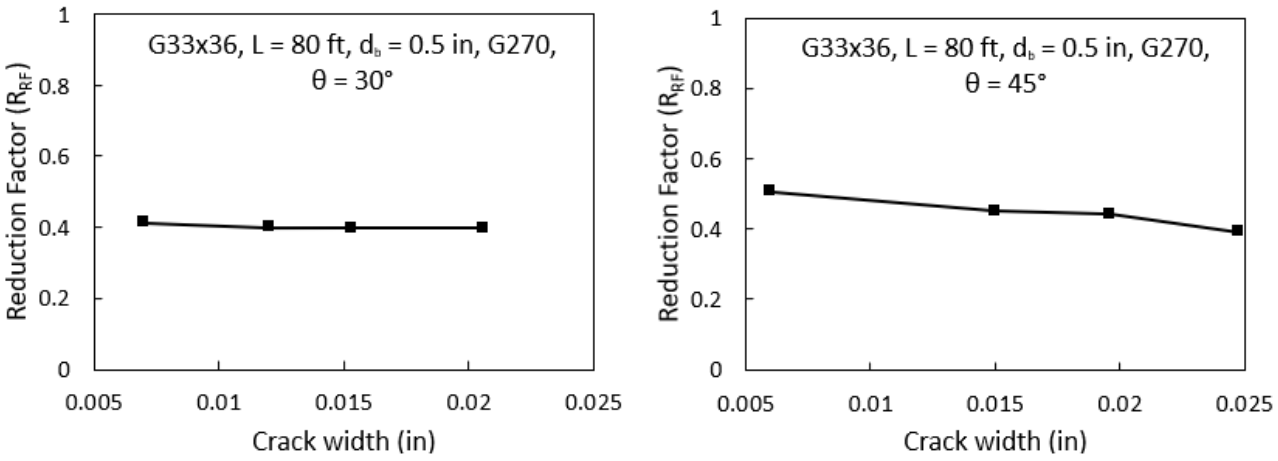

T. Results for 80 ft long beam with θ = 30° and 45°

Figure 36. Graph. Crack width vs. inventory rating for 33 × 36 PPC deck beams.

Variation in Strand Diameter

The diameter of the prestressing strands was identified as a significant parameter in the 2^n factorial analysis of the 33 × 36 PPC deck beam. Figure 37 presents the relationship between the reduction and crack width for the 10.97 m (36 ft) long non-skewed 33 × 36 PPC deck beam with G270 strand diameters varying from 11.11 mm (7/16 in.) and 12.7 mm (0.5 in.). The reduction factor (R_{RF}) is to be multiplied by the as-built rating factor to obtain the rating of the cracked beams. The analysis was performed on a 10.97 m (36 ft) long 33 × 36 PPC deck beam with six prestressing strands. The general trend in the behavior of the two PPC deck beams was the same. The inventory rating of the beams was governed by the capacity-based rating equations until a crack width of 0.51 mm (0.02 in.), after which the inventory rating for the prestressing strand in tension governed the rating.

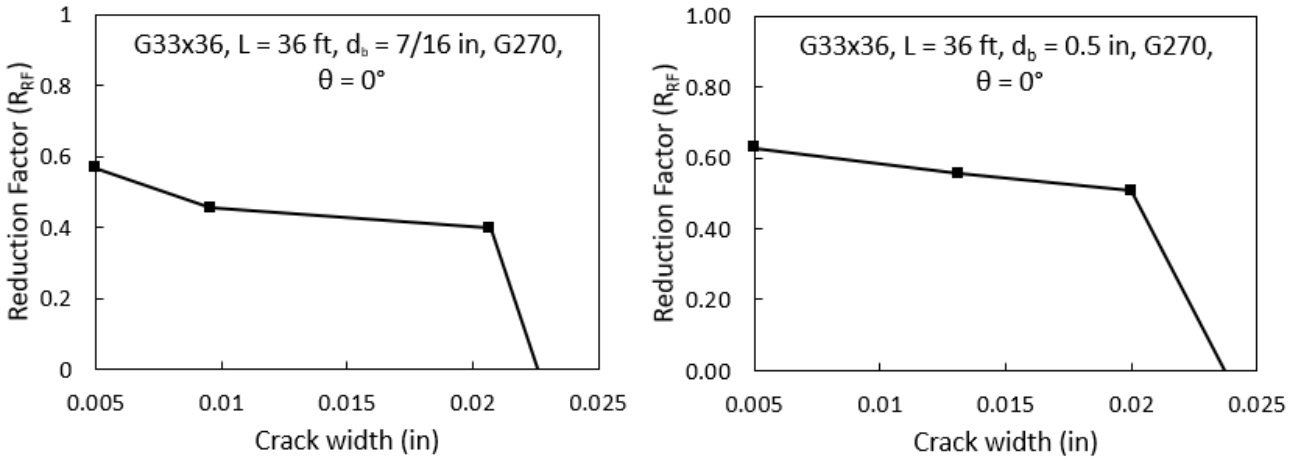

Figure 37. Graph. Results for variation in strand diameter for 33 × 36 PPC deck beam.

27 × 48 PPC DECK BEAM: ANALYSIS RESULTS

Similar to the 33 × 36 PPC deck beams, the 27 × 36 PPC deck beams exhibited a linear relationship between increasing crack width and decreasing inventory rating of prestressing strands. Initially, the capacity-based inventory rating declined sharply, attributed to using elastic capacity as the residual capacity of the cracked beam. As crack width increased, the capacity-based inventory rating gradually declined for both skewed and non-skewed beams. The inventory rating of cracked beams was determined as the minimum of the capacity-based and serviceability-based inventory ratings. The results of the reduced inventory rating and the reduction factors (R_{RF}) for the cracked 27 × 48 PPC deck beams for span lengths between 10.97 m (36 ft) to 18.29 m (60 ft) and four skew angles (0°, 15°, 30°, and 45°) are presented here. Figure 38 presents the results for the 27 × 48 PPC deck beams with spans ranging from 10.97 m (36 ft) to 13.7 m (45 ft). Findings indicate that the capacity-based inventory rating governed until the beam had a crack width of 0.51 mm (0.02 in.) for 10.97 m (36 ft) for all the skew angles. Similar trends were observed at 12.19 m (40 ft) and 13.72 m (45 ft) long for beams with skew angles of 0° to 30° and for 15.24 m (50 ft) for beams with zero skew. The inventory rating of the other beams was governed by capacity.

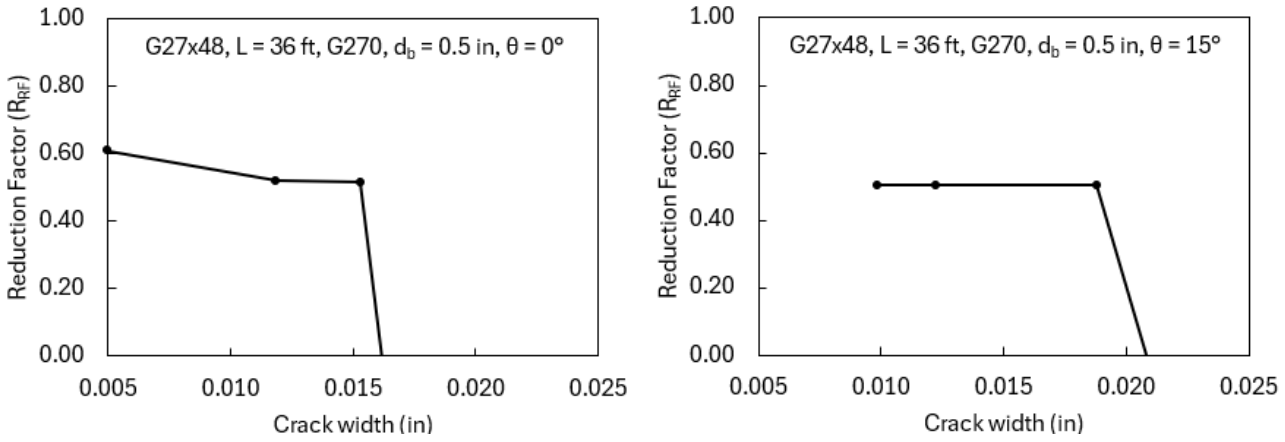

A. Results for 36 ft long beam with θ = 0° and 15°

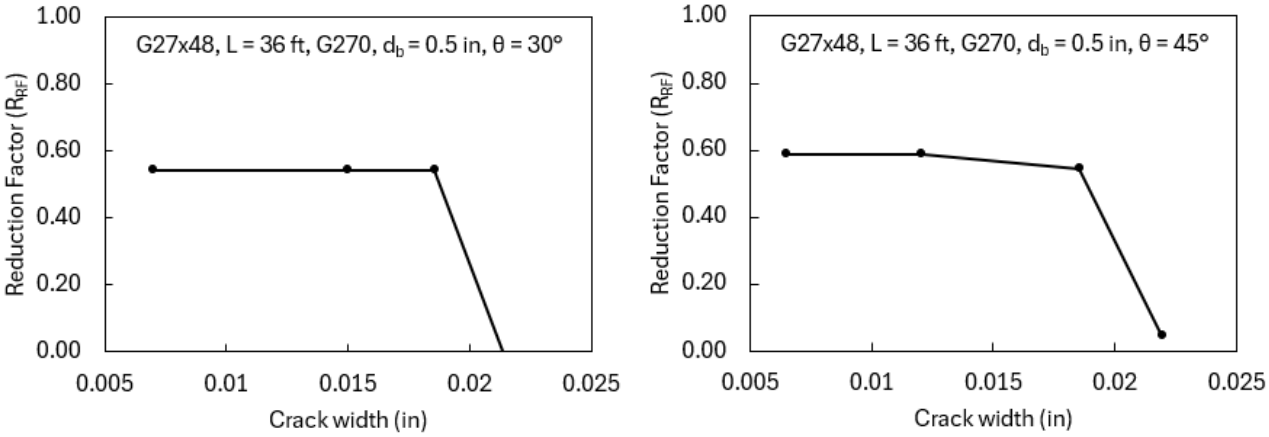

B. Results for 36 ft long beam with θ = 30° and 45°

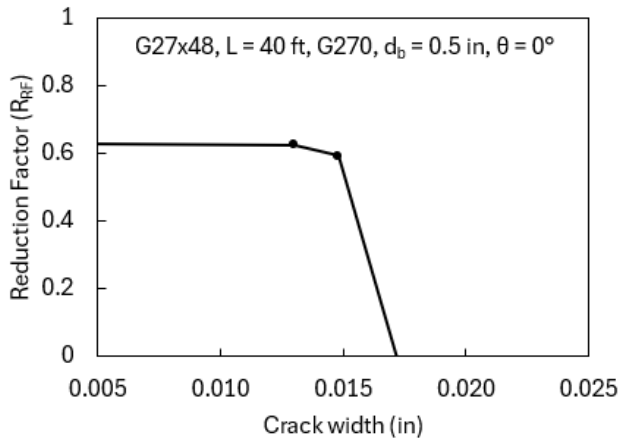

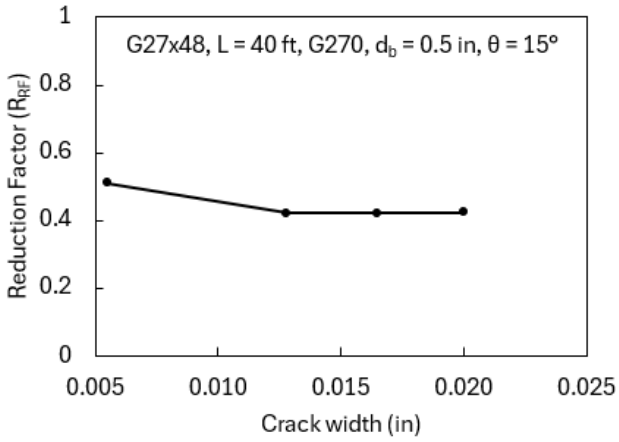

C. Results for 40 ft long beam with θ = 0° and 15°

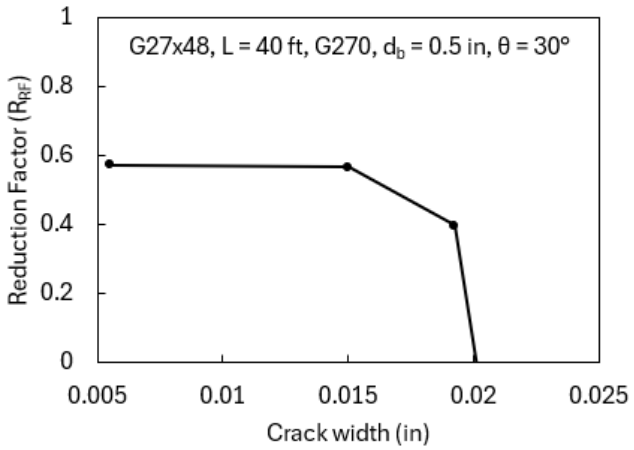

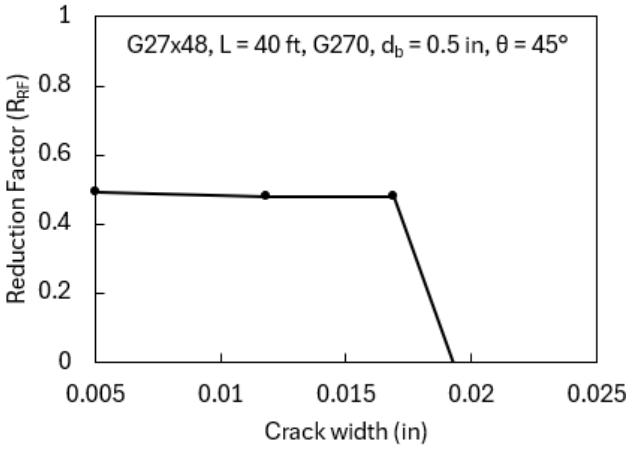

D. Results for 40 ft long beam with θ = 30° and 45°

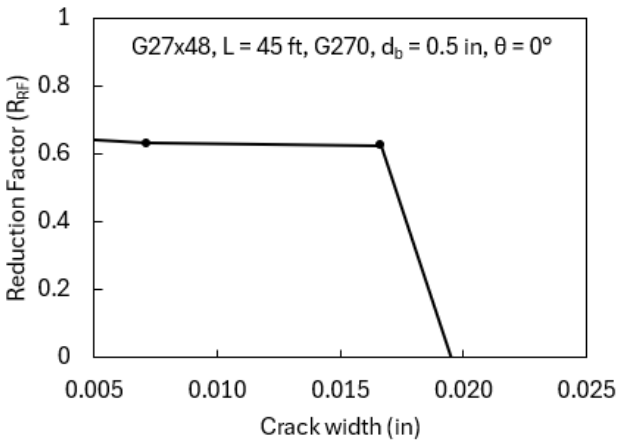

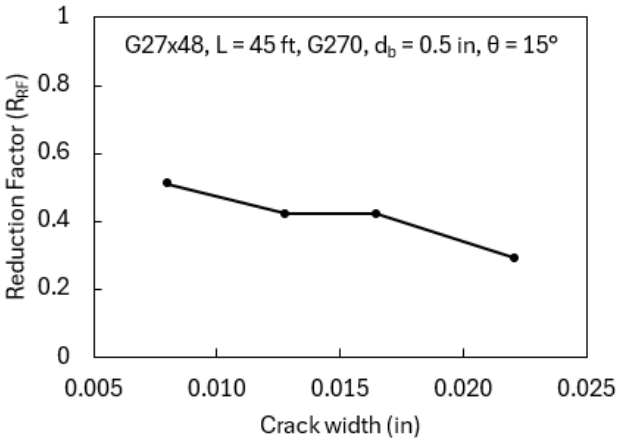

E. Results for 45 ft long beam with θ = 0° and 15°

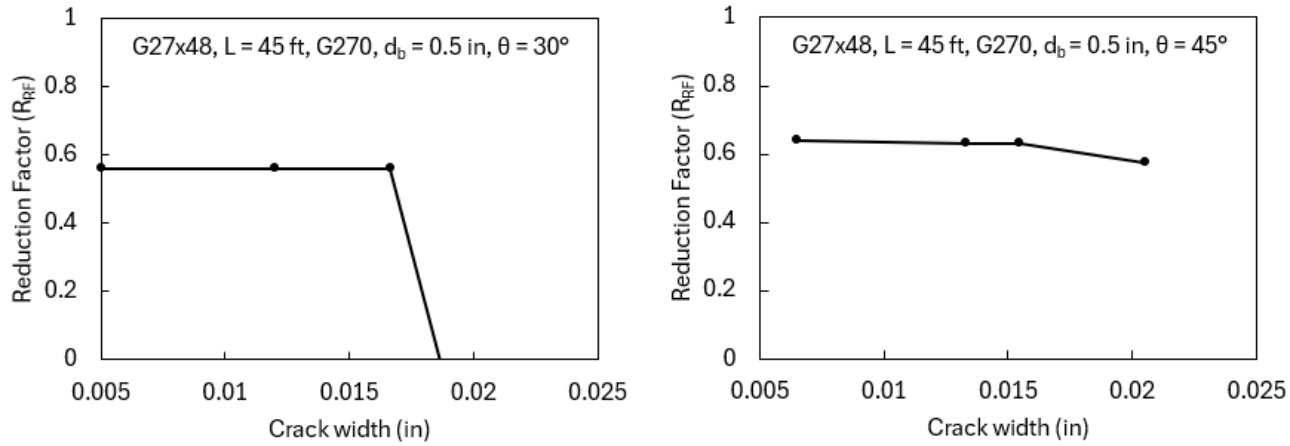

F. Results for 45 ft long beam with θ = 30° and 45°

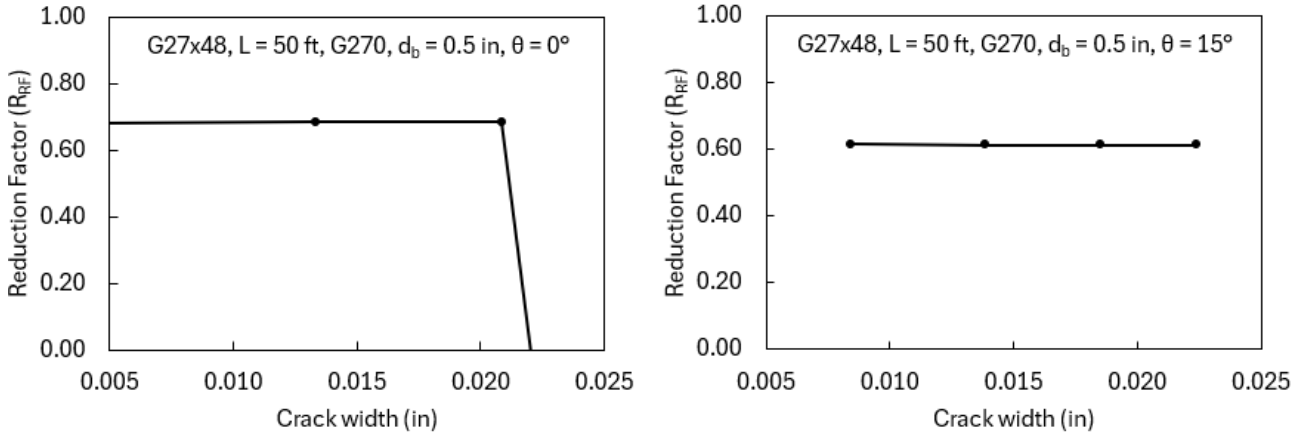

G. Results for 50 ft long beam with θ = 0° and 15°

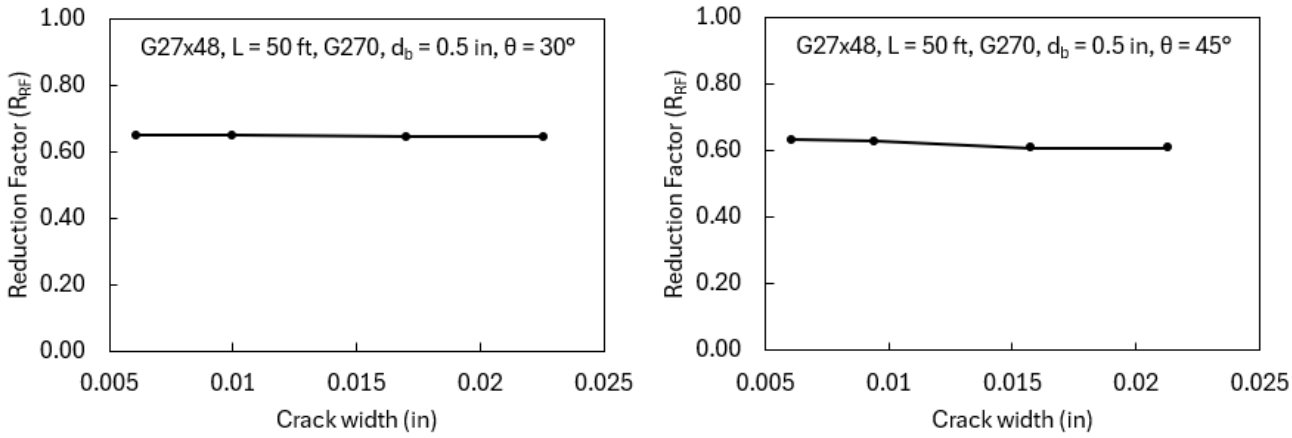

H. Results for 50 ft long beam with θ = 30° and 45°

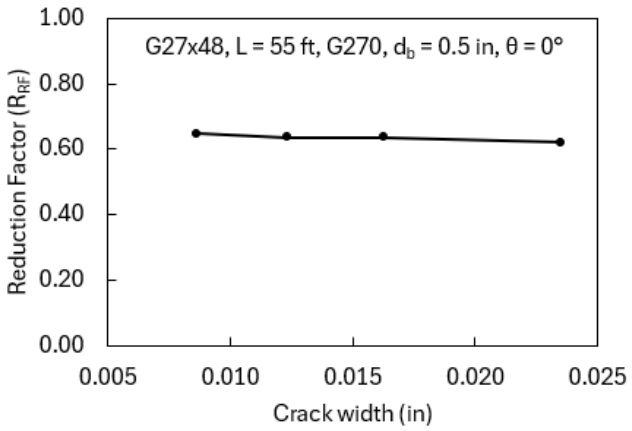

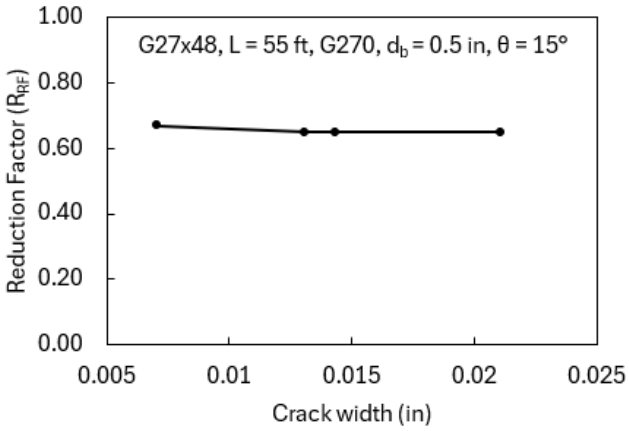

I. Results for 55 ft long beam with θ = 0° and 15°

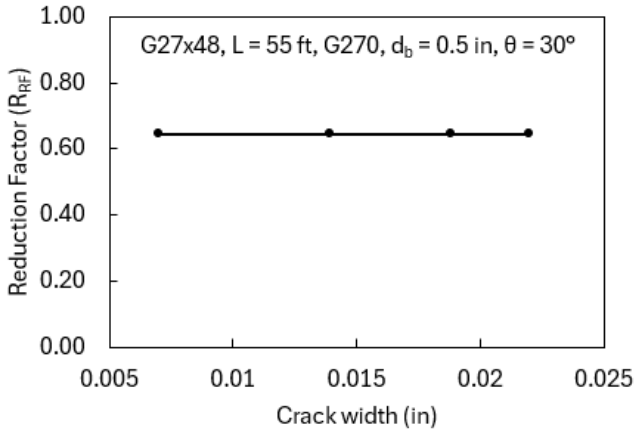

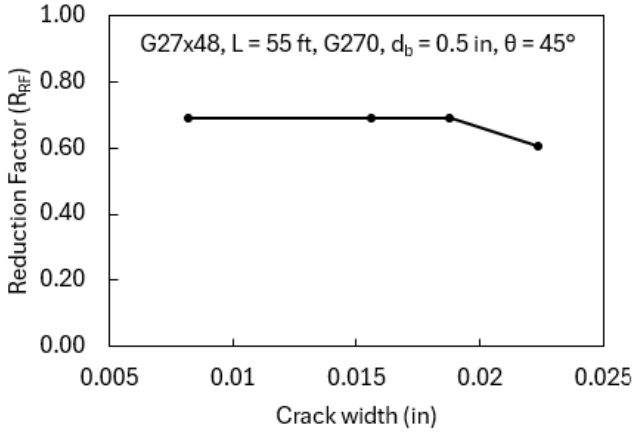

J. Results for 55 ft long beam with θ = 30° and 45°

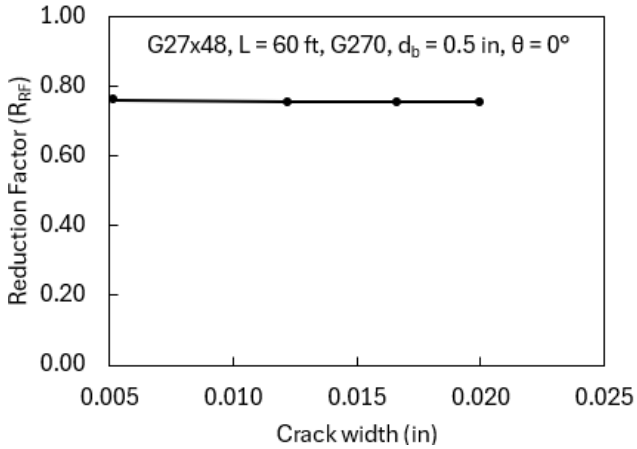

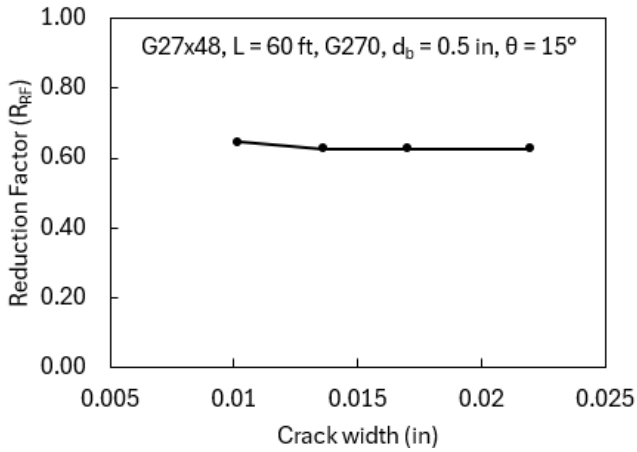

K. Results for 60 ft long beam with θ = 0° and 15°

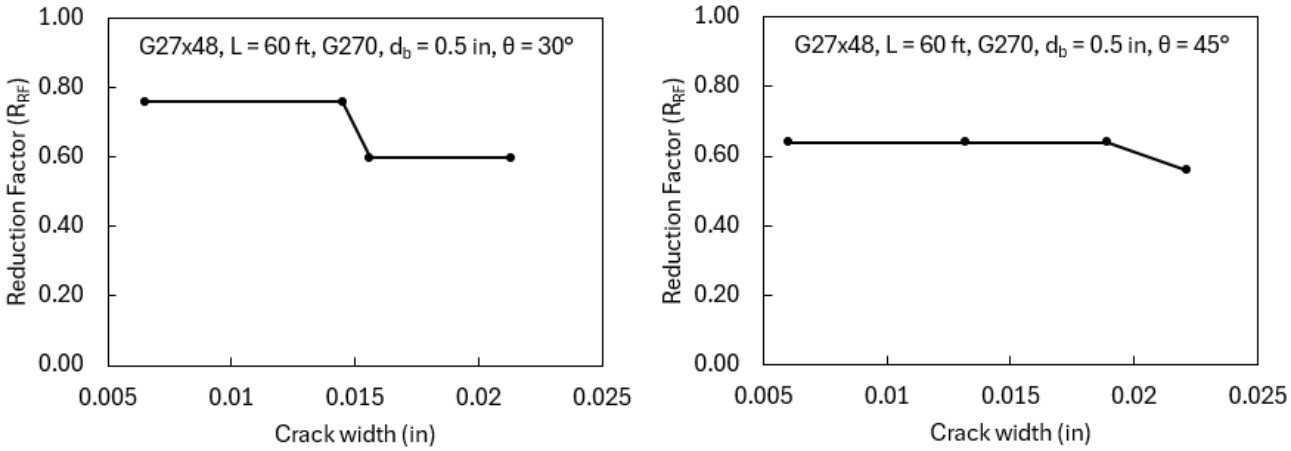

L. Results for 60 ft long beam with θ = 30° and 45°

Figure 38. Graph. Crack width vs. inventory rating for 27 × 48 PPC deck beams.

CHAPTER 7: RECOMMENDATIONS FOR CRACKED PPC DECK BEAMS

The following recommendations are based on the four-point bending tests on the 33 × 36 (G1) and 21 × 36 (G2) beams, the numerical simulations of the two test beams, theoretical cracked section analysis of the PPC deck beams with circular voids, and the parametric study on the PPC deck beams with rectangular voids.

RECOMMENDED LOAD RATING PROCEDURE FOR PPC DECK BEAMS WITH RECTANGULAR VOIDS

The following steps outline the recommended load rating procedure for cracked PPC deck beams with rectangular voids, which is also illustrated in Figure 39:

- Step 1: When transverse cracks are identified on the soffit of the beams, the crack width should be measured.
- Step 2: Determine the following design details: beam type (33 × 36, 27 × 36, or 27 × 48), beam span length (L), skew angle (θ), and prestressing strand diameter (d_b).
- Step 3: The reduction factor (R_{RF}) for the measured crack width should be obtained from Figures 36, 37, or 38 (from Chapter 6). Linear interpolation should be used if needed.
- Step 4: The reduction factor (R_{RF}) obtained from the graphs should be used to limit the rating factor of the cracked PPC deck beams. The rating factor of the cracked beam can be calculated using the formula in Figure 40. In the figure, $\mathrm{IR}_{\mathrm{Cracked\ beam}}$ and $\mathrm{IR}_{\mathrm{As-built\ beam}}$ refer to the inventory rating of the cracked and as-built beams, while $\mathrm{OR}_{\mathrm{Cracked\ beam}}$ and $\mathrm{OR}_{\mathrm{As-built\ beam}}$ refer to the operating rating of the cracked and as-built beams.

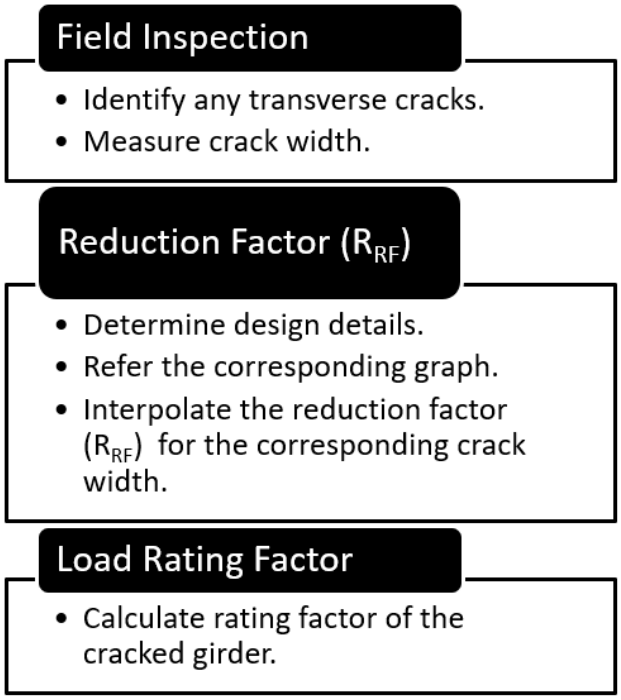

Figure 39. Flowchart. Recommended load rating procedure for cracked PPC deck beams with rectangular voids.

$$IR_{Cracked\ girder} = R_{RF} * IR_{As-built\ girder}$$

$$OR_{Cracked\ girder} = R_{RF} * OR_{As-built\ girder}$$

Figure 40. Equation. Rating factor of cracked beam.

The following are the recommendations for the cracked PPC deck beams with rectangular voids:

- Consider posting the bridge based on the reduction factors (R_{RF}) obtained from the parametric study.
- Assess the distributed loads on cracked beams to prevent exceeding their elastic capacity.
- Exercise caution when using cracked beams with crack widths greater than 0.02 in. These beams may be experiencing very high strand stresses.
- In new bridge designs, drain holes should be located away from the high-moment regions as they may act as nuclei for cracking.

PPC DECK BEAMS WITH CIRCULAR VOIDS

The following recommendations are based on the experimental and theoretical simulations of the PPC deck beams with circular voids. The steps are summarized in Figure 41:

- Step 1: If visible transverse cracks are identified on the soffit of the beams, the beam should be discarded/decommissioned from service.
- Step 2: If no transverse cracks are visible, the bridge can be load-rated according to standard practice.

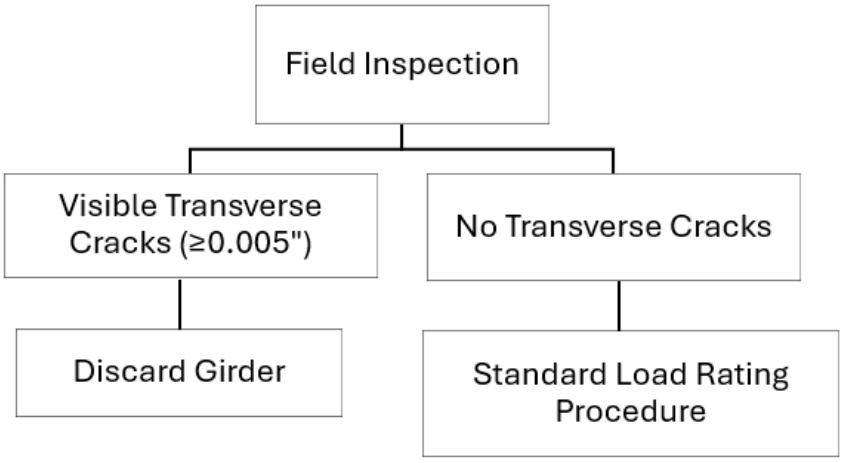

Figure 41. Flowchart. Recommendations for PPC deck beams with circular voids.

CHAPTER 8: SUMMARY AND CONCLUSIONS

This study investigated the impact of transverse cracking on in-service PPC deck beam bridges and developed recommendations for load rating procedures. Experimental testing and numerical simulation were conducted on a cracked PPC deck beam extracted from the field, and the results were used in the study. Finite element models were developed to assess the general behavior and determine the built-up stresses in the cracked beam due to transverse cracking. A parametric study was conducted to identify the variables influencing beam behavior, leading to the development of a new load rating procedure for cracked PPC deck beams. The following are the main conclusions of the study:

- The residual capacity (peak load) and the ductility of the cracked 33 × 36 (G1) beam were 45.9% and 56.3% lower than the as-built finite element predictions, respectively. Also, the cracked beam exhibited early flexible and nonlinear behavior compared to the as-built beam predictions.

- Based on the AASHTO *MBE* load rating approach, transverse cracking in the 33 × 36 (G1) beam resulted in a 34% reduction in load rating, which lowered the inventory and operating rating factors by 22% under HS-20 truck loading. Consequently, vehicular loads on the bridge must be reduced through posting.

- Finite element analysis of the damaged in-service 33 × 36 (G1) PPC deck beam predicted a 16.4% increase in strand stresses at the crack when considering bond-slip behavior. The predicted built-up strand stress was 11.8% lower than those predicted using finite element models assuming perfect bonds.

- In the parametric study, the behavior of cracked PPC deck beams with rectangular voids was influenced by the beam length (L), skew angle (θ), and the interaction between L and θ. Strand diameter (d_b) was also a significant parameter for the 33 × 36 PPC deck beams.

- The inventory rating factor of the prestressing strand in tension decreased linearly with increasing the crack width. For the shorter-span beams with a span of up to 16.8 m (55 ft), the strand tensile stresses governed the load rating once the crack width exceeded 0.51 mm (0.02 in.). The influence of the prestressing strands on the inventory rating reduced with increasing skew angle.

- The capacity-based rating factor of the cracked beam was 12.7% to 73.8% lower than that of the as-built beams since the predicted residual capacity of the cracked beam was 11.6% to 66.2% lower than the capacity of the as-built beam.

- For the G2 (21 × 36) PPC deck beam, the behavior of the beam materials was still in the elastic range even when it was loaded to 95.5% of its AASHTO live load capacity, exhibiting exceptional ductile behavior. After the beam was loaded to 95.5% of its AASHTO live load capacity and unloaded, the crack widths at rest were 0.13 mm (0.005 in.). This showed

that these types of beams have exceptional behavior, and if they have crack widths at rest, they may have been loaded to very high loads close to their nominal capacities and should be discarded/decommissioned.

- The load-deflection behavior obtained from the theoretical cracked section analysis captured the global behavior of the cracked and repaired beams. The elastic limit moments were predicted to be within a 6.7% difference from the experimental values.

The limitations of the analyses conducted in the study are:

- Theoretical cracked section analysis:
    - The analysis does not account for skew effects on beam behavior. The strains across the width of the section were assumed to be uniform.
    - The analysis assumed the applied load acts on the longitudinal axis of the beam with zero eccentricity, ignoring torsional and eccentric loading effects.
    - The analysis assumed that the beam's prestressing strands and other reinforcement were intact with no corrosion. Hence, the entire nominal area of the reinforcement was available.
    - The analysis assumed a perfect bond between the prestressing strands and the concrete beam, so the effect of the bond-slip was ignored.
- Parametric study on PPC deck beams with rectangular voids:
    - The analysis assumed the applied load would act on the longitudinal axis of the beam with zero eccentricity, ignoring torsional and eccentric loading effects.
    - The analysis assumed the beam sustains no damage other than transverse cracks. The analysis results present the reduction in load rating due to the effects of transverse cracks alone.
    - The analysis assumed that the beam's prestressing strands and other reinforcement were intact with no corrosion. Hence, the entire nominal area of the reinforcement was available.
    - The bond-slip model used in the analysis was based on the average bond strength obtained from the literature review. However, actual strand stresses at a crack may vary depending on the strand and beam condition during casting and service, concrete strength, and the bond condition at the crack.
    - Other forms of damage (e.g., longitudinal cracks, cover spalling, honeycombing, and corrosion) may further reduce beam capacity and load rating beyond what is predicted in this study. For example, in the G1 beam, the finite element analysis

predicted an elastic capacity 33% higher than the experimental beam's elastic capacity. The FEM model simulated the effects of the transverse crack. In contrast, the tested beam had other damages like (shear-torsional cracks and spalling of concrete cover near one end of the beam). This highlights that other damage can significantly affect the cracked beam's capacity.

- The inventory reduction factors (R_{RF}) presented in Chapter 6 apply only to beams similar to those analyzed in this study. Bridges other than those considered in this study must be assessed case by case.

- Even if bridges are posted and vehicular loads are limited, transverse cracks may continue to widen due to environmental loads (e.g., temperature changes, shrinkage effects, and corrosion) and additional damage mechanisms affecting the bridge structure. Hence, periodic monitoring is required to ensure that transverse cracks do not widen or that the strands at the cracks do not corrode. It is essential to conduct frequent and periodic inspections of these cracked beams.

REFERENCES

AASHTO. 2002. *Standard specifications for highway bridges, 17th Edition, HB-17.* American Association of State Highway and Transportation Officials.

AASHTO. 2018. *The manual for bridge evaluation, 3rd Edition.* American Association of State Highway and Transportation Officials.

ABAQUS. 2022. ABAQUS Analysis User's Manual version 6.14.

ACI. 2019. *Building code requirements for structural concrete.* (ACI 318-19). American Concrete Institute.

Anderson, G., H. Rider, and M. Sozen. 1964. *Bond characteristics of prestressing strands.* Structural Research Series 283, Structural Engineering Laboratory, University of Illinois Urbana-Champaign.

Andrawes, B. O., A. Pozolo, and M. Shin. 2009. *Transfer and development length of prestressing tendons in full-scale AASHTO prestressed concrete girders using self-consolidating concrete* (FHWA-ICT-09-038). Illinois Center for Transportation.

Attanayake, U., and H. Aktan. 2017. *Reflective cracking between precast prestressed box girders* (WHRP 0092-14-01). Wisconsin Department of Transportation.

Branson, Dan E. (1968). Design procedures for computing deflections. *ACI Journal*, *75*(9).

Cousins, T., M. Badeaux, and S. Moustafa. 1992. Proposed test for determining bond characteristics of prestressing strand. *PCI Journal* 66–73.

Dinsmore, G. A., P. L. Deutsch, and J. L. Montemayor. 1958. *Anchorage and bond in pretensioned prestressed concrete members.* Fritz Laboratory Rep. No. 223-19, Fritz Engineering Laboratory, Lehigh Univ.

Eurocode. 2004. *Design of concrete structures-part 1: General rules and rules for buildings.* Brussels: European Committee for Standardization.

Frosch, R. J. 1999. Another look at cracking and crack control in reinforced concrete. *ACI Structural Journal 96*, 437–42.

Grace, N. F., E. A. Jensen, and M. R. Bebawy. 2012. Transverse post-tensioning arrangement for side-by-side box-beam bridges. *PCI Journal* 48–63.

Gulyas, R. J., G. J. Wirthlin, and J. T. Champa. 1995. Evaluation of keyway grout test methods for precast concrete bridges. *PCI Journal* 44–57.

Hanson, N. W., and P. H. Kaar. 1959. Flexural bond tests of pretensioned prestressed beams. *ACI Journal Proceedings* 783–802.

Hognestad, E. 1951. *A study on combined bending and axial load in reinforced*. University of Illinois Urbana-Champaign.

Janney, J. R. 1954. Nature of bond in pre-tensioned prestressed concrete. *ACI Journal Proceedings* 717–736.

Johnson, R. A. 2018. *Miller & Freund's Probability and Statistics for Engineers.* Pearson.

Karthik, M. M., and J. B. Mander. (2011). Stress-block parameters for unconfined and confined concrete based on a unified stress-strain model. *Journal of Structural Engineering*, *137*(2), 270–273.

Lall, J., S. Alampalli, and E. F. DiCocco. 1998. Performance of full-depth shear keys in adjacent prestressed box beam bridges. *PCI Journal* 72–79.

Loflin, B. J. 2008. *Bond and material properties of grade 270 and Grade 300 prestressing strands.* M.S. Thesis, Virginia Polytechnic Institute and State University.

Logan, D. R. 1997. Acceptance criteria for bond quality of strand for pretensioned prestressed concrete applications. *PCI Journal* 52–90.

Menegotto, M., and P. E. Pinto. 1973. *Method of analysis of cyclically loaded RC plane frames including changes in geometry and non-elastic behavior of elements under normal force and bending.* Vol 13, Lisbon: IABSE Symposium on Resistance and Ultimate Deformability of Structures Acted on by Well-Defined Repeated Loads.

Miller, R. A., G. M. Hlavacs, T. Long, and A. Greuel. 1999. Full-scale testing of shear keys for adjacent box girder bridges. *PCI Journal* 80–99.

Moustafa, S. 1974. *Pullout strength of strand and lifting loops.* Technical Bulletin 74-B5. Concrete Technology Associates.

Motavalli, M., and C. Czaderski. 2007. FRP composites for retrofitting of existing civil structures in Europe: State-of-the-art review. *International Conference of Composites & Polycon.* American Composites Manufacturers Association.

Nawy, E. G. 2009. *Prestressed Concrete - A Fundamental Approach (5th Edition).* Pearson Education Inc.

NBI. 2024. *National Bridge Inventory.* https://www.fhwa.dot.gov/bridge/nbi/no10/mat16.cfm, Federal Highway Administration.

Nylen, R. 2020. *Residual capacity of concrete subjected to impulsive loads.* Georgia: PhD Thesis, Georgia Institute of Technology.

Peterman, R. J. 2009. Influence of flexure-shear cracking on strand development length in prestressed concrete members. *PCI Journal* 143–161.

Rao, S. V. K. M., and W. H. Dilger. 1992. Control of flexural crack width in cracked prestressed concrete members. *ACI Structural Journal* 89, 127–138.

Rose, D., and B. Russell. 1997. Investigation of standardized tests to measure the bond performance of prestressing strand. *PCI Journal*, 56–80.

Sharpe, G. P. 2007. *Reflective cracking in shear keys in multi-beam bridges.* MS Thesis, Texas A&M University.

Steensels, R., L. Vandewalle, B. Vandoren, and H. Degée. 2017. A two-stage modelling approach for the analysis of the stress distribution in anchorage zones of pre-tensioned, concrete elements.

Engineering Structures 384–397.

Stocker, M. F., and M. A. Sozen. 1969. *Investigation of prestressed reinforced concrete for highway bridges: Part VI – Bond characteristics of prestressing strand.* University of Illinois Urbana-Champaign.

Uijl, J. A. den. 1998. Bond modelling of prestressing strand. *SP-180: Bond and Development of Reinforcement, ACI Symposium Publication.*

Xiaohong, S. 2019. Cause analysis of transverse cracks and reinforcement measures for midspan of assembled box girder bridge. *IOP Conference Series: Earth and Environmental Science.*

Yu, Y., Z. Hang, W. Zhao, and X. Zhao. 2021. Fire-resistance mechanism and residual bearing capacity of prestressed concrete beams after fire exposure. *Journal of Structural Engineering, 147*(8).

Zhang, J., R. Wang, Z. Zhang, C. Tong, Z. Yu, and L. Feng. 2022. Residual performance and damage mechanism of prestressed concrete box beam bridge subjected to falling heavy object impact. *Structure and Infrastructure Engineering*, *19*(11).


Illinois Department
of Transportation


ILLINOIS